Contents of issue 2 vol. LV

Engineering Transactions, T. **LV**, nr 2, str. 99–194, Warszawa 2007

ENGINEERING TRANSACTIONS • *Engng. Trans.* • **55**, 2, 101–113, 2007
Polish Academy of Sciences • Institute of Fundamental Technological Research

THREE-PARAMETER OPTIMIZATION OF AN AXIALLY LOADED BEAM ON A FOUNDATION

A. S. Fryś, A. Fryś

Institute of Physics, Cracow University of Technology
1 Podchorążych Str., 30-084 Kraków, Poland

A beam of circular cross-section, made of viscoelastic material of Kelvin–Voigt type, is considered. The beam is symmetric with respect to its center, the length and volume of the beam are fixed and its ends are simply supported. The radius of the cross-section is a cubic function of co-ordinate. The beam interacts with a foundation of Winkler, Pasternak or Hetényi type and is axially loaded by a non-conservative force $P(t) = P_0 + P_1 \cos \vartheta t$. Only the first instability region is taken into account. The shape of the beam is optimal if the critical value of P_1 is maximal. A few numerical examples are presented on graphs.

1. Introduction

Problem of stability and parametric optimization of an axially loaded beam interacting with a foundation is considered. The radius of the circular cross-section of the beam is assumed to be a cubic polynomial of co-ordinate and an additional strength condition is added. Foundations of Winkler, Pasternak and Hetényi type are taken into account. Only the first instability region is considered. The optimal shape of the beam is characterized by variation of its cross-section radius. This paper is a continuation of the papers [1, 2] in which one-parameter and two-parameter optimization of the problem were considered.

Optimization of viscoelastic cantilever beam with respect to its dynamic stability was presented by A. Gajewski and A. S. Fryś during Euromech Colloquium 190 [3], cf. [4]. Optimization of structures is the subject of monograph by A. Gajewski and M. Życzkowski [5]. A study concerning to optimization of mechanical systems in conditions of parametric resonances was written by A. Fryś [6]. Some new approach to the solution of optimization problem for a compressed column is given by A. Gajewski [7, 8].

The Lagrange problem on an optimal column is analysed in the paper by A. P. Seyranian, O. G. Privalova [9]. Parametrically excited beam and its optimal shape is considered in the paper by A. A. Mailybaev, H. Yabuno and H. Kaneko [10].

2. Formulation of the problem

A straight beam of circular cross-section (see Fig. 1) is made of viscoelastic material of Kelvin–Voigt type. The undeformed beam axis coincides with the x-axis. In view of symmetry of the problem we assume that the beam is symmetric with respect to its centre $x = l/2$. The length l of the beam and its volume V are fixed. We assume that the cross-section of the beam is non-zero i.e. the radius $r(\xi)$ (where $\xi = x/l$) of the cross-section satisfies the assumption

$$r(\xi) > 0, \xi \in [0,1]. \tag{2.1}$$

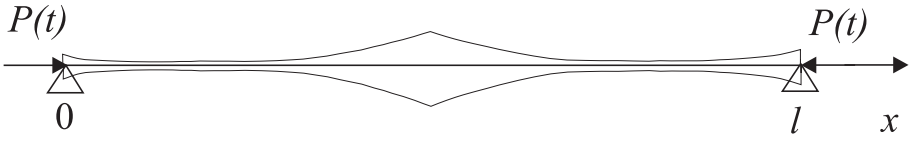

Fig. 1. The shape of the beam.

We assume that the radius is given by the following formulae:

$$r(\xi) \equiv r_0(\varepsilon_1,\varepsilon_2,\varepsilon_3)\varphi(\xi;\varepsilon_1,\varepsilon_2,\varepsilon_3) \tag{2.2}$$

$$= \begin{cases} r_0\left(1-\dfrac{\varepsilon_1}{2}-\dfrac{\varepsilon_2}{4}-\dfrac{\varepsilon_3}{8}+\varepsilon_1\xi+\varepsilon_2\xi^2+\varepsilon_3\xi^3\right), & \xi\in\left[0,\dfrac{1}{2}\right] \\ r_0\left[1+\dfrac{\varepsilon_1}{2}+\dfrac{3\varepsilon_2}{4}+\dfrac{7\varepsilon_3}{8}-(\varepsilon_1+2\varepsilon_2+3\varepsilon_3)\xi+(\varepsilon_2+3\varepsilon_3)\xi^2-\varepsilon_3\xi^3\right], & \xi\in\left[\dfrac{1}{2},1\right] \end{cases}$$

where $r_0 > 0$. Values of the parameters $\varepsilon_1, \varepsilon_2, \varepsilon_3$ determine the shape of the beam. For a prismatic beam $\varepsilon_1 = \varepsilon_2 = \varepsilon_3 = 0$. In this paper one assumes that $\varepsilon_3 \neq 0$. On the basis of the assumption (2.1) employed for $\xi = 0$ i.e. $r(0) > 0$, one has the inequality

$$1-\frac{\varepsilon_1}{2}-\frac{\varepsilon_2}{4}-\frac{\varepsilon_3}{8} > 0. \tag{2.3}$$

The volume of the beam is

$$V = 2\pi l\int_0^{1/2} r^2(\xi)d\xi = \pi r_0^2 l/f(\varepsilon_1,\varepsilon_2,\varepsilon_3),$$

where

$$f(\varepsilon_1,\varepsilon_2,\varepsilon_3) \tag{2.4}$$

$$= \left[1-\frac{\varepsilon_1}{2}-\frac{\varepsilon_2}{3}-\frac{3\varepsilon_3}{16}+\frac{\varepsilon_1^2}{12}+\frac{\varepsilon_2^2}{30}+\frac{9\varepsilon_3^2}{896}+\frac{5\varepsilon_1\varepsilon_2}{48}+\frac{9\varepsilon_1\varepsilon_3}{160}+\frac{7\varepsilon_2\varepsilon_3}{192}\right]^{-1}.$$

Therefore one obtains the following formula:

$$r_0 = \sqrt{\frac{Vf(\varepsilon_1, \varepsilon_2, \varepsilon_3)}{\pi l}}. \tag{2.5}$$

The three independent parameters $\varepsilon_1, \varepsilon_2, \varepsilon_3$ are the optimization parameters. Their admissible values must belong to a set in R^3 in which the inequality (2.1) is satisfied. One boundary (a plane) of this set is given by (2.3).

So we look for such values of parameters $\varepsilon_1, \varepsilon_2, \varepsilon_3$ for which the value of the cubic polynomial $\varphi(\xi; \varepsilon_1, \varepsilon_2, \varepsilon_3)$ given by the first formula (2.2) is positive for $\xi \in \left[0, \frac{1}{2}\right]$.

To this end the following reasoning is applied. Beacause of the assumption that $\varepsilon_3 \neq 0$, the possible graphs of this polynomial can be of the forms shown in Figs. 2–5, where $\varphi = \varphi(\xi; \varepsilon_1, \varepsilon_2, \varepsilon_3)$.

For the graphs shown in Figs. 2 and 3 the polynomial has no extremes, so the following condition is fulfilled:

$$\Delta \equiv 3\varepsilon_1\varepsilon_3 - \varepsilon_2^2 \geq 0. \tag{2.6}$$

For the graphs shown in Figs. 4 and 5 the polynomial has two extremes, so the following condition is fulfilled:

$$\Delta < 0. \tag{2.7}$$

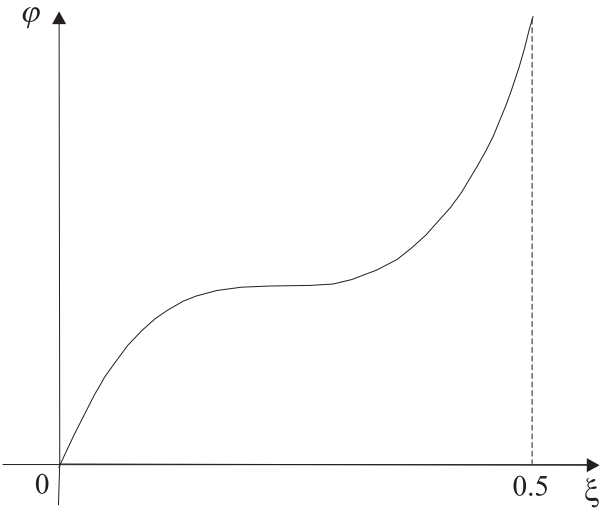

FIG. 2. The cubic polynomial.

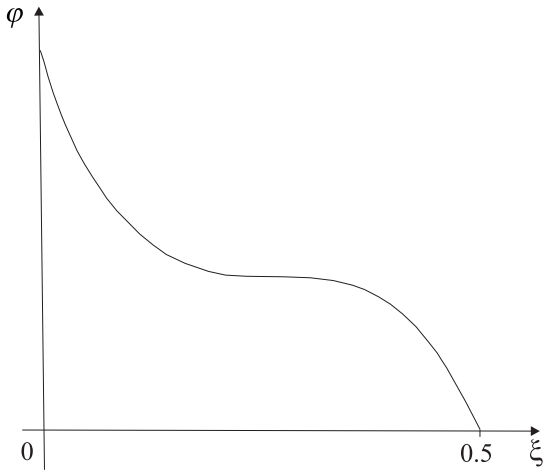

FIG. 3. The cubic polynomial.

For the cases shown in Figs. 2 and 3, from the inequalities $r(0) > 0, r\left(\frac{1}{2}\right) = r_0 > 0$ the condition (2.1) results. Therefore the conditions (2.3) and (2.6) define the set of admissible values of the optimization parameters for these cases.

If $\Delta < 0$ the situation is more complicated. In this case the polynomial φ given by the first formula (2.2) has two extremes at the points $\xi_{\min} = (-\varepsilon_2 + \sqrt{-\Delta})/3\varepsilon_3$ and $\xi_{\max} = (-\varepsilon_2 - \sqrt{-\Delta})/3\varepsilon_3$.

First we cosider the case $\varepsilon_3 > 0$, shown in Fig. 4. The points $\xi = 0$ and $\xi = \frac{1}{2}$ i.e. the ends of the interval $\left[0, \frac{1}{2}\right]$, can be situated in the following six positions: (11), (33), (22), (21), (31), (32), where each digit denotes the interval indicated in Fig. 4. To satisfy the condition (2.1) the following inequalities must be satisfied for succesive positions:

$$(11): \ \xi_{\min} \leq 0, \tag{2.8}$$

$$(33): \ \xi_{\max} \geq \frac{1}{2}, \tag{2.9}$$

$$(22): \ \xi_{\max} \leq 0 \wedge \xi_{\min} \geq \frac{1}{2}, \tag{2.10}$$

$$(21): \ \xi_{\max} \leq 0 \wedge \xi_{\min} \in \left(0, \frac{1}{2}\right] \wedge \varphi(\xi_{\min}) > 0, \tag{2.11}$$

$$(31): \ \xi_{\max} > 0 \wedge \xi_{\min} \leq \frac{1}{2} \wedge \varphi(\xi_{\min}) > 0, \tag{2.12}$$

$$(32): \ \xi_{\min} \geq \frac{1}{2} \wedge \xi_{\max} \in \left(0, \frac{1}{2}\right]. \tag{2.13}$$

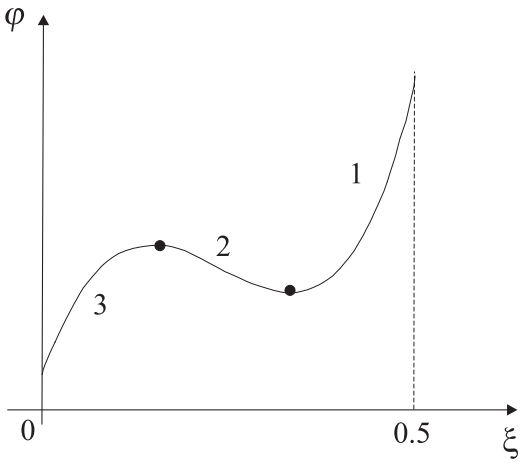

FIG. 4. The cubic polynomial.

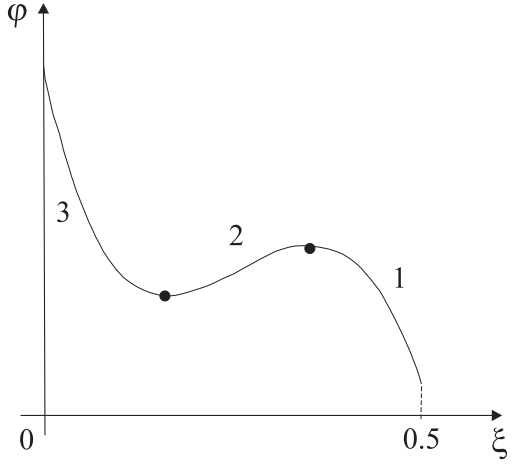

FIG. 5. The cubic polynomial.

Next we consider the case $\varepsilon_3 < 0$, illustrated in Fig. 5. To satisfy the condition (2.1), the following inequalities must be satisfied for succesive positions:

$$(11): \ \xi_{\max} \leq 0, \tag{2.14}$$

$$(33): \ \xi_{\min} \geq \frac{1}{2}, \tag{2.15}$$

$$(22): \ \xi_{\min} \leq 0 \wedge \xi_{\max} \geq \frac{1}{2}, \tag{2.16}$$

$$(21): \ \xi_{\min} \leq 0 \wedge \xi_{\max} > 0 \wedge \xi_{\max} \leq \frac{1}{2}, \tag{2.17}$$

$$(2.18)\qquad (31):\ \xi_{\min} > 0 \wedge \xi_{\max} < \frac{1}{2} \wedge \varphi(\xi_{\min}) > 0,$$

$$(2.19)\qquad (32):\ \xi_{\min} > 0 \wedge \xi_{\min} < \frac{1}{2} \wedge \xi_{\max} \geq \frac{1}{2} \wedge \varphi(\xi_{\min}) > 0.$$

For $\Delta < 0$ the above conditions define the admissible set in $\varepsilon_1\varepsilon_2\varepsilon_3$ space, i.e. the set in which the radius of cross-section of the beam is positive.

The beam under consideration is axially loaded by a non-conservative force of the form

$$(2.20)\qquad P(t) = P_0 + P_1 \cos \vartheta t,$$

where t is time and P_0, P_1, ϑ are positive constants. The beam interacts with a foundation of Winkler, Pasternak or Hetényi type with damping. A study of different foundation models has been presented by Kerr [11].

The following dimensionless quantities are introduced [1, 12]:

$$\upsilon = \frac{w}{l}, \qquad \tau = (\pi/2l^2)\sqrt{\pi EV/\rho l}\,t, \qquad \alpha = 4l^4P_0/\pi EV^2,$$
$$\beta = 4l^4P_1/\pi EV^2, \qquad \Lambda = (\pi\lambda/2l^2)\sqrt{\pi V/\rho l E}, \qquad \kappa = 4kl^6/\pi^3EV^2,$$
$$\mu = 4Gl^4/\pi EV^2, \qquad \theta = (2l^2/\pi)\sqrt{\rho l/\pi EV}\,\vartheta, \qquad \gamma = (2cl^4/\pi^2EV^2)\sqrt{\pi EV/\rho l},$$
$$\delta = 4\pi Dl^2/EV^2, \qquad f \equiv f(\varepsilon_1, \varepsilon_2, \varepsilon_3), \qquad \varphi \equiv \varphi(\xi; \varepsilon_1, \varepsilon_2, \varepsilon_3),$$

where $w(x,t)$ is the transverse displacement of the cross-section in the space coordinate x at the time t, E is Young's modulus, λ and c are the coefficients of internal and external damping respectively, ρ is the mass density of the beam, k is the foundation stiffness per unit length, G is the foundation modulus and D is the foundation flexural stiffness.

The equation of the transverse vibrations of the beam on its foundation has the form [1, 12]

$$(2.21)\qquad \frac{1}{\pi^2}f^2\frac{\partial^2}{\partial\xi^2}\left(\varphi^4\frac{\partial^2\upsilon}{\partial\xi^2} + \Lambda\varphi^4\frac{\partial^3\upsilon}{\partial\xi^2\partial\tau}\right) + \alpha\frac{\partial^2\upsilon}{\partial\xi^2} + \beta\frac{\partial^2\upsilon}{\partial\xi^2}\cos\theta\tau$$
$$+ \pi^2 f\varphi^2\frac{\partial^2\upsilon}{\partial\tau^2} + \pi^2\kappa\upsilon + \pi^2\gamma\frac{\partial\upsilon}{\partial\tau} + \frac{\delta}{\pi^2}\frac{\partial^4\upsilon}{\partial\xi^4} - \mu\frac{\partial^2\upsilon}{\partial\xi^2} = 0,$$

where $\mu \equiv \delta \equiv 0$ for a Winkler foundation, $\delta \equiv 0$ for a Pasternak foundation and $\mu \equiv 0$ for a Hetényi foundation respectively.

It is assumed that the two ends of the beam are simply supported:

$$(2.22)\qquad \begin{aligned} &\upsilon(0,\tau) = 0, \quad [\varphi^4(\partial^2\upsilon/\partial\xi^2 + \Lambda\partial^3\upsilon/\partial^2\xi\partial\tau)](0,\tau) = 0,\\ &\upsilon(1,\tau) = 0, \quad [\varphi^4(\partial^2\upsilon/\partial\xi^2 + \Lambda\partial^3\upsilon/\partial^2\xi\partial\tau)](1,\tau) = 0. \end{aligned}$$

From the Eq. (2.21) with the boundary conditions (2.22) one can determine the first instability region for the beam under consideration. Parametric optimization of the shape of the beam consists in finding those admissible values of the parameters $\varepsilon_1, \varepsilon_2, \varepsilon_3$ for which the value of P_1 i.e. the oscillatory component of the loading force, causing beam's instability, is maximal.

3. Solution of the problem

The problem is approximately solved by the Galerkin method; cf. [1, 2]. Therefore one looks for the solution of Eq. (2.21) in the form

$$v(\xi,\tau) = \sum_{n=1}^{N} q_n(\tau)\sin n\pi\xi \tag{3.1}$$

and obtains the set of ordinary differerential equations for the unknown functions $q_n(\tau)$

$$\sum_{k=1}^{N}(A_{nk}\ddot{q}_k + B_{nk}\dot{q}_k + C_{nk}q_k + D_{nk}q_k\cos\theta\tau) = 0, \qquad n = 1,...,N, \tag{3.2}$$

where

$$A_{nk} = f(\varepsilon_1,\varepsilon_2,\varepsilon_3)\int_0^1 \varphi^2(\xi;\varepsilon_1,\varepsilon_2,\varepsilon_3)\sin n\pi\xi\sin k\pi\xi d\xi,$$

$$B_{nk} = \frac{1}{2}\gamma\delta_{nk} + \Lambda n^2k^2f^2(\varepsilon_1,\varepsilon_2,\varepsilon_3)\int_0^1 \varphi^4(\xi;\varepsilon_1,\varepsilon_2,\varepsilon_3)\sin n\pi\xi\sin k\pi\xi d\xi,$$

$$C_{nk} = \frac{1}{2}(\kappa + \mu n^2 + \delta n^4 - \alpha n^2)\delta_{nk} + n^2k^2f^2(\varepsilon_1,\varepsilon_2,\varepsilon_3)\int_0^1 \varphi^4(\xi;\varepsilon_1,\varepsilon_2,\varepsilon_3)\sin n\pi\xi\sin k\pi\xi d\xi, \tag{3.3}$$

$$D_{nk} = -\frac{1}{2}\beta n^2\delta_{nk}.$$

Here δ_{nk} is the Kronecker delta.

In further considerations only the first two Eqs. (3.2) are retained; these are equations for the functions $q_1(\tau), q_2(\tau)$. From these two equations the boundaries

of the first instability region of the beam are determined. The instability region occurs in the neighbourhood of twice the value of the first natural frequency of the beam [3, 4].

To determine the boundaries of the first instability region one assumes the solution of Eqs. (3.2) in the following form [13, 14]:

$$q_k(\tau) = A_k \sin\frac{\theta\tau}{2} + B_k \cos\frac{\theta\tau}{2}, \qquad k = 1, 2, \tag{3.4}$$

where A_k, B_k are constants. After inserting (3.4) into the system of Eq. (3.2), a system of four algebraic linear homogeneous equations for A_k, B_k is obtained. The non-zero solution of these equations exists if the determinant of the system equals zero. This leads to the biquadratic equation for dimensionless amplitude β of the oscillating component of loading, in the form ([1])

$$\frac{1}{16}\beta^4 - \left[h_{11}^2 + \frac{1}{16}h_{22}^2 + (\theta^2/4)B_{11}^2 + (\theta^2/64)B_{22}^2\right]\beta^2 + h_{11}^2 h_{22}^2 + (\theta^2/4)\left[h_{11}^2 B_{22}^2 + h_{22}^2 B_{11}^2 + (\theta^2/4)B_{11}^2 B_{22}^2\right] = 0, \tag{3.5}$$

where

$$h_{11} = -(\theta^2/4)A_{11} + C_{11}, h_{22} = -(\theta^2/4)A_{22} + C_{22}. \tag{3.6}$$

From Eq. (3.5) one determines the boundaries of the first instability region i.e. the critical value of β as a function of θ. Inside the instability region the critical value attains its minimal value given by the formula

$$\beta_{\min} = 4\,|B_{11}|\sqrt{\frac{C_{11}}{A_{11}} - \frac{{B_{11}}^2}{4A_{11}^2}}. \tag{3.7}$$

The critical value of β depends on the values of optimization parameters $\varepsilon_1, \varepsilon_2, \varepsilon_3$. The shape of the beam is optimal if the value of $\beta_{\min}$ is maximal.

The results of paper [2] show one difficulty: in many cases the radius of the cross-section of the beam attains very small values. This fact undoubtedly questions the obtained results. Thus in the present paper the following strength condition is added – one assumes that the maximal stress, i.e. the stress, at the smallest cross-section of the beam, does not exceed the limity stress σ_0 of the material:

$$\frac{P_0 + P_1}{\pi r_{\min}^2} \leq \sigma_0. \tag{3.8}$$

4. Parametric optimization of the shape of the beam

To realize a few numerical calculations one assumes: $E = 2.1 \cdot 10^{11}$ Pa, $\sigma_0 = 2.2 \cdot 10^8$ Pa, $V/l^3 = 10^{-4}$. Therefore the strength condition (3.8) takes the form

$$\frac{\alpha + \beta}{f(\varepsilon_1, \varepsilon_2, \varepsilon_3)\varphi^2_{\min}} \leq 13.37. \tag{4.1}$$

The numerical calculations have been performed for $\varepsilon_k \in [-10, 10]$, $k = 1, 2, 3$ with step 0.1 and the maximum of $\beta_{\min}$ has been found out.

The following denotations are adopted:

Winkler model ($\mu = \delta = 0$)

case 1: $\gamma = 0.03$, $\kappa = 0.1$, $\alpha = 0.5$, $\Lambda = 0.01$,

case 2: $\gamma = 0.1$, $\kappa = 0.1$, $\alpha = 0.5$, $\Lambda = 0.01$,

case 3: $\gamma = 0.1$, $\kappa = 0.1$, $\alpha = 0.8$, $\Lambda = 0.01$.

Pasternak model ($\delta = 0$)

case 4: $\gamma = 0.005$, $\kappa = 0.1$, $\mu = 0.2$, $\alpha = 0.5$, $\Lambda = 0.002$,

case 5: $\gamma = 0.1$, $\kappa = 0.1$, $\mu = 0.2$, $\alpha = 0.5$, $\Lambda = 0.01$.

Hetényi model ($\mu = 0$)

case 6: $\gamma = 0.005$, $\kappa = 0.1$, $\delta = 0.2$, $\alpha = 0.5$, $\Lambda = 0.002$,

case 7: $\gamma = 0.1$, $\kappa = 0.1$, $\delta = 0.2$, $\alpha = 0.5$, $\Lambda = 0.01$.

The results are tabulated and illustrated on the graphs which are shown in Figs. 6–10, where

$$R(\xi) = r(\xi)/l. \tag{4.2}$$

For comparison in Figs. 8–10 the graphs obtained in virtue of reference [2] are shown by dashed lines.

Case	ε_1	ε_2	ε_3	β_{opt}
1	−1.0	0.2	9.9	0.382
2	−1.1	0.5	9.5	0.623
3	−1.2	0.3	10.0	0.584
4, 6	−3.4	4.2	8.8	0.316
5, 7	−3.2	4.4	7.4	1.404

The optimal shape of the beam depends on the values of parameters describing materials of the beam and foundation. The optimal shape of the beam is not a universal one.

Sensitivity of the shape of the beam i.e. $R(\xi)$ to the values of $\varepsilon_1, \varepsilon_2, \varepsilon_3$ is presented by Fig. 11 where the graphs for optimal case and for $\varepsilon_k - 0.1$, $k = 1, 2, 3$ are shown.

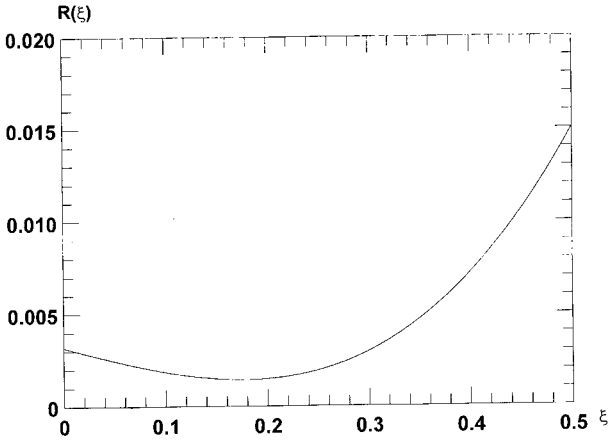

FIG. 6. The graph $R(\xi)$, case 1.

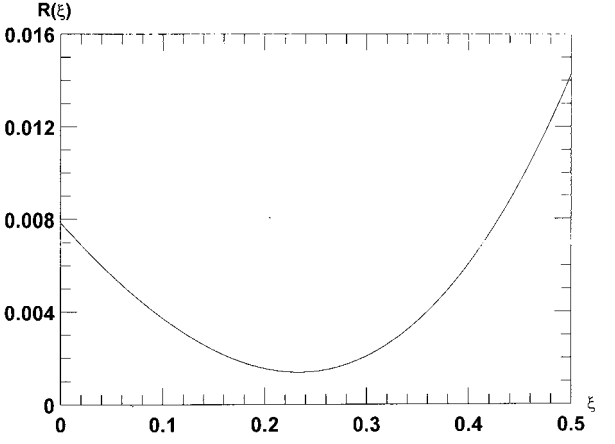

FIG. 7. The graph $R(\xi)$, case 4, 6.

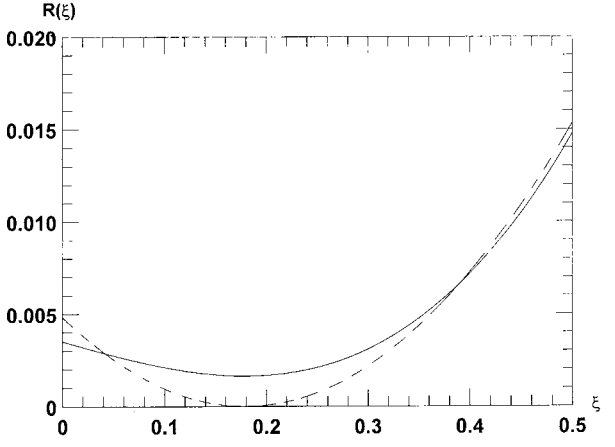

FIG. 8. The graph $R(\xi)$, case 2.

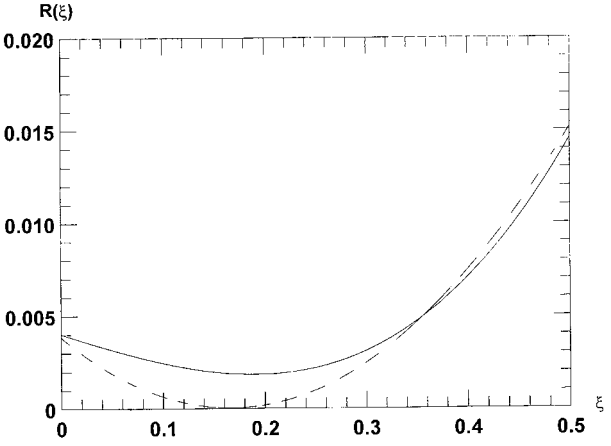

FIG. 9. The graph $R(\xi)$, case 3.

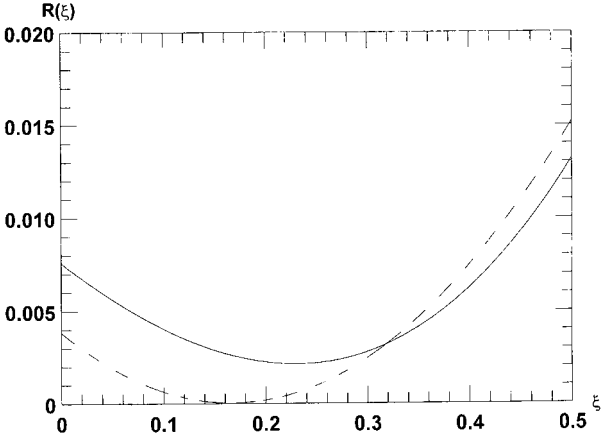

FIG. 10. The graph $R(\xi)$, case 5, 7.

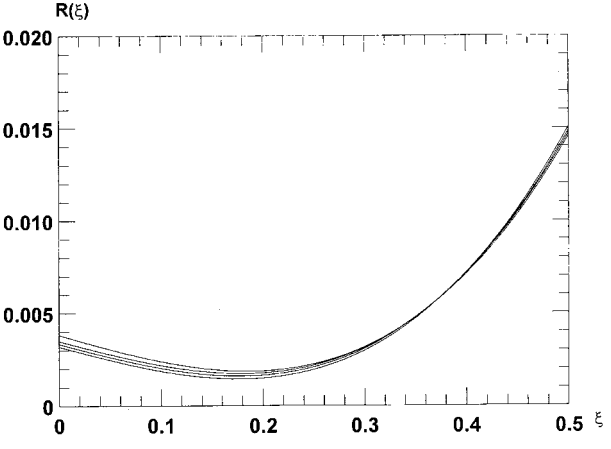

FIG. 11. The graph $R(\xi)$, case 1, for different ε_k.

5. Final remarks

The parametrical optimization of an axially loaded viscoelastic beam on a foundation has been discussed. The radius of the cross-section of the beam is a cubic function of co-ordinate. The beam performs transverse vibration and interacts with a foundation of Winkler, Pasternak or Hetényi type. The values of three optimization parameters defining optimal shape of the beam are calculated for a number cases. Results are shown on the graphs.

The results of the paper are the extension and confirmation of the results obtained in the previous papers [1, 2].

References

1. A. S. Foryś, *Optimization of an axially loaded beam on a foundation*, Journal of Sound and Vibration, **178**, 607–613, 1994.

2. A. S. Foryś, *Two-parameter optimization of an axially loaded beam on a foundation*, Journal of Sound and Vibration, **199**, 801–812, 1997.

3. A. Gajewski and A. S. Foryś *Optimal structural design of a nonconservative viscoelastic system with respect to dynamic stability*, Euromech Colloquium 190, Hamburg-Harburg, 1984.

4. A. S. Foryś and A. Gajewski, *Parametric optimization of a viscoelastic rod with respect to its dynamic stability* [in Polish], Engineering Transactions, **35**, 297–308, 1987.

5. A. Gajewski and M. Życzkowski, *Optimal structural design under stability constraints*, Kluwer Academic Publishers, Dordrecht/Boston /London 1988.

6. A. Foryś, *Optimization of mechanical systems in conditions of parametric resonance and in autoparametric resonances* [in Polish], Monograph 199, Cracow University of Technology, Kraków 1996.

7. A. Gajewski, *Optimization of a compressed column under dynamical stability constraints*, XVIII Symposium – Vibration in Physical Systems, Poznań – Błażejewko 1998.

8. A. Gajewski, *Optimization of a compressed column under dynamical stability constraints,* Third World Congress of Structural and Multidisciplinary Optimization, Buffalo, New York 1999.

9. A. P. Seyranian, O. G. Privalova, *The Lagrange problem on an optimal column: old and new results*, Struct. Multidisc. Optim., **25**, 393–410, 2003.

10. A. A. Mailybaev, H. Yabuno and H. Kaneko, *Optimal shapes of parametrically excited beams,* Struct. Multidisc. Optim., **27**, 435–445, 2004.

11. A. D. Kerr, *Elastic and viscoelastic foundation models*, Journal of Applied Mechanics, **31**, 491–498, 1964.

12. R. S. Engel, *Dynamic stability of an axially loaded beam on an elastic foundation with damping,* Journal of Sound and Vibration, **146**, 463–477, 1991.

13. V. V. Bolotin, *Dynamic Stability of Elastic Systems* [in Russian], Moscow: Izd. Teor. Lit., 1956.

14. A. S. Volmir, *Stability of Deformable Systems* [in Russian]. Moscow: Nauka, 1967

Received May 16, 2005; revised version March 23, 2006.

ENGINEERING TRANSACTIONS • *Engng. Trans.* • **55**, 2, 115–128, 2007
Polish Academy of Sciences • Institute of Fundamental Technological Research

MODELLING OF CONTINUUM DAMAGE FOR APPLICATION ELASTO-VISCOPLASTIC BODNER-PARTOM CONSTITUTIVE EQUATIONS

A. Ambroziak

Gdańsk University of Technology
Faculty of Civil and Environmental Engineering
Department of Structural Mechanics and Bridge Structures
Narutowicza 11/12, 80–952 Gdańsk, Poland

The aim of the paper is to propose an application of the continuum damage model proposed by Lemaitre to the elasto-viscoplastic constitutive equations of the Bodner–Partom model. The proposed approach has been implemented into subroutines of the FE code MSC.Marc as the user's viscoplastic subroutine UVSCPL and has been used to perform the FE numerical simulations. Comparison is given of the following two variants: 1) uniaxial creep test results for a nickel-based B1900+Hf superalloy at high temperatures and 2) calculation based on the constitutive equations with the inclusion of isotropic damage models.

Key words: elasto-viscoplastic, Bodner–Partom, damage, FEM.

1. Introduction

The Bodner–Partom constitutive model belongs to the group of unified theories, proposed by Bodner and Partom [7] at the beginning of the 1970s. These constitutive equations have been frequently utilized in modelling of the elasto-viscoplastic hardening of a number of materials, with a great many practical engineering applications [2]. Its application in the elasto-viscoplastic static and dynamic analysis of plates and shells is shown in many examples: Kłosowski *et al.* [21] and [23], Sansour and Kollmann [30], Woźnica [39], Kłosowski [20], Stoffel [34] and [35], Sansour and Wagner [31] and [32], Steck [33], Kłosowski and Woźnica [22]. Description of the behaviour of glassy polymers (see e.g.: Frank and Brockman [16], Zaïri *et al.* [42]) and technical coated fabrics (see e.g.: Kłosowski *et al.* [24]) is also shown with reference to the presented model. On the other hand, Chełmiński and Gwiazda [14] studied application to the model of Bodner–Partom monotonicity of operators of the viscoplastic response.

In the present paper the author makes a detailed investigation of modelling of continuum damage for application in the elasto-viscoplastic Bodner–Partom

model. In the second part of the paper, which is preceded by an introduction, the detailed description of the model is given. In the third part the author proposes an application of the continuum damage model proposed by LEMAITRE [25] to the elasto-viscoplastic constitutive equations of the Bodner–Partom model. Next section concerns the description of the finite element procedure which was used for the open commercial FE program implementation. The last part gives numerical simulation examples of the creep tests for B1900+Hf alloy.

2. BODNER–PARTOM EQUATIONS

At the beginning it is necessary to assume the isotropic material and strain additivity, where the total strain rate $\dot{\boldsymbol{\varepsilon}}$ is decomposed into the elastic part $\dot{\boldsymbol{\varepsilon}}^E$ and the inelastic part $\dot{\boldsymbol{\varepsilon}}^I$ according to the formula

$$\dot{\boldsymbol{\varepsilon}} = \dot{\boldsymbol{\varepsilon}}^E + \dot{\boldsymbol{\varepsilon}}^I. \tag{2.1}$$

Therefore, the relation between the stress rate $\dot{\boldsymbol{\sigma}}$ and strain rate $\dot{\boldsymbol{\varepsilon}}^E$, for the assumed isotropic material, is defined as:

$$\dot{\boldsymbol{\sigma}} = \mathbf{B}^* : \dot{\boldsymbol{\varepsilon}}^E = (1-D) \cdot \mathbf{B} : \left(\dot{\boldsymbol{\varepsilon}} - \dot{\boldsymbol{\varepsilon}}^I \right), \tag{2.2}$$

where $D \in \langle 0, 1 \rangle$ is the scalar parameter of the isotropic damage and $\mathbf{B}^*$ is the effective tensor of elasticity for the damaged material, which is expressed by the standard elasticity tensor $\mathbf{B}$, reduced by the damage parameter.

Since KACHANOV [19] and RABOTNOV [29] have proposed the concept of effective stress, numerous damage models have been developed (see e.g.: KACHANOV [18] or LEMAITRE [26]). Most of the investigations on continuum damage use a power law for the damage equation evolution. BODNER and CHAN [6] proposed an alternative functional form of the evaluation equation which leads to an exponential equation for damage development:

$$\dot{D} = \frac{h}{H} \cdot \left[\ln \left(\frac{1}{D} \right)^{(h+1)/h} \right] \cdot D \cdot \dot{Q}, \tag{2.3}$$

where h and H are the damage material parameters and Q is the multiaxial stress function obtained from the equation included in [17]:

$$\dot{Q} = \left(\alpha_1 \cdot \sigma^+_{\max} + \alpha_2 \cdot J(\boldsymbol{\sigma}) + \alpha_3 \cdot \operatorname{tr}(\boldsymbol{\sigma})^+ \right)^z, \tag{2.4}$$

where $\sigma^+_{\max}$ and $\operatorname{tr}(\boldsymbol{\sigma})^+$ are the maximum principal tensile stress and the first stress invariant, respectively. Next α_1, α_2, α_3, z are the material constants. It should be noted that the parameters α_1, α_2 and α_3 satisfy the condition $\alpha_1 + \alpha_2 + \alpha_3 = 1.0$.

It is necessary to point out that Bodner and Chan [6], besides of the isotropic damage model, described the procedure considering the directional damage by the load-history dependent softening variables. In this procedure the directional damage is expressed by the second-order symmetric tensor with a scalar effective value.

The inelastic strain rate $\dot{\boldsymbol{\varepsilon}}^I$ in the Bodner–Partom model is calculated according to the equation

$$\dot{\boldsymbol{\varepsilon}}^I = \frac{3}{2} \cdot \dot{p} \cdot \frac{\boldsymbol{\sigma}'}{J(\boldsymbol{\sigma}')}, \tag{2.5}$$

where $\dot{p}$ is the equivalent plastic strain, $\boldsymbol{\sigma}'$ and $J(\boldsymbol{\sigma}') = \sqrt{\frac{3}{2}\left(\boldsymbol{\sigma}' : \boldsymbol{\sigma}'\right)}$ are the deviatoric parts of stress and the stress invariant. It should be noted that in the literature it is possible to find two ways of calculating $\dot{p}$ – the rate of the equivalent plastic strain, which includes the isotropic damage evolution (see e.g. [6] and [7] for details)

$$\dot{p} = \frac{2}{\sqrt{3}} \cdot D_0 \cdot \exp\left[-\frac{1}{2} \cdot \left(\frac{\left(R + \left(\mathbf{X} : \dfrac{\boldsymbol{\sigma}}{J(\boldsymbol{\sigma})}\right)\right) \cdot (1 - D)}{J(\boldsymbol{\sigma}')}\right)^{2 \cdot n} \cdot \frac{n+1}{n}\right], \tag{2.6}$$

or

$$\dot{p} = \frac{2}{\sqrt{3}} \cdot D_0 \cdot \exp\left[-\frac{1}{2} \cdot \left(\frac{\left(R + \left(\mathbf{X} : \dfrac{\boldsymbol{\sigma}}{J(\boldsymbol{\sigma})}\right)\right) \cdot (1 - D)}{J(\boldsymbol{\sigma}')}\right)^{2 \cdot n}\right], \tag{2.7}$$

where the material parameters D_0 and n represent the limiting plastic strain rate and the strain rate sensitivity parameter, respectively. The isotropic hardening R is given as

$$\dot{R} = m_1 \cdot (Z_1 - R) \cdot \left(\boldsymbol{\sigma} : \dot{\boldsymbol{\varepsilon}}^I\right) - A_1 \cdot Z_1 \cdot \left(\frac{R - Z_2}{Z_1}\right)^{r_1}, \tag{2.8}$$

where m_1, A_1, r_1, Z_1 and Z_2 are the material parameters. The material constants m_1, A_1, r_1 are the hardening rate coefficient, recovery coefficient, and recovery exponent for isotropic hardening, respectively. The values Z_1 and Z_2 are the limiting value of isotropic hardening and the fully recovered value of isotropic hardening, respectively.

Subsequently, the kinematic hardening $\mathbf{X}$ is defined as

$$\dot{\mathbf{X}} = m_2 \cdot \left(\frac{3}{2} \cdot Z_3 \cdot \frac{\boldsymbol{\sigma}}{J(\boldsymbol{\sigma})} - \mathbf{X}\right) \cdot \left(\boldsymbol{\sigma} : \dot{\boldsymbol{\varepsilon}}^I\right) - A_2 \cdot Z_1 \cdot \frac{3}{2} \cdot \left[\frac{\frac{2}{3} J(\mathbf{X})}{Z_1}\right]^{r_2} \cdot \frac{\mathbf{X}}{J(\mathbf{X})}, \tag{2.9}$$

where m_2, A_2, r_2, Z_3 are material parameters. The material constants m_2, A_2, r_2 are the hardening rate coefficient, recovery coefficient, recovery exponent for kinematic hardening, respectively, and Z_3 is the limiting value of the kinematic hardening. Additionally, at the beginning of calculations the initial value of the isotropic hardening is assumed as $R(t=0) = Z_0$. It should be noted that the relation $\left(\boldsymbol{\sigma} : \dot{\boldsymbol{\varepsilon}}^I\right)$, used in Eq. (2.8) and Eq. (2.9), is called the plastic work rate.

In this described model the 20 parameters have to be determined; 14 parameters of the base model: E, ν, D_0, n, Z_0, Z_1, Z_2, Z_3, m_1, m_2, A_1, A_2, r_1, r_2, and 6 parameters of damage evolution: h, H, α_1, α_2, α_3, z. In the work [8] BODNER proposed the concept of reduction of the number of parameters, where $Z_0 = Z_2 = Z$, $A_1 = A_2 = A$ and $r_1 = r_2 = r$. According to this assumption 11 parameters of base model have to be determined: E, ν, D_0, n, $Z_0 = Z_2 = Z$, Z_1, Z_3, m_1, m_2, $A_1 = A_2 = A$, $r_1 = r_2 = r$. Detailed description of the identification procedure for the material parameters is described by CHAN *et al.* [11] and WOŹNICA and KŁOSOWSKI [40].

In the work [6], BODNER and CHAN investigated a nickel based super alloy B1900+Hf. For this material the uniaxial creep test results at various temperatures are given. The material constants for Bodner–Partom constitutive equations have been established, see Table 1. It should be noted that the damage evolution, under constant stress conditions (creep tests), was described by the equation:

$$D = \exp\left[-\frac{H}{Q}\right]^h, \tag{2.10}$$

where the stress function Q has the simplified form:

$$Q = t \cdot \sigma^z. \tag{2.11}$$

Table 1. Parameters for Bodner–Partom model for B1900+Hf [6].

	base parameters of the model								
temp. T [°C]	E [MPa]	ν [–]	D_0 [s^{-1}]	n [–]	Z_0 [MPa]	m_1 [MPa^{-1}]	Z_1 [MPa]	A_1 [s^{-1}]	temp. T [°C]
871	141525	0.3	10^4	1.03	2400	0.270	3000	0.0055	871
982	125391	0.3	10^4	0.85	1900	0.270	3000	0.02	982
1093	107539	0.3	10^4	0.70	1200	0.270	3000	0.25	1093
	base parameters of the model						damage parameters		
temp. T [°C]	Z_2 [MPa]	r_1 [–]	m_2 [MPa^{-1}]	Z_3 [MPa]	A_2 [s^{-1}]	r_2 [–]	H [$(MPa)^z \cdot s$]	h [–]	z [–]
871	2400	2.0	1.52	1150	0.0055	2.0	$2 \cdot 10^{27}$	1.0	8.3
982	1900	2.0	1.52	1150	0.02	2.0	$4 \cdot 10^{24}$	1.0	8.3
1093	1200	2.0	1.52	1150	0.25	2.0	$5 \cdot 10^{20}$	1.0	8.3

3. Proposed approach of damage evolution in Bodner–Partom model

The author of the present paper proposed the application of the damage concept described by Lemaitre [25] in the Bodner–Partom model. The damage evolution is specified by the following expression:

$$\dot{D} = \left(\frac{Y}{S}\right)^{s} \cdot \dot{p}, \tag{3.1}$$

where the variables s, S are the damage material parameters and $\dot{p}$ is the rate of the equivalent plastic strain assumed according to Eqs. (2.6) or (2.7). The function Y, used in Eq. (3.1), is specified by the Young's modulus E, Poisson's ratio ν, the current values of damage D, the Huber–Mises equivalent stress σ_{eq} and the hydrostatic stress σ_H, and is called the damage strain energy release rate. It is expressed by the equation

$$Y = \frac{\sigma_{eq}^2}{2 \cdot (1-D)^2 \cdot E} \cdot \left(\frac{2}{3} \cdot (1+\nu) + 3 \cdot (1-2\cdot\nu) \cdot \left(\frac{\sigma_H}{\sigma_{eq}}\right)^2\right). \tag{3.2}$$

The function of the energy density Y, in above equation, in the case of uniaxial stress state can be rewritten as

$$Y = \frac{\sigma^2}{2 \cdot (1-D)^2 \cdot E}. \tag{3.3}$$

The proposal of Lemaitre damage evolution is not the only one which can be found in the literature (see e.g.: Tai [36], Wang [38], Chandrakanth [12] and [13], Dhar [15], Bonora [9], Xiao [41], Życzkowski [43]), where the authors propose alternative versions of the Eq. (3.1).

The damage model proposed by Lemaitre [25] is successfully applied to the Chaboche model [10], see e.g.: Amar and Dufailly [1]. It should be noted that the Chaboche model is an extension of the Perzyna law [28], based on the orthogonal condition in the plastic law, which requires an established yield criterion. On the other hand in the Bodner–Partom model the existence is assumed of the inelastic deformation from the beginning of the deformation process, without references to the yield limit.

Identification of the values of damage material parameters s and S is based on the concept proposed by Amar and Dufailly [1]. The present author also investigates the identification and validation of the damage parameters for the Lemaitre model, described in the paper [3]. Referring to paper [1], the value of the parameter s is chosen arbitrarily; only the factor S has to be determined. It should be noted that only the parameter S is accepted as temperature-dependent.

At the beginning of the identification process, the numerical simulation of the uniaxial tensile tests were performed on the basis on the known material parameters (see Table 1) for the Bodner–Partom model with damage. From the numerical simulation the rupture time t_r was defined. Then we can make the following transformation of the Eq. (3.1):

$$\dot{D} \cdot (1-D)^{2\cdot s} = \left(\frac{\sigma^2}{2\cdot E\cdot S}\right)^s \cdot \dot{p},$$

$$\int_0^1 (1-D)^{2\cdot s}\, dD = \frac{1}{2\cdot s+1} = \int_0^{t_r} \left(\frac{\sigma^2}{2\cdot E\cdot S}\right)^s \cdot \dot{p}\, dt \tag{3.4}$$

which leads to the specified value of the parameter S:

$$S = \frac{(2\cdot s+1)^{1/s}}{2\cdot E} \cdot \left(\int_0^{t_r} \left(\sigma^{2\cdot s}\cdot \dot{p}\right)\, dt\right)^{1/s}. \tag{3.5}$$

In this variant of identification, the value of the parameter $s = 3.0\,[-]$ is predetermined. According to the assumed procedure, the following damage parameters for the investigated superalloy B1900+Hf are specified and given in Table 2. The basic parameters for Bodner–Partom model are known and have been collected in Table 1. The detailed identification procedure of the damage parameters s and S, for the Lemaitre model of damage evolution, is described by the author in the paper [3].

Table 2. Damage parameters of the Bodner–Partom model for B1900+Hf.

temp. $T\,[^\circ\mathrm{C}]$	S [MPa]	s [–]
871	0.900	3.0
982	0.275	3.0
1093	0.023	3.0

In practical applications it is necessary to specify the value of the critical damage D_c, which indicates the limit of the theory. It should be noted that this factor must be lower than 1.0. It usually lies between 0.2 and 0.8, depending on the type of material [25].

It is worth pointing out that in the proposed approach, the damage parameter has the additive character. It is dependent on the rate of the equivalent plastic strain, see Eq. (3.1), when in the concept proposed by Bodner and Chan the damage is directly calculated as a function of time and stresses, see Eq. (2.10). However, both concepts belong to the group of the isotropic continuum damage models.

4. Description of applied program and procedure

In the numerical analysis the MSC.Marc system was used. To apply the Bodner-Partom model to the MSC.Marc system the user-defined subroutines UVSCPL [37] are applied. The fundamental part of the algorithm used in the implementation of UVSCPL subroutines is presented in Figs. 1 and 2 in the form of flow charts. Early this subroutine was used successfully by the author for implementation of the Chaboche model with damage [4] and for the introduced Bodner–Partom model without damage (see e.g.: [2] and [5]).

$$[\text{step 1}] \rightarrow \left[\begin{array}{ll} \Delta\mathbf{X} = \dfrac{\Delta t}{2}\cdot\left(\dot{\mathbf{X}}_{j-1}+\dot{\mathbf{X}}_{j}\right), & \mathbf{X}_j = \mathbf{X}_{j-1}+\Delta\mathbf{X} \\ \Delta R = \dfrac{\Delta t}{2}\cdot\left(\dot{R}_{j-1}+\dot{R}_{j}\right), & R_j = R_{j-1}+\Delta R \end{array}\right]$$

$$[\text{step 2}] \rightarrow [\boldsymbol{\sigma'}_j j,\ J(\boldsymbol{\sigma'}_j j),\ J(\boldsymbol{\sigma'}_j),\ J(\mathbf{X}_j)]$$

$$[\text{step 3}] \rightarrow D_j = \exp\cdot\left[-\frac{H}{(t\cdot\sigma^z)}\right]^h$$

$$[\text{step 4}] \rightarrow \left[\dot{p}_j = \frac{2}{\sqrt{3}}\cdot D_0\cdot\exp\left[-\frac{1}{2}\cdot\left(\frac{\left(R+\left(\mathbf{X}_j:\dfrac{\boldsymbol{\sigma}_j}{J(\boldsymbol{\sigma}_j)}\right)\right)\cdot(1-D_j)}{J\left(\boldsymbol{\sigma}'_j\right)}\right)^{2\cdot n}\cdot\frac{n+1}{n}\right]\right]$$

$$[\text{step 5}] \rightarrow \left[\dot{\boldsymbol{\varepsilon}}^I_j = \frac{3}{2}\cdot\dot{p}_j\cdot\frac{\boldsymbol{\sigma'}_j}{J(\boldsymbol{\sigma'}_j)}\right]$$

$$[\text{step 6}] \rightarrow \left[\dot{W}^I_j = \boldsymbol{\sigma}_j:\dot{\boldsymbol{\varepsilon}}^I_j\right]$$

$$[\text{step 7}] \rightarrow \left[\dot{\mathbf{X}}_j = m_2\cdot\left(\frac{3}{2}\cdot Z_3\cdot\frac{\boldsymbol{\sigma}_j}{J(\boldsymbol{\sigma}_j)}-\mathbf{X}_j\right)\cdot\dot{W}^I_j - A_2\cdot Z_1\cdot\frac{3}{2}\cdot\left(\frac{\frac{2}{3}\cdot J(\mathbf{X}_j)}{Z_1}\right)^{r_2}\cdot\frac{\mathbf{X}_j}{J(\mathbf{X}_j)}\right]$$

$$[\text{step 8}] \rightarrow \left[\dot{R}_j = m_1\cdot(Z_1-R_j)\cdot\dot{W}^I_j - A_1\cdot Z_1\cdot\left(\frac{R_j-Z_2}{Z_1}\right)^{r_1}\right]$$

$$[\text{step 9}] \rightarrow \left[\Delta\boldsymbol{\varepsilon}^I_j = \dot{\boldsymbol{\varepsilon}}^I_j\cdot\Delta t_j\right]$$

$$[\text{step 10}] \rightarrow \left[\Delta\boldsymbol{\sigma}_j = (1-D_j)\cdot\mathbf{B}\cdot\left(\Delta\boldsymbol{\varepsilon}_j-\Delta\boldsymbol{\varepsilon}^I_j\right)\right]$$

Fig. 1. Flow chart of the UVSCPL subroutine with the damage model proposed by Bodner and Chan.

$$[\text{step 1}] \rightarrow \left[\begin{array}{ll} \Delta \mathbf{X} = \dfrac{\Delta t}{2} \cdot \left(\dot{\mathbf{X}}_{j-1} + \dot{\mathbf{X}}_j \right), & \mathbf{X}_j = \mathbf{X}_{j-1} + \Delta \mathbf{X} \\ \Delta R = \dfrac{\Delta t}{2} \cdot \left(\dot{R}_{j-1} + \dot{R}_j \right), & R_j = R_{j-1} + \Delta R \\ \Delta D = \dfrac{\Delta t}{2} \cdot \left(\dot{D}_{j-1} + \dot{D}_j \right), & D_j = D_{j-1} + \Delta D \end{array} \right]$$

$$[\text{step 2}] \rightarrow \left[\boldsymbol{\sigma}'_j,\ J\left(\boldsymbol{\sigma}'_j \right),\ J\left(\boldsymbol{\sigma}_j \right),\ J\left(\mathbf{X}_j \right) \right]$$

$$[\text{step 3}] \rightarrow \left[\dot{p}_j = \frac{2}{\sqrt{3}} \cdot D_0 \cdot \exp \left[-\frac{1}{2} \cdot \left(\frac{\left(R_j + \left(\mathbf{X}_j : \dfrac{\boldsymbol{\sigma}_j}{J\left(\boldsymbol{\sigma}_j \right)} \right) \right) \cdot \left(1 - D_j \right)}{J\left(\boldsymbol{\sigma}'_j \right)} \right)^{2 \cdot n} \cdot \frac{n+1}{n} \right] \right]$$

$$[\text{step 4}] \rightarrow \left[\dot{\boldsymbol{\varepsilon}}^I_j = \frac{3}{2} \cdot \dot{p}_j \cdot \frac{\boldsymbol{\sigma}'_j}{J\left(\boldsymbol{\sigma}'_j \right)} \right]$$

$$[\text{step 5}] \rightarrow \left[\dot{W}^I_j = \boldsymbol{\sigma}_j : \dot{\boldsymbol{\varepsilon}}^I_j \right]$$

$$[\text{step 6}] \rightarrow \left[\dot{\mathbf{X}}_j = m_2 \cdot \left(\frac{3}{2} \cdot Z_3 \cdot \frac{\boldsymbol{\sigma}_j}{J\left(\boldsymbol{\sigma}_j \right)} - \mathbf{X}_j \right) \cdot \dot{W}^I_j - A_2 \cdot Z_1 \cdot \frac{3}{2} \cdot \left(\frac{\dfrac{2}{3} \cdot J\left(\mathbf{X}_j \right)}{Z_1} \right)^{r_2} \cdot \frac{\mathbf{X}_j}{J\left(\mathbf{X}_j \right)} \right]$$

$$[\text{step 7}] \rightarrow \left[\dot{R}_j = m_1 \cdot \left(Z_1 - R_j \right) \cdot \dot{W}^I_j - A_1 \cdot Z_1 \cdot \left(\frac{R_j - Z_2}{Z_1} \right)^{r_1} \right]$$

$$[\text{step 8}] \rightarrow Y_j = \frac{\sigma^2_{eq}}{2 \cdot \left(1 - D_j \right)^2 \cdot E} \cdot \left(\frac{2}{3} \cdot \left(1 + \nu \right) + 3 \cdot \left(1 - 2 \cdot \nu \right) \cdot \left(\frac{\sigma_H}{\sigma_{eq}} \right)^2 \right)$$

$$[\text{step 9}] \rightarrow \dot{D}_j = \left(\frac{Y}{S} \right)^s \cdot \dot{p}_j$$

$$[\text{step 10}] \rightarrow \left[\Delta \boldsymbol{\varepsilon}^I_j = \dot{\boldsymbol{\varepsilon}}^I_j \cdot \Delta t_j \right]$$

$$[\text{step 11}] \rightarrow \left[\Delta \boldsymbol{\sigma}_j = \left(1 - D_j \right) \cdot \mathbf{B} \cdot \left(\Delta \boldsymbol{\varepsilon}_j - \Delta \boldsymbol{\varepsilon}^I_j \right) \right]$$

FIG. 2. Flow chart of the UVSCPL subroutine with the proposed damage evolution in the Bodner–Partom model.

5. Numerical simulation of creep tests for B1900+Hf alloy

In the paper two concepts of the damage evolution in the Bodner–Partom model are described. Numerical simulations of strain-time relations based on the constitutive equations with the damage models are performed for the nickel-based superalloy B1900+Hf. The results of numerical simulations obtained from the procedure described by Bodner and Chan (see Fig. 1, B–P v1) are compared with the proposed procedure (see Fig. 2, B–P v2).

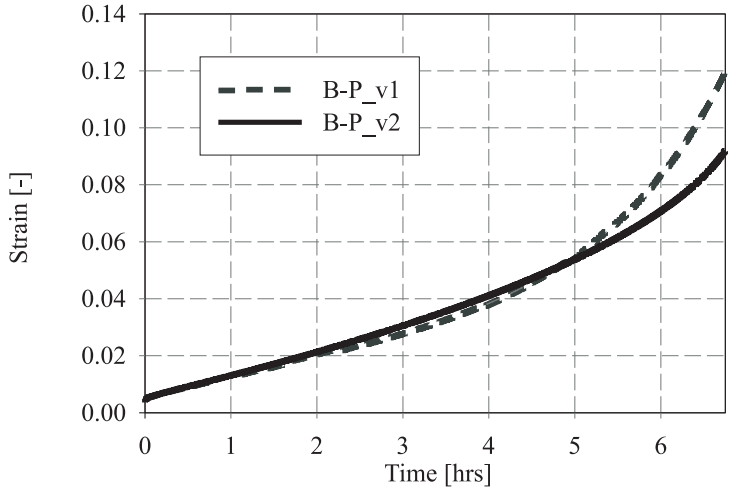

Fig. 3. Creep curves for B1900+Hf at 871° C, $\sigma = 517$ [MPa] = const.

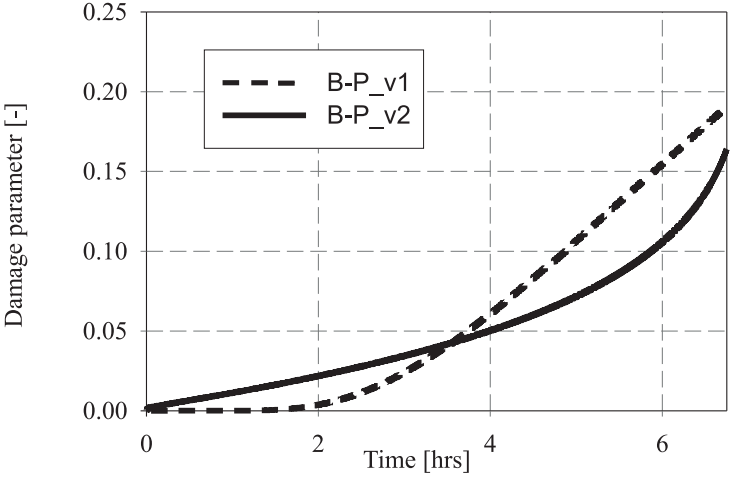

Fig. 4. Damage parameter evolution for B1900+Hf at 871° C, $\sigma = 517$ [MPa] = const.

Like in the paper [6], the numerical simulations of the uniaxial creep tests at various temperatures (see Fig. 3, Fig. 5, Fig. 7) were carried out. Additionally the damage evolution parameters for these variants of simulation are given in Fig. 4, Fig. 6 and Fig. 8. The strain-time functions obtained from the two investigated damage models gave similar results (very small differences can be observed only) in the considered range of time. The functions of the damage evolution (see Fig. 4, Fig. 8 and Fig. 6) also gave small differences.

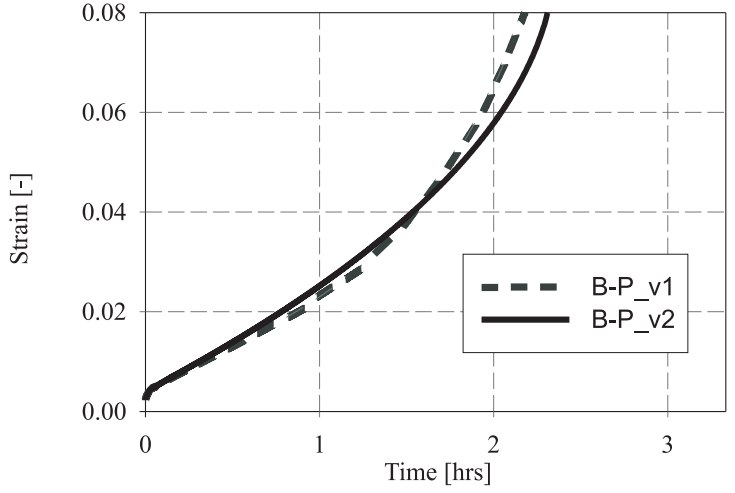

FIG. 5. Creep curves for B1900+Hf at 982° C, $\sigma = 283$ [MPa] = const.

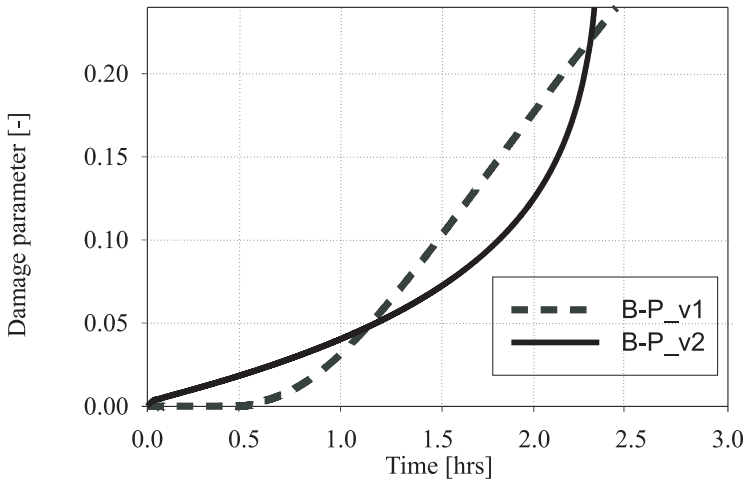

FIG. 6. Damage parameter evolution for B1900+Hf at 982° C, $\sigma = 283$ [MPa] = const.

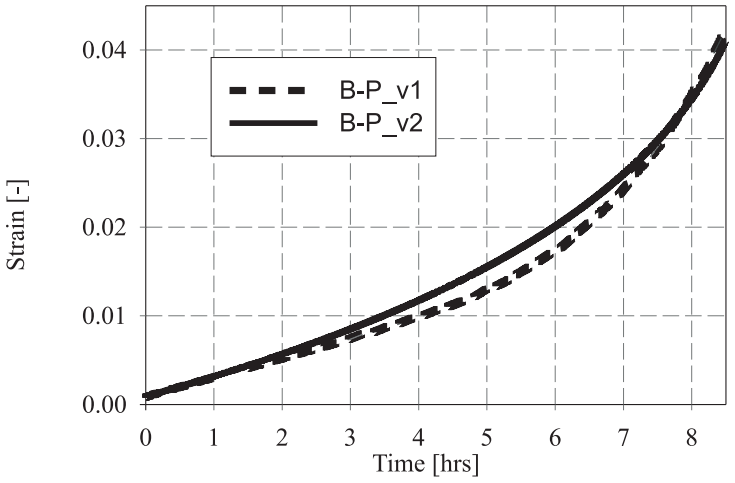

FIG. 7. Creep curves for B1900+Hf at 1093° C, $\sigma = 79.5$ [MPa] = const.

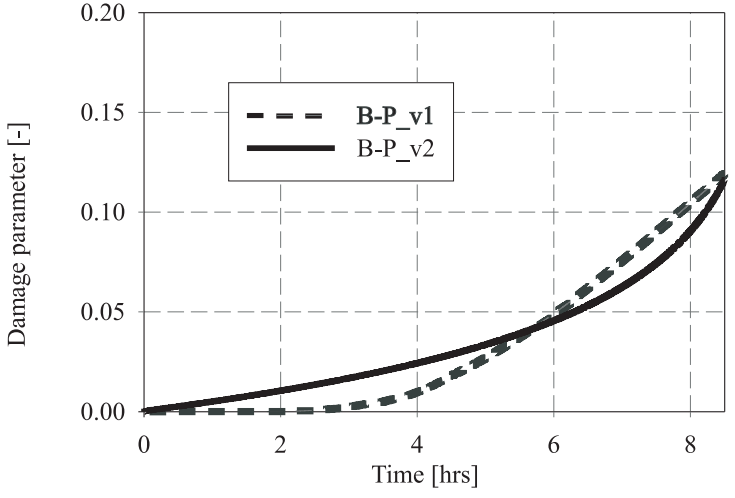

FIG. 8. Damage parameter evolution for B1900+Hf at 1093° C, $\sigma = 79.3$ [MPa] = const.

6. Concluding remarks

A new approach is proposed to the problem of continuum damage modelling for application in elasto-viscoplastic Bodner–Partom constitutive equations. The proposed method combines the damage model developed by Lemaitre and the Bodner–Partom model. The results obtained in numerical simulations of creep tests for B1900+Hf confirms the validity of the approach. Moreover, the obtained results encourage the author to continue the outlined research based on

broader experimental data. Such experiment can provide a perspective of application of other types of damage evolution equation to various elasto-viscoplastic constitutive models.

Acknowledgments

The research was performed as part of the Polish-French cooperation program Polonium 2005 (KBN 5598.II/2004/2005) and the Polish-German cooperation program (KBN/DAAD 2004/2005 no. 09).

Calculations presented in the paper have been performed at the Academic Computer Centre in Gdańsk (TASK).

The study was supported by the European Community under the FP5 Programme, key-action "City of Tomorrow and Cultural Heritage" (Contract No. EVK4-CT-2002-80005). This support is greatly acknowledged.

References

1. Amar G., Dufailly J, *Identification of viscoplastic and damage constitutive equations*, European Journal of Mechanics, **2**, 197–218, 1985.
2. Ambroziak A., *Application of elasto-viscoplastic Bodner-Partom constitutive equations in finite element analysis*, Computer Assisted Mechanics and Engineering Sciences (accepted).
3. Ambroziak A., *Identification and validation of damage parameters for elasto-viscoplastic Chaboche model*, Engineering Transactions, **55**, 1, 1–26, 2006.
4. Ambroziak A., *Numerical modelling of elasto-viscoplastic Chaboche constitutive equations using MSC.Marc*, Task Quarterly, **2**, 167–178, 2005.
5. Ambroziak A., *Viscoplastic analysis of damped vibrations of circular plate,* [in:] *Shell Structures: Theory and applications*, W. Pietraszkiewicz, C. Szymczak [Eds.], Taylor and Francis Group, (Balkema – Proceedings and Monographs in Engineering, Water and Earth Sciences), 445–449, 2005.
6. Bodner S.R., Chan K.S., *Modelling of continuum damage for application in elastic-viscoplastic constitutive equations*, Engineering Fracture Mechanics, **25**, 705–712, 1986.
7. Bodner S.R., Partom Y., *Constitutive equations for elastic-viscoplastic strain-hardening materials*, Journal of Applied Mechanics, ASME, **42**, 385–389, 1975.
8. Bodner S.R., *Review of a unified elastic-viscoplastic theory*, Unified Constitutive Equations for Creep and Plasticity, K. Miller [Ed.], Elsewier, 273–301, 1987.
9. Bonora N., *A nonlinear CDM model for ductile failure*, Engineering Fracture Mechanics, **58**, 11–28, 1997.
10. Chaboche J.–L., *Constitutive equations for cyclic plasticity and cyclic viscoplasticity*, International Journal of Plasticity, **5**, 247–302, 1989.

11. Chan K.S., Bodner S.R., Lindholm U.S., *Phenomenological modelling of hardening and thermal recovery in metals*, Journal of Engineering Material and Technology, **110**, 1–8, 1988.

12. Chandrakanth S. and Pandey P.C., *An exponential ductile continuum damage model for metals*, International Journal of Fracture, **72**, 293–310, 1995.

13. Chandrakanth S. and Pandey P.C., *An isotropic damage model for ductile materials*, Engineering Fracture Mechanics, **50**, 457–465, 1995.

14. Chełmiński, K., Gwiazda, P., *Monotonicity of operators of viscoplastic response: Application to the model of Bodner-Partom*, **3**, 191–208, 1999.

15. Dhar S, Sethuraman R. and Dixit P.M., *A continuum damage mechanics model for void growth and micro-crack initiation*, Engineering Fracture Mechanics, **53**, 917–928, 1996.

16. Frank G.J., Brockman R.A., *A viscoelastic-viscoplastic constitutive model for glassy polymerst*, International Journal of Solids and Structures, **38**, 5149–5164, 2001.

17. Hayhurst D.R., *Creep rupture under multi-axial state of stress*, Journal of Mechanical Physical Solids, **20**, 381–390, 1972.

18. Kachanov L.M., *Introduction to continuum damage mechanics*, Martinus Nijhoff Publishers, Dordecht, 1986.

19. Kachanov L.M., *Time of rupture process under creep conditions*, TVZ Akad. Nauk. S.S.R. Otd. Tech. Nauk., **8**, 26–31, 1958.

20. Kłosowski P., *Nonlinear numerical analysis and experiments on vibrations of elasto-viscoplastic plates and shells* [in Polish], Politechnika Gdańska, Gdańsk 1999.

21. Kłosowski P., Weichert D., Woznica K., *Dynamic of elasto-viscoplastic plates and shells*, Archive of Applied Mechanics, **5**, 326–345, 1995.

22. Kłosowski P., Woźnica K., *Numerical treatment of elasto viscoplastic shells in the range of moderate and large rotations*, Computational Mechanics, **34**, 194–212, 2004.

23. Kłosowski P., Woźnica K., Weichert D., *Comparison of numerical modelling and experiments for the dynamic response of circular elasto-viscoplastic plates*, European Journal of Mechanics A/Solid, **19**, 343–359, 2000.

24. Kłosowski P., Zagubień A., Woźnica K., *Investigation on rheological properties of technical fabric Panama*, Archive of Applied Mechanics, **9–10**, 661–681, 2004.

25. Lemaitre J., *A continuous damage mechanics. Model for ductile fracture,* Journal of Engineering Materials and Technology, **107**, 83–89, 1985.

26. Lemaitre J., *A course on damage mechanics*, Springer-Verlag, New York 1992.

27. Miller A.K. [Ed.], *Unified constitutive equations for creep and plasticity*, Elsevier Applied Science, London 1987.

28. Perzyna P., *Fundamental problems in viscoplasticity*, Advances in Mechanics, **9**, 243–377, 1966.

29. Rabotnov Y.N., *Creep problems of structural members*, North–Holland, Amsterdam 1969.

30. Sansour C., Kollmann F.G., *Large viscoplastic deformations of shells. Theory and finite formulation*, Computational Mechanics, **6**, 512–525, 1998.

31. Sansour C., Wagner W., *A model of finite strain viscoplasticity based on unified constitutive equations. Theoretical and computational considerations with applications to shell*, Computer Methods in Applied Mechanics and Engineering, **191**, 423–450, 2001.

32. Sansour C., Wagner W., *Viscoplasticity based on additive decomposition of logarithmic strain and unified constitutive equations. Theoretical and computational considerations with reference to shell applications*, Composite Structures, **81**, 1583–1594, 2003.

33. Steck E.A., *A stochastic model for the high-temperature plasticity of metals*, International Journal of Plasticity, **1**, 243–258, 1985.

34. Stoffel M., *An experimental method to validate viscoplastic constitutive equations in the dynamic response of plates*, Mechanics of Materials, **37**, 1210–1222, 2005.

35. Stoffel M., *Nichtlineare Dynamik von Platten*, der Rheinisch-Westfälischen Technischen Hochschule Aachen, Aachen, 2000.

36. Tai W.H. and Yang B.X., *A new microvoid-damage model for ductile fracture*, Engineering Fracture Mechanics, **25**, 377–384, 1986.

37. Users handbook: *MSC.MARC Volume B: Element library* and *MSC.MARC Volume D: User subroutines and special routines, Version 2003*, MSC.Software Corporation 2003.

38. Wang T.-J., *Prediction of sheet forming limits using a new continuum damage mechanics criterion for ductile fracture*, Engineering Fracture Mechanics, **51**, 275–279, 1995.

39. Woźnica K., *Dynamique des structures elasto-viscoplastique*, Cahiers de Mechanique, Lille, 1998.

40. Woźnica K., Kłosowski P., *Evaluation of viscoplastic parameters and its application for dynamic behaviour of plates*, Archive of Applied Mechanics, **70**, 561–570, 2000.

41. Xiao Y.C., Li S. and Gao Z., *A continuum damage mechanics model for high cycle fatigue*, International Journal of Fatigue, **20**, 503–508, 1998.

42. Zaïri F., Woźnica K., Naït-Abdelaziz M., *Phenomenological nonlinear modelling of glassy polymers*, Compites Rendus Mecanique, **333**, 359–364, 2005.

43. Życzkowski M., *Creep damage evolution equations expressed in terms of dissipated power*, International Journal of Mechanical Science, **42**, 755–769, 2000.

Received July 18, 2005; revised version March 27, 2006.

ENGINEERING TRANSACTIONS • *Engng. Trans.* • **55**, 2, 129–153, 2007
Polish Academy of Sciences • Institute of Fundamental Technological Research

WAVE POLYNOMIALS IN ELASTICITY PROBLEMS

A. M a c i ą g

Department of Mathematics
Faculty of Management and Computer Modelling
Kielce University of Technology
Al. 1000–lecia P.P. 7, Poland
e-mail: matam@tu.kielce.pl

The paper demonstrates a new technique of obtaining the approximate solution of the two- and three-dimensional elasticity problems. The system of equations of elasticity can be converted to the system of wave equation. In this case, as solving functions (Trefftz functions), the so-called wave polynomials can be used. The presented method is useful for a finite body of a certain shape. Then the obtained solutions are coupled through initial and boundary conditions. Recurrent formulas for the two- and three-dimensional wave polynomials and their derivatives are obtained. The methodology for solution of systems of partial differential equations with common initial and boundary conditions by means of solving functions is presented. The advantage of using the method of solving functions is that the solution exactly satisfies the given equation (or system of equations). Some examples are included.

Key words: elasticity, Trefftz method, wave equation, wave polynomials.

1. Introduction

The method of solving functions applied for linear partial differential equations has been developed recently. The key idea of the method is to determine functions (polynomials) satisfying a given differential equation and fitted to the governing initial and boundary conditions. In this sense it is a variant of the Trefftz method [1, 2].

The method was first described in the paper [3] where it was applied to one-dimensional heat conduction problems. Heat polynomials were used for solving unsteady heat conduction problems in [4]. The method is continued in the Cartesian coordinate system in [5, 6], describing heat polynomials for the two- and three-dimensional case. Application of heat polynomials in polar and cylindrical coordinates is shown in the papers [7–9]. Application of this method to inverse heat-conduction problems is described in [5–11]. Reference [12] contains the highly interesting idea of using heat polynomials as a new type of finite-element base functions.

The work [13] deals with numerous cases involving other differential equations such as the Laplace, Poisson, Helmholtz and one-dimensional wave equations. Dimensionless wave polynomials for solving the two-dimensional wave equation are presented in [14, 15] and three-dimensional wave equation in [16, 17]. The wave functions can be obtained by using symbolic operations (for example in Maple or Mathematica) or inverse operations. These techniques are described correspondingly in [19, 20] and [21, 22]. Basically a linear differential equations (or system of equations) can be solved by means of various methods. Some of them are better for infinite bodies and others are suitable for finite bodies but of simple shape. The method presented here is useful for finite bodies but the shape of the body can be more complicated.

In Sec. 2 two- and three-dimensional wave polynomials and their properties in the Cartesian coordinate system are considered. Section 3 contains equations of elasticity. The method applied for a system of equations is presented in Sec. 4. In Sec. 5 some examples are discussed. Concluding remarks are given in Sec. 6.

2. Wave polynomials

The elasticity problems will be solved by means of wave polynomials. The papers [14, 16] show the way to obtain two- and three-dimensional wave equation for dimensionless wave equation. In engineering practice it is often convenient to use the dimensional wave equation. Analogously to the papers mentioned above, the dimensional wave polynomials can be obtained. There are two methods to obtain the wave polynomials. The first one is using a "generating function". The second one (giving the error estimator) is the expansion of the function satisfying the wave equation in Taylor series. Both methods lead to equivalent wave polynomials.

2.1. Two-dimensional wave polynomials

2.1.1. Generating function. Let us consider the wave equation

$$\frac{1}{v^2}\frac{\partial^2 w}{\partial t^2} = \frac{\partial^2 w}{\partial x^2} + \frac{\partial^2 w}{\partial y^2}. \tag{2.1}$$

By using the separating variables method, we get a function called a generating function for wave polynomials

$$g = \mathrm{e}^{\mathrm{i}(ax+by+cvt)} \tag{2.2}$$

satisfying Eq. (2.1) when $c^2 = a^2 + b^2$. The power series expansion for (2.2) is

$$\mathrm{e}^{\mathrm{i}(ax+by+cvt)} = \sum_{n=0}^{\infty}\sum_{k=0}^{n}\sum_{l=0}^{n-k} S_{(n-k-l)kl}(x,y,t)a^{n-k-l}b^k c^l, \tag{2.3}$$

where $S_{(n-k-l)kl}(x,y,t)$ are polynomials of variables x, y, t containing v.

Substituting $c^2 = a^2 + b^2$ in (2.3), we obtain

$$\mathrm{e}^{\mathrm{i}(ax+by+ct)} = \sum_{n=0}^{\infty}\sum_{k=0}^{n}\sum_{\substack{l=0\\ l<2}}^{n-k} R_{(n-k-l)kl}(x,y,t)a^{n-k-l}b^k c^l. \tag{2.4}$$

The real and imaginary parts of polynomials R satisfy Eq. (2.1) and are called wave polynomials:

$$\begin{aligned} P_{(n-k-l)kl}(x,y,t) &= \Re(R_{(n-k-l)kl}(x,y,t)),\\ Q_{(n-k-l)kl}(x,y,t) &= \Im(R_{(n-k-l)kl}(x,y,t)), \end{aligned} \tag{2.5}$$

e.g.

$$\begin{aligned} &P_{000}(x,y,t) = 1, && Q_{000}(x,y,t) = 0,\\ &P_{100}(x,y,t) = 0, && Q_{100}(x,y,t) = x,\\ &P_{010}(x,y,t) = 0, && Q_{010}(x,y,t) = y,\\ &P_{001}(x,y,t) = 0, && Q_{001}(x,y,t) = vt,\\ &P_{200}(x,y,t) = -\frac{x^2}{2} - \frac{v^2t^2}{2}, && Q_{200}(x,y,t) = 0,\\ &P_{110}(x,y,t) = -xy, && Q_{110}(x,y,t) = 0,\\ &P_{101}(x,y,t) = -vxt, && Q_{101}(x,y,t) = 0,\\ &P_{011}(x,y,t) = -vyt, && Q_{011}(x,y,t) = 0,\\ &P_{020}(x,y,t) = -\frac{y^2}{2} - \frac{v^2t^2}{2}, && Q_{020}(x,y,t) = 0, \quad \ldots \end{aligned} \tag{2.6}$$

Notice that here R_{002} does not appear, because $l < 2$ (see Eq. (2.4)).

2.1.2. Partial derivatives of wave polynomials. To obtain the recurrent formulas of partial derivatives for wave polynomials we follow analogously as in [14]. Because function (2.4) is analytical, the Taylor series on the right-hand side of (2.4) is convergent. Therefore we can differentiate consecutive terms

$$\frac{\partial g}{\partial x} = \mathrm{i}ag = \sum_{n=0}^{\infty}\sum_{k=0}^{n}\sum_{\substack{l=0\\ l<2}}^{n-k} \frac{\partial R_{(n-k-l)kl}}{\partial x} a^{n-k-l}b^k c^l,$$

hence

$$\sum_{n=0}^{\infty}\sum_{k=0}^{n}\sum_{\substack{l=0\\ l<2}}^{n-k} \mathrm{i}R_{(n-k-l)kl}a^{n-k-l+1}b^k c^l = \sum_{n=0}^{\infty}\sum_{k=0}^{n}\sum_{\substack{l=0\\ l<2}}^{n-k} \frac{\partial R_{(n-k-l)kl}}{\partial x} a^{n-k-l}b^k c^l,$$

and

$$\frac{\partial R_{(n-k-l)kl}}{\partial x} = \mathrm{i}R_{(n-k-l-1)kl},$$

so that finally

$$\begin{aligned} \frac{\partial P_{(n-k-l)kl}}{\partial x} &= -Q_{(n-k-l-1)kl}, \\ \frac{\partial Q_{(n-k-l)kl}}{\partial x} &= P_{(n-k-l-1)kl}. \end{aligned} \tag{2.7}$$

Similarly we get

$$\begin{aligned} \frac{\partial P_{(n-k-l)kl}}{\partial y} &= -Q_{(n-k-l)(k-1)l}, \\ \frac{\partial Q_{(n-k-l)kl}}{\partial y} &= P_{(n-k-l)(k-1)l}, \end{aligned} \tag{2.8}$$

and

$$\begin{aligned} \frac{\partial P_{(n-k)k0}}{\partial t} &= -vQ_{(n-k-2)k1} - vQ_{(n-k)(k-2)1}, \\ \frac{\partial P_{(n-k-1)k1}}{\partial t} &= -vQ_{(n-k-1)k0}, \\ \frac{\partial Q_{(n-k)k0}}{\partial t} &= vP_{(n-k-2)k1} + vP_{(n-k)(k-2)1}, \\ \frac{\partial Q_{(n-k-1)k1}}{\partial t} &= vP_{(n-k-1)k0}. \end{aligned} \tag{2.9}$$

The starting values for the derivatives (2.7), (2.8) and (2.9) are obtained either from (2.6) or directly by putting zero instead of the polynomial, in which any of its subscripts takes a negative value.

2.1.3. Recurrent formulas for wave polynomials. In numerical practice the recurrent formulas are very useful. Theorem 1 enables us to obtain the two-dimensional wave polynomials.

THEOREM 1: *Let* $P_{000} = 1$, $Q_{000} = 0$ *and* $P_{(n-k-l)kl} = Q_{(n-k-l)kl} = 0$ *when any subscript is negative. Then, the polynomials*

$$\begin{aligned} P_{(n-k)k0} = \frac{1}{n}(&-xQ_{(n-k-1)k0} - yQ_{(n-k)(k-1)0} \\ &- vtQ_{(n-k-2)k1} - vtQ_{(n-k)(k-2)1}), \end{aligned} \tag{2.10}$$

$$P_{(n-k-1)k1} = \frac{1}{n}(-xQ_{(n-k-2)k1} - yQ_{(n-k-1)(k-1)1} - vtQ_{(n-k-1)k0}), \tag{2.11}$$

$$Q_{(n-k)k0} = \frac{1}{n}(xP_{(n-k-1)k0} + yP_{(n-k)(k-1)0} + vtP_{(n-k-2)k1} + vtP_{(n-k)(k-2)1}), \tag{2.12}$$

$$Q_{(n-k-1)k1} = \frac{1}{n}(xP_{(n-k-2)k1} + yP_{(n-k-1)(k-1)1} + vtP_{(n-k-1)k0}), \tag{2.13}$$

satisfy the wave equation (2.1).

P r o o f. For relation (2.10) we assume that all polynomials on the right-hand side either satisfy Eq. (2.1) or equal zero. Substituting (2.10) in (2.1) we get

$$x\left(\underbrace{\frac{1}{v^2}\frac{\partial^2 Q_{(n-k-1)k0}}{\partial t^2} - \frac{\partial^2 Q_{(n-k-1)k0}}{\partial x^2} - \frac{\partial^2 Q_{(n-k-1)k0}}{\partial y^2}}_{=0}\right)$$

$$+ y\left(\underbrace{\frac{1}{v^2}\frac{\partial^2 Q_{(n-k)(k-1)0}}{\partial t^2} - \frac{\partial^2 Q_{(n-k)(k-1)0}}{\partial x^2} - \frac{\partial^2 Q_{(n-k)(k-1)0}}{\partial y^2}}_{=0}\right)$$

$$+ vt\left(\underbrace{\frac{1}{v^2}\frac{\partial^2 Q_{(n-k-2)k1}}{\partial t^2} - \frac{\partial^2 Q_{(n-k-2)k1}}{\partial x^2} - \frac{\partial^2 Q_{(n-k-2)k1}}{\partial y^2}}_{=0}\right)$$

$$+ vt\left(\underbrace{\frac{1}{v^2}\frac{\partial^2 Q_{(n-k)(k-2)1}}{\partial t^2} - \frac{\partial^2 Q_{(n-k)(k-2)1}}{\partial x^2} - \frac{\partial^2 Q_{(n-k)(k-2)1}}{\partial y^2}}_{=0}\right)$$

$$+ \frac{2}{v}\left(\frac{\partial Q_{(n-k-2)k1}}{\partial t} + \frac{\partial Q_{(n-k)(k-2)1}}{\partial t}\right) = 2\frac{\partial Q_{(n-k-1)k0}}{\partial x} + 2\frac{\partial Q_{(n-k)(k-1)0}}{\partial y},$$

hence

$$\frac{\partial Q_{(n-k-2)k1}}{\partial t} + \frac{\partial Q_{(n-k)(k-2)1}}{\partial t} = v\left(\frac{\partial Q_{(n-k-1)k0}}{\partial x} + \frac{\partial Q_{(n-k)(k-1)0}}{\partial y}\right)$$

and according to (2.7), (2.8) and (2.9), we obtain

$$vP_{(n-k-2)k0} + vP_{(n-k)(k-2)0} = v(P_{(n-k-2)k0} + P_{(n-k)(k-2)0}).$$

□

This proves the theorem. The proof for (2.11), (2.12), and (2.13) is similar.

Starting values of the polynomials (2.10)–(2.13) can be obtained either from (2.6) or directly by putting zero instead of the polynomial in which any of its subscripts takes a negative value.

2.1.4. Expansion of the function satisfying wave equation in Taylor series. Another way to obtain the wave polynomials is to expand the function satisfying the wave equation in Taylor series. Similarly as for other equations [13] and for dimensionless wave equation [14], the wave polynomials can be obtained by means of Taylor series for the function w. Let the function $w(x, y, t)$ satisfy the wave equation (2.1). We assume that $w \in C^{N+1}$ in the neighborhood of (x_0, y_0, t_0). Let $\hat{x} = x - x_0, \hat{y} = y - y_0, \hat{t} = t - t_0$. Then, the Taylor series for function w and for $N = 2$ is

$$\begin{aligned} w(x,y,t) = w(x_0,y_0,t_0) &+ \frac{\partial w}{\partial x}\hat{x} + \frac{\partial w}{\partial y}\hat{y} + \frac{\partial w}{\partial t}\hat{t} + \frac{\partial^2 w}{\partial x^2}\frac{\hat{x}^2}{2} \\ &+ \frac{\partial^2 w}{\partial y^2}\frac{\hat{y}^2}{2} + \frac{\partial^2 w}{\partial t^2}\frac{\hat{t}^2}{2} + \frac{\partial^2 w}{\partial x \partial y}\hat{x}\hat{y} + \frac{\partial^2 w}{\partial x \partial t}\hat{x}\hat{t} + \frac{\partial^2 w}{\partial y \partial t}\hat{y}\hat{t} + R_3. \end{aligned} \tag{2.14}$$

Eliminating the derivative $\dfrac{\partial^2 w}{\partial t^2}$ by Eq. (2.1) we obtain

$$\begin{aligned} w(x,y,t) = w(x_0,y_0,t_0) &+ \frac{\partial w}{\partial x}\hat{x} + \frac{\partial w}{\partial y}\hat{y} + \frac{\partial w}{\partial t}\hat{t} + \frac{\partial^2 w}{\partial x^2}\left(\frac{\hat{x}^2}{2} + \frac{v^2\hat{t}^2}{2}\right) \\ &+ \frac{\partial^2 w}{\partial y^2}\left(\frac{\hat{y}^2}{2} + \frac{v^2\hat{t}^2}{2}\right) + \frac{\partial^2 w}{\partial x \partial y}\hat{x}\hat{y} + \frac{\partial^2 w}{\partial x \partial t}\hat{x}\hat{t} + \frac{\partial^2 w}{\partial y \partial t}\hat{y}\hat{t} + R_3. \end{aligned} \tag{2.15}$$

The coefficients following the derivative terms on the right-hand side represent, within the accuracy of a constant, the non-zero wave polynomials (2.6). As a solution of (2.1) we take a linear combination of wave polynomials. Therefore the constants in the polynomials are insignificant. Similarly, we get polynomials for $N = 3, 4, ...$

The procedure described above is important. If w is the solution of the problem described by Eq. (2.1) and the corresponding initial and boundary conditions and if w is analytical, then we can control the accuracy of approximation by

the properties of Taylor series. Moreover, using this procedure we can separate the stationary and nonstationary parts of expansion. For example, substituting $\dfrac{\partial^2 w}{\partial x^2} = \dfrac{\partial^2 w}{v^2 \partial t^2} - \dfrac{\partial^2 w}{\partial y^2}$ into (2.14) we obtain

$$w(x,y,t) = w(x_0,y_0,t_0) + \frac{\partial w}{\partial x}\hat{x} + \frac{\partial w}{\partial y}\hat{y} + \frac{\partial^2 w}{\partial y^2}\left(\frac{\hat{y}^2}{2} - \frac{\hat{x}^2}{2}\right) + \frac{\partial^2 w}{\partial x \partial y}\hat{x}\hat{y} + \frac{\partial w}{\partial t}\hat{t} + \frac{\partial^2 w}{\partial t^2}\left(\frac{\hat{x}^2}{2v^2} + \frac{\hat{t}^2}{2}\right) + \frac{\partial^2 w}{\partial x \partial t}\hat{x}\hat{t} + \frac{\partial^2 w}{\partial y \partial t}\hat{y}\hat{t} + R_3.$$

The coefficients $1,\ \hat{x},\ \hat{y},\ \dfrac{\hat{y}^2}{2} - \dfrac{\hat{x}^2}{2},\ \hat{x}\hat{y}$ are harmonic polynomials and satisfy the Laplace equation (stationary part) and coefficients $\hat{t},\ \dfrac{\hat{x}^2}{2v^2} + \dfrac{\hat{t}^2}{2},\ \hat{x}\hat{t},\ \hat{y}\hat{t}$ satisfy the wave equation (nonstationary part).

2.2. Three-dimensional wave polynomials

The wave polynomials for three-dimensional wave equation

$$\frac{1}{v^2}\frac{\partial^2 w}{\partial t^2} = \frac{\partial^2 w}{\partial x^2} + \frac{\partial^2 w}{\partial y^2} + \frac{\partial^2 w}{\partial z^2} \tag{2.16}$$

we obtain in a similar manner. Recurrent formulas for partial derivatives of wave polynomial are

$$\begin{aligned} \frac{\partial P_{(n-k-l-m)klm}}{\partial x} &= -Q_{(n-k-l-m-1)klm}, \\ \frac{\partial Q_{(n-k-l-m)klm}}{\partial x} &= P_{(n-k-l-m-1)klm}. \end{aligned} \tag{2.17}$$

$$\begin{aligned} \frac{\partial P_{(n-k-l-m)klm}}{\partial y} &= -Q_{(n-k-l-m)(k-1)lm}, \\ \frac{\partial Q_{(n-k-l-m)klm}}{\partial y} &= P_{(n-k-l-m)(k-1)lm}, \end{aligned} \tag{2.18}$$

$$\begin{aligned} \frac{\partial P_{(n-k-l-m)klm}}{\partial z} &= -Q_{(n-k-l-m)k(l-1)m}, \\ \frac{\partial Q_{(n-k-l-m)klm}}{\partial z} &= P_{(n-k-l-m)k(l-1)m}, \end{aligned} \tag{2.19}$$

$$
\begin{aligned}
\frac{\partial P_{(n-k-l)kl0}}{\partial t} &= -vQ_{(n-k-l-2)kl1} - vQ_{(n-k-l)(k-2)l1} - vQ_{(n-k-l)k(l-2)1},\\
\frac{\partial P_{(n-k-l-1)kl1}}{\partial t} &= -vQ_{(n-k-l-1)k0},\\
\frac{\partial Q_{(n-k-l)kl0}}{\partial t} &= vP_{(n-k-l-2)kl1} + vP_{(n-k-l)(k-2)l1} + vP_{(n-k-l)k(l-2)1},\\
\frac{\partial Q_{(n-k-l-1)kl1}}{\partial t} &= vP_{(n-k-l-1)kl0}.
\end{aligned} \tag{2.20}
$$

Theorem 2 enables us to obtain the three-dimensional wave polynomials $P_{(n-k-l-m)klm)}$ and $(Q_{(n-k-l-m)klm}$.

THEOREM 2: *Let $(P_{0000} = 1)$ and $(Q_{0000} = 0)$. Let $(P_{(n-k-l-m)klm} = Q_{(n-k-l-m)klm} = 0)$ when any subscript is negative. Then, the polynomials*

$$
\begin{aligned}
P_{(n-k-l)kl0} = -\frac{1}{n}(&xQ_{(n-k-l-1)kl0} + yQ_{(n-k-l)(k-1)l0}\\
&+ zQ_{(n-k-l)k(l-1)0} + vtQ_{(n-k-l-2)kl1} + vtQ_{(n-k-l)(k-2)l1}\\
&+ vtQ_{(n-k-l)k(l-2)1}),
\end{aligned} \tag{2.21}
$$

$$
\begin{aligned}
P_{(n-k-l-1)kl1} = -\frac{1}{n}(&xQ_{(n-k-l-2)kl1}\\
&+ yQ_{(n-k-l-1)(k-1)l1} + zQ_{(n-k-l-1)k(l-1)1} + vtQ_{(n-k-l-1)kl0}),
\end{aligned} \tag{2.22}
$$

$$
\begin{aligned}
Q_{(n-k-l)kl0} = \frac{1}{n}(&xP_{(n-k-l-1)kl0} + yP_{(n-k-l)(k-1)l0}\\
&+ zP_{(n-k-l)k(l-1)0} + vtP_{(n-k-l-2)kl1} + vtP_{(n-k-l)(k-2)l1}\\
&+ vtP_{(n-k-l)k(l-2)1}),
\end{aligned} \tag{2.23}
$$

$$
\begin{aligned}
Q_{(n-k-l-1)kl1} = \frac{1}{n}(&xP_{(n-k-l-2)kl1} + yP_{(n-k-l-1)(k-1)l1}\\
&+ zP_{(n-k-l-1)k(l-1)1} + vtP_{(n-k-l-1)kl0})
\end{aligned} \tag{2.24}
$$

satisfy the wave equation (2.16).

We prove Theorem 2 similarly to Theorem 1.

For example, from formulas (2.21)–(2.24) we get

$$
\begin{aligned}
&P_{0000} = 1,\\
&Q_{1000} = x, \qquad Q_{0100} = y, \qquad Q_{0010} = z, \qquad Q_{0001} = vt,
\end{aligned} \tag{2.25}
$$

$$
\begin{aligned}
&P_{2000} = -\frac{x^2}{2} - \frac{v^2t^2}{2}, \qquad P_{1100} = -xy, \qquad P_{1010} = -xz,\\
&P_{1001} = -vxt, \qquad P_{0200} = -\frac{y^2}{2} - \frac{v^2t^2}{2}, \qquad P_{0110} = -yz,\\
&P_{0101} = -vyt, \qquad P_{0020} = -\frac{z^2}{2} - \frac{v^2t^2}{2}, \qquad P_{0011} = -vzt, \dots
\end{aligned}
\tag{2.25 [cont.]}
$$

and

$$
Q_{0000} = P_{1000} = P_{0100} = P_{0010} = P_{0001} = Q_{2000} = Q_{1100} = Q_{1010} = Q_{1001} = \dots = 0
$$

Notice that there is no R_{0002} because $m < 2$.

3. Equations of elasticity

In general, elasticity problems are described by the following system of equations [18]:

$$
\mu\nabla^2\mathbf{u} + (\lambda+\mu)\text{grad div } \mathbf{u} + \mathbf{X} = \rho\ddot{\mathbf{u}} \tag{3.1}
$$

where $\mathbf{u}$ – displacement vector, $\mathbf{X}$ – body force vector, ∇ – nabla operator, μ, λ, ρ – constants. If we omit the body forces, we obtain

$$
\mu\nabla^2\mathbf{u} + (\lambda+\mu)\text{grad div } \mathbf{u} = \rho\ddot{\mathbf{u}}. \tag{3.2}
$$

Equations (3.2) are completed by initial and boundary conditions for displacements and/or stresses. The relationship between the displacements and stresses is given by Hooke's law:

$$
\sigma_{ij} = 2\mu\varepsilon_{ij} + \lambda\delta_{ij}\varepsilon_{kk} \tag{3.3}
$$

where $\varepsilon_{ij} = \dfrac{1}{2}\left(\dfrac{\partial u_i}{\partial x_j} + \dfrac{\partial u_j}{\partial x_i}\right)$ – strain tensor. The system of equations (3.2) can be simplified by substitution:

$$
\mathbf{u} = \text{grad } \phi + \text{rot } \mathbf{\Psi} \tag{3.4}
$$

Then we obtain

$$
\left(\nabla^2 - \frac{1}{v_1^2}\frac{\partial^2}{\partial t^2}\right)\phi = 0, \tag{3.5}
$$

$$
\left(\nabla^2 - \frac{1}{v_2^2}\frac{\partial^2}{\partial t^2}\right)\psi_i = 0, \qquad i = 1,2,3 \tag{3.6}
$$

where $v_1^2 = \dfrac{\lambda + 2\mu}{\rho}$, $v_2^2 = \dfrac{\mu}{\rho}$. The Eqs. (3.5) and (3.6) are wave equations, but for a finite domain they are still coupled by initial and boundary conditions. The main purpose of this work is to solve the system of (3.5), (3.6) by means of to solve functions' method.

4. Method of solving functions

The wave-polynomial method discussed below belongs to the class of Trefftz methods. As a solution of each wave equation (3.5), (3.6) we take a linear combination of the corresponding wave polynomials. The succeeding non-zero polynomials satisfying Eqs. (3.5) and (3.6) we denote correspondingly by V_n^0 and V_n^i, $\quad i = 1, 2, 3$

As approximations for the solution of Eqs. (3.5) and (3.6) we take correspondingly

$$\phi \approx \widehat{\phi} = \sum_{n=1}^{N} c_n^0 V_n^0 \tag{4.1}$$

and

$$\psi_i \approx \widehat{\psi}_i = \sum_{n=1}^{N} c_n^i V_n^i, \quad i = 1, 2, 3. \tag{4.2}$$

Then

$$\mathbf{u} \approx \widehat{\mathbf{u}} = \operatorname{grad} \widehat{\phi} + \operatorname{rot} \widehat{\mathbf{\Psi}}. \tag{4.3}$$

Because polynomials V_n satisfy the corresponding wave equation, also the linear combination satisfies this equation. The coefficients c_n in (4.1) and (4.2) are chosen so that the error of fulfilling the given boundary and initial conditions corresponding to Eqs. (3.5) and (3.6) is minimized (see examples).

5. Examples

Some examples presented in this section show the application of the method of solving functions in elasticity. The first two concern the two-dimensional and the next two the three-dimensional elasticity problems. In all examples presented here the constants are established as follows: $\lambda = 10^{11}$ [Pa], $\mu = 8 \cdot 10^{10}$ [Pa], $\rho = 8000$ [kg/m^3].

5.1. Example 1 – two-dimensional problem in a square

First we consider the plane state of strain when the strain tensor depends on time and two variables $\varepsilon_{ij} = \varepsilon_{ij}(x, y, t), (i, j = 1, 2)$ and $\varepsilon_{i3} = 0, (i = 1, 2, 3)$. Then

$$\begin{aligned}\mathbf{u} &= [u_x(x, y, t), u_y(x, y, t)] \\ &= \left[\frac{\partial\phi(x, y, t)}{\partial x} + \frac{\partial\psi(x, y, t)}{\partial y}, \frac{\partial\phi(x, y, t)}{\partial y} - \frac{\partial\psi(x, y, t)}{\partial x}\right],\end{aligned}$$

$$\begin{aligned}\sigma_{xx} &= (2\mu + \lambda)\frac{\partial u_x}{\partial x} + \lambda\frac{\partial u_y}{\partial y}, \qquad \sigma_{xy} = \mu\left(\frac{\partial u_x}{\partial y} + \frac{\partial u_y}{\partial x}\right), \\ \sigma_{yy} &= \lambda\frac{\partial u_x}{\partial x} + (2\mu + \lambda)\frac{\partial u_y}{\partial y}, \qquad \sigma_{zz} = \lambda\left(\frac{\partial u_x}{\partial x} + \frac{\partial u_y}{\partial y}\right).\end{aligned} \tag{5.1}$$

The system of equations (3.5) and (3.6) has the form:

$$\frac{1}{v_1^2}\frac{\partial^2\phi}{\partial t^2} = \frac{\partial^2\phi}{\partial x^2} + \frac{\partial^2\phi}{\partial y^2}, \tag{5.2}$$

$$\frac{1}{v_2^2}\frac{\partial^2\psi}{\partial t^2} = \frac{\partial^2\psi}{\partial x^2} + \frac{\partial^2\psi}{\partial y^2}. \tag{5.3}$$

Let us consider the two-dimensional elasticity problem in a square $(x, y) \in [0, 1]\times[0, 1]$, described by the system of Eqs. (5.2)–(5.3) and conditions:

$$u_x(x, y, 0) = u_{x0}(x, y) = -\frac{x}{10000}, \qquad u_y(x, y, 0) = 0, \tag{5.4}$$

$$\frac{\partial u_x(x, y, 0)}{\partial t} = \frac{\partial u_y(x, y, 0)}{\partial t} = 0, \tag{5.5}$$

$$u_x(0, y, t) = u_y(0, y, t) = 0, \tag{5.6}$$

$$\begin{aligned}&\sigma_{xx} = \sigma_{xy} = \sigma_{yy} = 0, \\ &\text{for} \quad x = 1, \quad y = 0, \quad y = 1.\end{aligned} \tag{5.7}$$

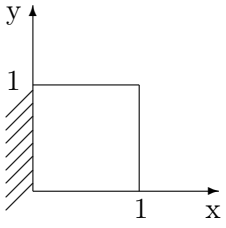

FIG. 1. Fixation of the square.

The problem described by relationships (5.2)–(5.7) can be solved approximately by means of the method of solving functions. Let us denote the non-zero two-dimensional wave polynomials (2.6) by

$$V_1^0 = 1, \quad V_2^0 = x, \quad V_3^0 = y, \quad V_4^0 = v_1 t, \quad V_5^0 = -\frac{x^2}{2} - \frac{v_1^2 t^2}{2}, \quad V_6^0 = -xy,$$

$$V_7^0 = -v_1 xt, \quad V_8^0 = -v_1 yt, \quad V_9^0 = -\frac{y^2}{2} - \frac{v_1^2 t^2}{2}, \quad \ldots$$

$$V_1^1 = 1, \quad V_2^1 = x, \quad V_3^1 = y, \quad V_4^0 = v_2 t, \quad V_5^1 = -\frac{x^2}{2} - \frac{v_2^2 t^2}{2}, \quad V_6^1 = -xy,$$

$$V_7^1 = -v_2 xt, \quad V_8^1 = -v_2 yt, \quad V_9^1 = -\frac{y^2}{2} - \frac{v_2^2 t^2}{2}, \quad \ldots.$$

As the approximations for the solutions of Eqs. (5.2)–(5.3), we take correspondingly

$$\phi \approx \widehat{\phi} = \sum_{n=1}^{N} c_n^0 V_n^0. \tag{5.8}$$

and

$$\psi \approx \widehat{\psi} = \sum_{n=1}^{N} c_n^1 V_n^1. \tag{5.9}$$

The coefficients c_n in (5.8) and (5.9) are chosen so that the error of fulfilling the boundary and initial conditions (5.4)–(5.7) is minimized. After applyting the least squares method, the functional describing this error can be written in the

time interval $(0, \Delta t)$ as:

$$
\begin{aligned}
(5.10)\quad I \;=\; & w_u \int_0^1\int_0^1 \Big\{ \underbrace{\big[\widehat{u}_x(x,y,0) - u_{x0}(x,y)\big]^2 + \big[\widehat{u}_y(x,y,0)\big]^2}_{\text{cond.}(5.4)} \Big\} dydx \\
& + w_u \int_0^1\int_0^1 \Big\{ \underbrace{\Big[\frac{\partial \widehat{u}_x(x,y,0)}{\partial t}\Big]^2 + \Big[\frac{\partial \widehat{u}_y(x,y,0)}{\partial t}\Big]^2}_{\text{cond.}(5.5)} \Big\} dydx \\
& + w_u \int_0^{\Delta t}\int_0^1 \Big\{ \underbrace{\big[\widehat{u}_x(0,y,t)\big]^2 + \big[\widehat{u}_y(0,y,t)\big]^2}_{\text{cond.}(5.6)} \Big\} dydt \\
& + w_\sigma \int_0^{\Delta t}\int_0^1 \Big\{ \underbrace{\big[\widehat{\sigma}_{xx}(1,y,t)\big]^2 + \big[\widehat{\sigma}_{xy}(1,y,t)\big]^2}_{\text{cond.}(5.7)} \Big\} dydt \\
& + w_\sigma \int_0^{\Delta t}\int_0^1 \Big\{ \underbrace{\big[\widehat{\sigma}_{yx}(x,0,t)\big]^2 + \big[\widehat{\sigma}_{yy}(x,0,t)\big]^2}_{\text{cond.}(5.7)} \Big\} dxdt \\
& + w_\sigma \int_0^{\Delta t}\int_0^1 \Big\{ \underbrace{\big[\widehat{\sigma}_{yx}(x,1,t)\big]^2 + \big[\widehat{\sigma}_{yy}(x,1,t)\big]^2}_{\text{cond.}(5.7)} \Big\} dxdt.
\end{aligned}
$$

The constants μ, λ are large. They appear in the second power by conditions connected with stresses. Therefore in functional I we have to introduce weights by each condition. The sum of all weights equals one. Because in functional (5.10) there are six conditions connected with stresses and six conditions connected with displacements, the weight $w_\sigma = 1/(6 \cdot 10^{24})$.

The necessary condition to minimize the functional I is

$$
\frac{\partial I}{\partial c_1^0} = \cdots = \frac{\partial I}{\partial c_N^0} = \frac{\partial I}{\partial c_1^1} = \cdots = \frac{\partial I}{\partial c_N^1} = 0. \tag{5.11}
$$

The linear system of equations (5.11) can be written as

$$
AC = B \tag{5.12}
$$

where $C = [c_1^0, \ldots, c_N^0, c_1^1, \ldots, c_N^1]^T$ and $A = \underbrace{\begin{bmatrix} A^1 & A^2 \\ A^3 & A^4 \end{bmatrix}}_{\substack{c_j^0 \\ \quad}} \begin{matrix} \} \frac{\partial I}{\partial c_i^0} \\ \} \frac{\partial I}{\partial c_i^1} \end{matrix}$.

For example, the elements of matrix A^2 are

$$
\begin{aligned}
a^2_{i,j} &= w_u \int_0^1 \int_0^1 \left\{ \frac{\partial V_i^0(x,y,0)}{\partial x} \frac{\partial V_j^1(x,y,0)}{\partial x} - \frac{\partial V_i^0(x,y,0)}{\partial y} \frac{\partial V_j^1(x,y,0)}{\partial x} \right. \\
&+ \left. \frac{\partial^2 V_i^0(x,y,0)}{\partial x \partial t} \frac{\partial^2 V_j^1(x,y,0)}{\partial y \partial t} - \frac{\partial^2 V_i^0(x,y,0)}{\partial y \partial t} \frac{\partial^2 V_j^1(x,y,0)}{\partial x \partial t} \right\} dydx \\
&+ \int_0^1 \int_0^{\Delta t} \left\{ w_u \left(\frac{\partial V_i^0(0,y,t)}{\partial x} \frac{\partial V_j^1(0,y,t)}{\partial y} - \frac{\partial V_i^0(0,y,t)}{\partial y} \frac{\partial V_j^1(0,y,t)}{\partial x} \right) \right. \\
&+ w_\sigma \left(2\mu \left((2\mu+\lambda) \frac{\partial^2 V_i^0(1,y,t)}{\partial x^2} + \lambda \frac{\partial^2 V_i^0(1,y,t)}{\partial y^2} \right) \frac{\partial^2 V_j^1(1,y,t)}{\partial x \partial y} \right. \\
&+ \left. \left. 2\mu^2 \frac{\partial^2 V_i^0(1,y,t)}{\partial x \partial y} \left(\frac{\partial^2 V_j^1(1,y,t)}{\partial y^2} - \frac{\partial^2 V_j^1(1,y,t)}{\partial x^2} \right) \right) \right\} dtdy \\
&+ w_\sigma 2\mu \int_0^1 \int_0^{\Delta t} \left\{ \mu \frac{\partial^2 V_i^0(x,0,t)}{\partial x \partial y} \left(\frac{\partial^2 V_j^1(x,0,t)}{\partial y^2} - \frac{\partial^2 V_j^1(x,0,t)}{\partial x^2} \right) \right. \\
&- \left((2\mu+\lambda) \frac{\partial^2 V_i^0(x,0,t)}{\partial y^2} + \lambda \frac{\partial^2 V_i^0(x,0,t)}{\partial x^2} \right) \frac{\partial^2 V_j^1(x,0,t)}{\partial x \partial y} \\
&+ \mu \frac{\partial^2 V_i^0(x,1,t)}{\partial x \partial y} \left(\frac{\partial^2 V_j^1(x,1,t)}{\partial y^2} - \frac{\partial^2 V_j^1(x,1,t)}{\partial x^2} \right) \\
&- \left. \left((2\mu+\lambda) \frac{\partial^2 V_i^0(x,1,t)}{\partial y^2} + \lambda \frac{\partial^2 V_i^0(x,1,t)}{\partial x^2} \right) \frac{\partial^2 V_j^1(x,1,t)}{\partial x \partial y} \right\} dtdx.
\end{aligned}
$$

From Eq. (5.12) we obtain the coefficients c_n. In practice it turns out that this system of linear equations is indeterminate. Nevertheless, for different values of the parameter we get the same solution. In the time intervals $(\Delta t, 2\Delta t)$, $(2\Delta t, 3\Delta t)$,..., we proceed analogously. Here, the initial condition for time interval $((m-1)\Delta t, m\Delta t)$ is the value of function u at the end of interval $((m-2)\Delta t, (m-1)\Delta t)$. All results below have been obtained for $\Delta t = 0.00016$. Then $v_1 \Delta t = 0.91214034, v_2 \Delta t = .5059644256$. We obtain an approximation in the entire time interval $(0, \Delta t)$. For example, Fig. 2 shows an approximation of displacement u_x by polynomials from order 0 to 9 for times a) $t = 0$,

b) $t = 0.00008$, c) $t = 0.00014$. Figures 2 show that the initial and boundary conditions for displacement u_x are well approximated

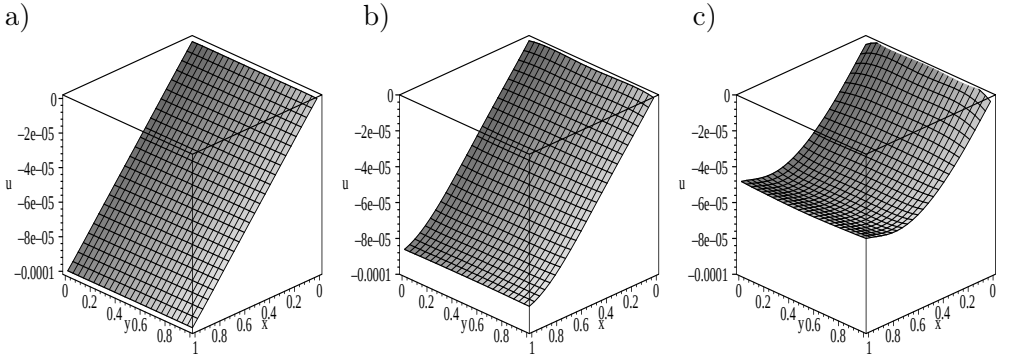

FIG. 2. Approximation of displacement u_x for time a) $t = 0$, b) $t = 0.00008$, c) $t = 0.00014$.

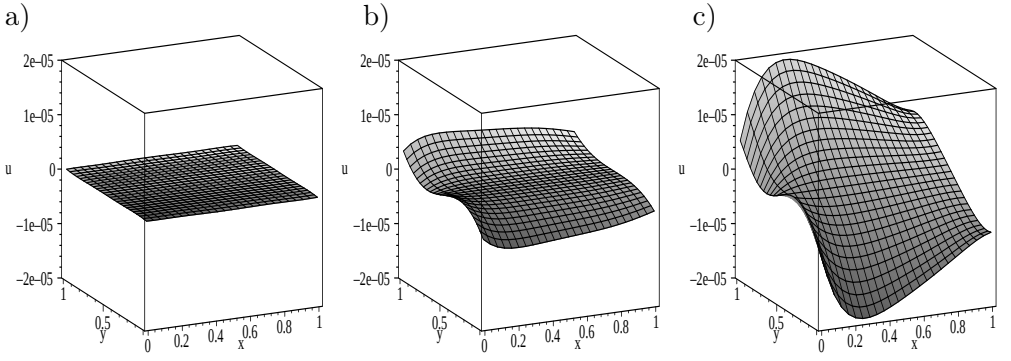

FIG. 3. Approximation of displacement u_y for time a) $t = 0$, b) $t = 0.00008$, c) $t = 0.00014$.

Figure 3 show an approximation of displacement u_y by polynomials from order 0 to 9 for times a) $t = 0$, b) $t = 0.00008$, c) $t = 0.00014$. Figures 2 and 3 shows that the the physical character of the displacement is preserved.

In approximations (5.8) and (5.9) we take all wave polynomials of orders from 0 to K. Table 1 shows the value of functional I which depends on the order K. The error decreases when the number of polynomials in the approximation increases.

Table 1. I dependence of the polynomial order.

Order K	1	2	3	4	5
I	$0.139 \cdot 10^{-9}$	$0.234 \cdot 10^{-13}$	$0.233 \cdot 10^{-13}$	$0.211 \cdot 10^{-13}$	$0.166 \cdot 10^{-13}$

5.2. Example 2 – two-dimensional problem in a triangle

The majority of analytical methods used for solving partial differential equations are effective for simple shapes of the body (square, circle, cube or sphere). Solving functions' method can be applied for more complicated domains. The only difficulty for such a shape may be the calculation of the integrals determining the coefficients c_n – for most shapes this does not create any problem.

Similarly as in Sec. 5.1, we consider a plane state of strain when the strain tensor depends on time and two variables. Let us consider the two-dimensional elasticity problem in a triangle $0 \leq x \leq 1,\ 0 \leq y \leq 1-x$, described by the system of Eqs. (5.2)–(5.3) and conditions:

$$u_x(x,y,0) = u_{x0}(x,y) = \frac{y(1-y)(1-x-y)}{1000}, \qquad u_y(x,y,0) = 0, \tag{5.13}$$

$$\frac{\partial u_x(x,y,0)}{\partial t} = \frac{\partial u_y(x,y,0)}{\partial t} = 0, \tag{5.14}$$

$$u_x(x,0,t) = u_y(x,0,t) = u_x(x,1-x,t) = u_y(x,1-x,t) = 0, \tag{5.15}$$

$$\sigma_{xx}(0,y,t) = \sigma_{xy}(0,y,t) = 0. \tag{5.16}$$

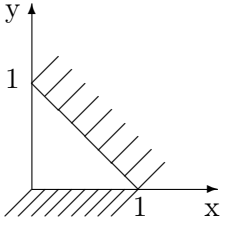

Fig. 4. Fixation of the triangle.

Similarly as in Sec. 5.1, approximations for the solution of Eqs. (5.2)–(5.3) we take correspondingly (5.8) and (5.9). The coefficients c_n in the linear combinations are chosen such that the error in fulfilling the boundary and initial conditions (5.13)–(5.16) is minimized. The functional describing this error is

similar to (5.10). Here we have other domains for integrals:

$$
\begin{aligned}
(5.17)\quad I &= w_u \int_0^1 \int_0^{1-x} \left\{ \underbrace{[\widehat{u}_x(x,y,0) - u_{x0}(x,y)]^2 + [\widehat{u}_y(x,y,0)]^2}_{\text{cond.}(5.13)} \right\} dydx \\
&+ w_u \int_0^1 \int_0^{1-x} \left\{ \underbrace{\left[\frac{\partial \widehat{u}_x(x,y,0)}{\partial t}\right]^2 + \left[\frac{\partial \widehat{u}_y(x,y,0)}{\partial t}\right]^2}_{\text{cond.}(5.14)} \right\} dydx \\
&+ w_u \int_0^{\Delta t} \int_0^1 \{ \underbrace{[\widehat{u}_x(x,0,t)]^2 + [\widehat{u}_y(x,0,t)]^2}_{\text{cond.}(5.15)} \, dxdt \\
&+ w_u \sqrt{2} \int_0^{\Delta t} \int_0^1 \underbrace{[\widehat{u}_x(x,1-x,t)]^2 + [\widehat{u}_x(x,1-x,t)]^2}_{\text{cond.}(5.15)} \} dxdt \\
&+ w_\sigma \int_0^{\Delta t} \int_0^1 \{ \underbrace{[\widehat{\sigma}_{xx}(0,y,t)]^2 + [\widehat{\sigma}_{xy}(0,y,t)]^2}_{\text{cond.}(5.16)} \} dydt
\end{aligned}
$$

There are two conditions connected with stresses and eight conditions connected with displacements. Therefore in functional I the weight $w_\sigma = 2/10^{23}$. The sum of all weights equals one. We obtain the coefficients c_n in the same manner as in Sec. 5.1. All results below have been obtained for $\Delta t = 0.00016[s]$. Figure 5 shows the initial condition for displacement u_x a) the exact solution, b) an approximation by polynomials from order 0 to 9, c) the difference between a) and b). Figure 5 shows that the initial condition for displacement u_x is well approximated. Figure 6 shows an approximation of displacement $u_y(0,y,t)$ in time by polynomials from order 0 to 9. Let u_K denote the approximation of $u_y(0,y,t)$ by polynomials of order from 0 to K. We define the average, relative difference between solutions u_K and u_{K-1}:

$$
D(K) = \sqrt{\frac{\int_0^{\Delta t} \int_0^1 (u_K(0,y,t) - u_{K-1}(0,y,t))^2 \mathrm{d}y\mathrm{d}t}{\int_0^{\Delta t} \int_0^1 (u_{K-1}(0,y,t))^2 \mathrm{d}y\mathrm{d}t}}
$$

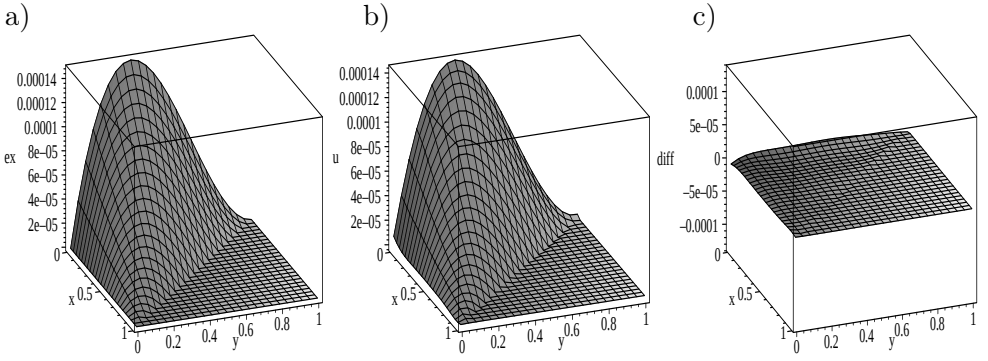

FIG. 5. Initial condition for displacement u_x: a) exact, b) approximation, c) difference.

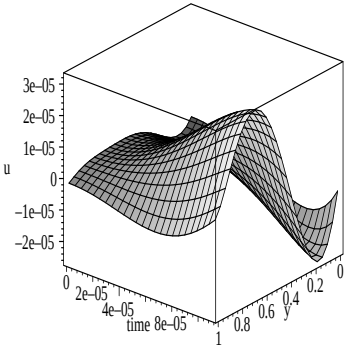

FIG. 6. Approximation in time of displacement $u_y(0, y, t)$.

Table 2 shows the difference $D(K)$ which depends on the order K. The error decreases when the number of polynomials in the approximation u increases. It suggests that the method is convergent.

Table 2. Error dependence of the polynomial order.

Order K	3	5	7	9
$D(K)$	201.2	1.235	1.256	0.558

Stresses can be calculated by means of formula (3.3). For example, Fig. 7 shows the approximation of stress σ_{xx} by polynomials of order from 0 to 9 for times a) $t = 0.00001$, b) $t = 0.00008$, c) $t = 0.00011$. Figures 6 and 7 show that the physical character of the displacements and stresses is preserved.

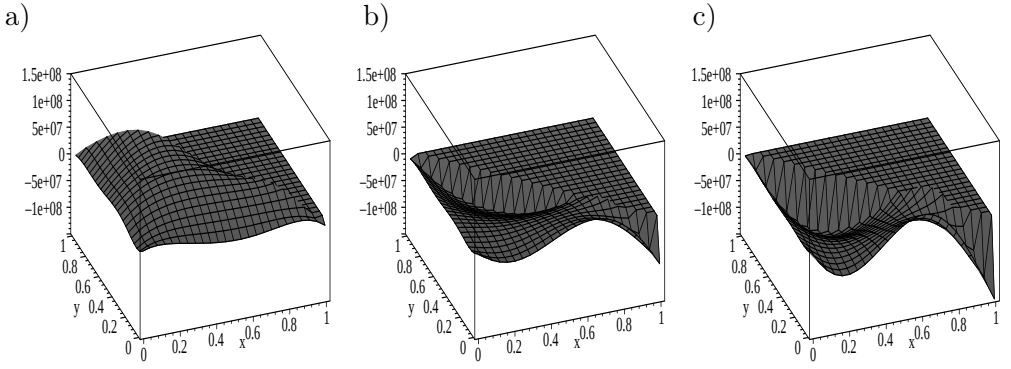

FIG. 7. Approximation of stress σ_{xx} for times a) $t = 0.00001$, b) $t = 0.00008$, c) $t = 0.00011$.

5.3. Example 3 – three-dimensional problem in a cube

The method presented here can be also applied to three-dimensional elasticity problems. Let us consider the elasticity problem described for a cube $(x, y, z) \in [0, 1] \times [0, 1] \times [0, 1]$ by the system of Eqs. (3.5)–(3.6) and conditions:

$$
\begin{aligned}
&u_x(x, y, z, 0) = 0, \qquad u_y(x, y, z, 0) = 0, \\
&u_z(x, y, z, 0) = u_{x0}(x, y, z) = -\frac{z}{10000},
\end{aligned}
\tag{5.18}
$$

$$
\frac{\partial u_x(x, y, z, 0)}{\partial t} = \frac{\partial u_y(x, y, z, 0)}{\partial t} = \frac{\partial u_z(x, y, z, 0)}{\partial t} = 0,
\tag{5.19}
$$

$$
u_x(x, y, 0, t) = u_y(x, y, 0, t) = u_z(x, y, 0, t) = 0,
\tag{5.20}
$$

$$
\begin{aligned}
&\sigma_{xx}(0, y, z, t) = \sigma_{xy}(0, y, z, t) = \sigma_{xz}(0, y, z, t) = 0, \\
&\sigma_{xx}(1, y, z, t) = \sigma_{xy}(1, y, z, t) = \sigma_{xz}(1, y, z, t) = 0, \\
&\sigma_{yx}(x, 0, z, t) = \sigma_{yy}(x, 0, z, t) = \sigma_{yz}(x, 0, z, t) = 0, \\
&\sigma_{yx}(x, 1, z, t) = \sigma_{yy}(x, 1, z, t) = \sigma_{yz}(x, 1, z, t) = 0, \\
&\sigma_{zx}(x, y, 1, t) = \sigma_{zy}(x, y, 1, t) = \sigma_{zz}(x, y, 1, t) = 0.
\end{aligned}
\tag{5.21}
$$

The problem described by relationships (5.18)–(5.21) can be solved approximately by means of the method of solving functions. Let us denote the non-zero

two-dimensional wave polynomials (2.25) as

$$V_1^0 = 1, \quad V_2^0 = x, \quad V_3^0 = y, \quad V_4^0 = z, \quad V_5^0 = v_1 t, \quad V_6^0 = -\frac{x^2}{2} - \frac{v_1^2 t^2}{2},$$
$$V_7^0 = -xy, \quad V_8^0 = -xz, \quad V_9^0 = -v_1 xt, \quad V_{10}^0 = -\frac{y^2}{2} - \frac{v_1^2 t^2}{2},$$
$$V_{11}^0 = -yz, \quad V_{12}^0 = -v_1 yt, \quad V_{13}^0 = -\frac{z^2}{2} - \frac{v_1^2 t^2}{2}, \quad V_{14}^0 = -v_1 zt, \ldots$$

and

$$V_1^i = 1, \quad V_2^i = x, \quad V_3^i = y, \quad V_4^i = z, \quad V_5^i = v_2 t, \quad V_6^i = -\frac{x^2}{2} - \frac{v_2^2 t^2}{2},$$
$$V_7^i = -xy, \quad V_8^i = -xz, \quad V_9^i = -v_2 xt, \quad V_{10}^i = -\frac{y^2}{2} - \frac{v_2^2 t^2}{2},$$
$$V_{11}^i = -yz, \quad V_{12}^i = -v_2 yt, \quad V_{13}^i = -\frac{z^2}{2} - \frac{v_2^2 t^2}{2}, \quad V_{14}^i = -v_2 zt, \ldots \quad i = 1, 2, 3$$

Notice that we take the same polynomials for Eqs. (3.6). As approximations for the solution of Equations (3.5)–(3.6) we take correspondingly

$$\phi \approx \widehat{\phi} = \sum_{n=1}^{N} c_n^0 V_n^0. \tag{5.22}$$

and

$$\psi_i \approx \widehat{\psi}_i = \sum_{n=1}^{N} c_n^i V_n^i, \quad i = 1, 2, 3. \tag{5.23}$$

The coefficients c_n in (5.22) and (5.23) are chosen so that the error for fulfilling the boundary and initial conditions (5.18)–(5.21) is minimized. Further we progress as in Secs. 5.1 and 5.2. Of course, here we have more conditions. Therefore the functional I and matrices A, C and B are "bigger". In functional I we introduce weights by each condition. In this case there are fifteen conditions connected with stresses and nine conditions connected with displacements – the weight $w_\sigma = 15/10^{22}$.

All results below have been obtained for $\Delta t = 0.00016$. Figure 8 shows an approximation of displacement $u_z(x, 0.5, z, t)$ by polynomials from order 0 to 4 for time a) $t = 0$, b) $t = 0.0001$, c) $t = 0.00016$. Figures 8 show that the initial and boundary conditions are well approximated.

Figure 9 shows an approximation of displacement $u_x(x, y, 0.5, t)$ by polynomials of order from 0 to 4 for times a) $t = 0$, b) $t = 0.0001$, c) $t = 0.00016$. Figures 8 and 9 show that the physical character of the displacement is preserved.

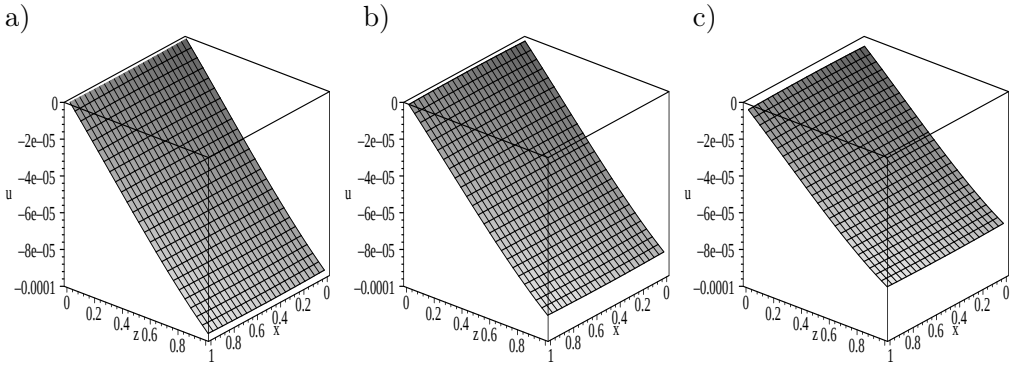

FIG. 8. Approximation of displacement $u_z(x, 0.5, z, t)$ for time a) $t = 0$, b) $t = 0.0001$, c) $t = 0.00016$.

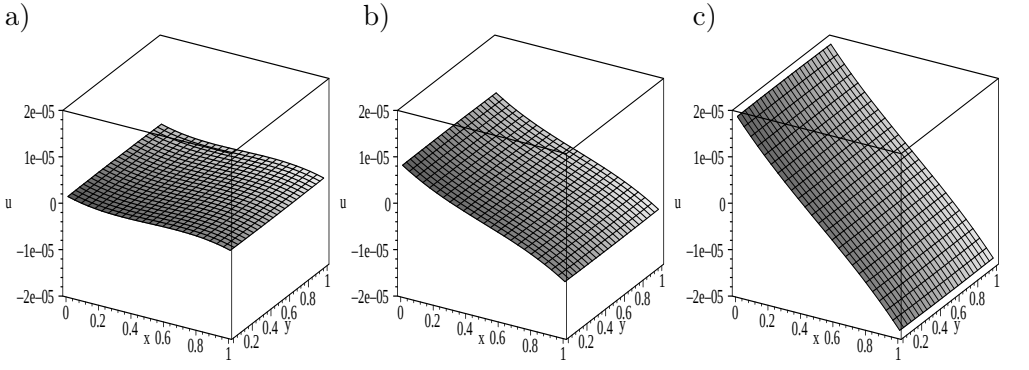

FIG. 9. Approximation of displacement $u_x(x, y, 0.5, t)$ for time a) $t = 0$, b) $t = 0.0001$, c) $t = 0.00016$.

5.4. Example 4 – three-dimensional problem in a triangular prism

Let us consider the elasticity problem described in a triangular prism $0 \leq x \leq 1$, $0 \leq y \leq 1 - x$, $0 \leq z \leq 1$ by the system of Eqs. (3.5)–(3.6) and conditions:

$$
\begin{aligned}
&u_x(x, y, z, 0) = 0, \quad u_y(x, y, z, 0) = 0, \\
&u_z(x, y, z, 0) = u_{x0}(x, y, z) = -\frac{z}{10000},
\end{aligned}
\tag{5.24}
$$

$$
\frac{\partial u_x(x, y, z, 0)}{\partial t} = \frac{\partial u_y(x, y, z, 0)}{\partial t} = \frac{\partial u_z(x, y, z, 0)}{\partial t} = 0,
\tag{5.25}
$$

$$u_x(x,y,0,t) = u_y(x,y,0,t) = u_z(x,y,0,t) = 0, \tag{5.26}$$

$$\begin{aligned}
&\sigma_{xx}(0,y,z,t) = \sigma_{xy}(0,y,z,t) = \sigma_{xz}(0,y,z,t) = 0,\\
&\sigma_{yx}(x,0,z,t) = \sigma_{yy}(x,0,z,t) = \sigma_{yz}(x,0,z,t) = 0,\\
&\sigma_{zx}(x,y,1,t) = \sigma_{zy}(x,y,1,t) = \sigma_{zz}(x,y,1,t) = 0,\\
&\sigma_{xx}(x,1-x,z,t) = \sigma_{xy}(x,1-x,z,t) = \sigma_{xz}(x,1-x,z,t) = 0,\\
&\sigma_{yy}(x,1-x,z,t) = \sigma_{yz}(x,1-x,z,t) = \sigma_{zz}(x,1-x,z,t) = 0.
\end{aligned} \tag{5.27}$$

The problem described by relationships (5.24)–(5.27) can be solved in the same manner as in Secs. 5.1, 5.2 and 5.3. In this case we have other domain for integrals in functional I where there are fourteen conditions connected with stresses and nine conditions connected with displacements – the weight $w_\sigma = 14/10^{22}$.

All results given below given have been obtained for $\Delta t = 0.00016$.

Figure 10 shows the approximation of displacement $u_x(x,y,0.5,t)$ by polynomials of order from 0 to 4 for times a) $t = 0$, b) $t = 0.0001$, c) $t = 0.00015$. Figure 10 shows that the physical character of the displacement is preserved. Figure 11 shows an approximation of displacement $u_z(x,x,z,t)$ by polynomials of order from 0 to 4 for times a) $t = 0$, b) $t = 0.0001$, c) $t = 0.00016$. Figures 11 shows that the initial and boundary conditions for u_z are well approximated.

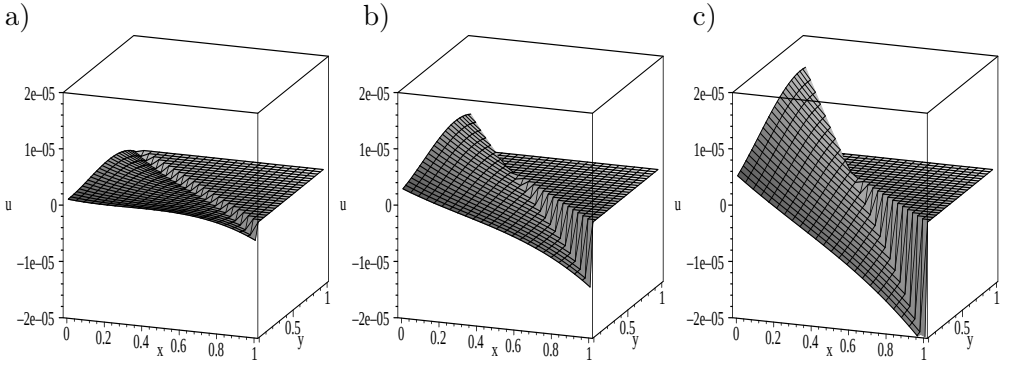

FIG. 10. Approximation of displacement $u_x(x,y,0.5,t)$ for time a) $t = 0$, b) $t = 0.0001$, c) $t = 0.00015$.

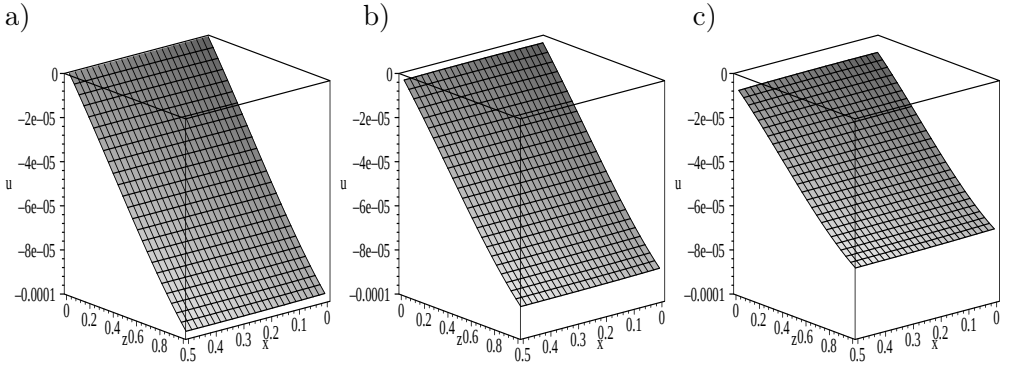

FIG. 11. Approximation of displacement $u_z(x, x, z, t)$ for time a) $t = 0$, b) $t = 0.0001$, c) $t = 0.00016$.

6. Concluding remarks

As a rule, the elasticity problems are difficult. A new simple technique for solving these two- and three- dimensional problems has been developed. The method of solving functions presented in this paper is a straightforward method for solving elasticity problems in finite bodies. This method is also useful when the shape of the body is complicated. We must calculate the integrals determining the coefficients c_n. For most shapes this does not present any problem. The simple examples presented in this paper show that in the obtained approximations, the physical character of displacements and stresses is preserved. The solution, which is a linear combination of wave polynomials, satisfies exactly the wave equation and approximately – the initial and boundary conditions. The next step of the research should be the application of this method to thermoelasticity problems. Moreover, wave polynomials can be used as finite-element base functions.

Acknowledgments

The author would like to thank the University of Karlsruhe where most of the calculations have been made.

References

1. E. Trefftz, *Ein Gegenstück zum Ritzschen Verfahren*, [in:], Proceedings of the 2-nd International Congress of Applied Mechanics. Zurich 131–137, 1926.

2. A.P. Zieliński and I.Herrera, *Trefftz method: fitting boundary conditions.* Int. J. Num. Meth. Eng., **24**, 871–891, 1987.

3. P.C. Rosenbloom and D.V. Widder, *Expansion in terms of heat polynomials and associated functions,* Trans. Am. Math. Soc., **92**, 220–266, 1956.

4. H. Yano, S. Fukutani and A. Kieda, *A boundary residual method with heat polynomials for solving unsteady heat conduction problems,* Franklin Inst, **316**, 291–298, 1983.

5. S. Futakiewicz and L. Hożejowski, *Heat polynomials method in the n-dimensional direct and inverse heat conduction problems,* [in:] A.J. Nowak, C.A. Brebbia, R. Bielecki and M. Zerroukat [Eds.], Advanced Computational Method in Heat Transfer V. Southampton, UK and Boston, USA: Computational Mechanics Publications, 103–112, 1998.

6. L. Hożejowski, *Heat polynomials and their application for solving direkt and inverse heat condutions problems* (PhD-Thesis) [in Polish], Kielce University of Technology, pp. 115, 1999.

7. S. Futakiewicz and L. Hożejowski, *Heat polynomials in solving the direct and inverse heat conduction problems in a cylindrical system of coordinates*, [in:] A.J. Nowak, C.A. Brebbia, R. Bielecki and M. Zerroukat [Eds.], Advanced Computational Method in Heat Transfer V. Southampton UK and Boston USA: Computational Mechanics Publications 71–80, 1998.

8. S. Futakiewicz, K. Grysa and L. Hożejowski, *On a problem of boundary temperature identification in a cylindrical layer,* [in:] B.T. Maruszewski, W. Muschik and A. Radowicz [Eds.], Proceedings of the International Symposium on Trends in Continuum Physics, World Scientific Publishing, Singapore, New Jersey, London, Hong Kong 119–125, 1999.

9. S. Futakiewicz, *Heat functions method for solving direct and inverse heat condutions problems* (PhD-Thesis) [in Polish], Poznań University of Technology 120pp, 1999.

10. M.J. Ciałkowski, S. Futakiewicz and L. Hożejowski, *Method of heat polynomials in solving the inverse heat conduction problems,* ZAMM, **79**, 709–710, 1999.

11. M.J. Ciałkowski, S. Futakiewicz and L. Hożejowski, *Heat polynomials applied to direct and inverse heat conduction problems,* [in:] B.T. Maruszewski, W. Muschik and A. Radowicz [Eds.], Proceedings of the International Symposium on Trends in Continuum Physics, World Scientific Publishing, Singapore, New Jersey, London, Hong Kong 79–88, 1999.

12. M.J. Ciałkowski, *Solution of inverse heat conduction problem with use of a new type of finite element base functions,* [in:] B.T. Maruszewski, W. Muschik and A.Radowicz [Eds.], Proceedings of the International Symposium on Trends in Continuum Physics, Singapore, New Jersey, London, Hong Kong: World Scientific Publishing, 64–78, 1999.

13. M.J. Ciałkowski and A. Frąckowiak, *Heat functions and their application for solving heat transfer and mechanical problems* [in Polish], University of Technology Publishers pp. 360, Poznań 2000.

14. A. Maciąg and J. Wauer, *Solution of the two-dimensional wave equation by using wave polynomials*, J. Engrg. Math., **51**, 4, 339–350, 2005,

15. A. Maciąg, J. Wauer, *Wave polynomials for solving different types of two-dimensional wave equations*, Computer Assisted Mechanics and Engineering Sciences, **12**, 87–102, 2005.

16. A. Maciąg *Solution of the three-dimensional wave polynomials*, Mathematical Problems in Engineering, **5**, 583–598, 2005.

17. A. Maciąg, *Solution of the three-dimensional wave equation by using wave polynomials*, PAMM – Proc. Math. Mech., **4**, 706–707, 2004.

18. W. Nowacki, *Thermoelascity,* Pergamon Press, Oxford–Warsaw 1962.

19. M.J. Ciałkowski, M. Jarosławski, *Application of symbolic calculations in generating the solution of the wave equation* [in Polish], Zeszyty Naukowe Politechniki Poznańskiej nr 56, Maszyny Robocze i Transport, 2003.

20. M.J. Ciałkowski, A. Frąckowiak, *Application of symbolic operations to the determination of Trefftz functions for a heat flow wave equation* [in Polish], Zeszyty Naukowe Politechniki Poznańskiej nr 57, Maszyny Robocze i Transport, 2004.

21. M.J. Ciałkowski, *Thermal and related functions used in solving certain problems of mechanics. Part I - Solution of certain differential equations by means of inverse operations* [in Polish], Studia i materiały. Technika 3. Uniwersytet Zielonogórski, 7–70, 2003.

22. M.J. Ciałkowski, A. Frąckowiak, *Thermal and related functions in solving certain problems of mechanics. Part II – Effective determination of inverse operations applied to harmonic functions* [in Polish], Studia i materiały. Technika 3. Uniwersytet Zielonogórski, 71–98, 2003.

Received February 10, 2006.

ENGINEERING TRANSACTIONS • *Engng. Trans.* • **55**, 2, 155–180, 2007
Polish Academy of Sciences • Institute of Fundamental Technological Research

IMPROVEMENT OF HANDLING BY MEANS OF ACTIVE SUSPENSION CONTROL

T. R. O r i[1)], M. N. I c h c h o u[2)], P. P. G b a h a[1)], L. J e z e q u e l[2)]

[1)]**Institut National Polytechnique Houphouët Boigny**
Côte d'Ivoire

[2)]**Ecole Centrale Lyon**
France

Brake systems have become increasingly complex. They must not only slow down or stop a vehicle under extreme conditions within short distances, but also reduce the effort exerted by the driver. This phenomenon is difficult to approach because it depends on the vehicle's architecture. This is why, in this paper, the first part will give the basis for modelling of the complete vehicle including the frame and the tires, in a 3D format. A 2D control law model will be synthesized to obtain the best performances for road behaviour. This control law is based on the theory of Linear Quadratic control (LQ). It is also extended to cover the 3D vehicle model. The last part gives the numerical simulation results which demonstrate the effectiveness of this law for vehicle performances.

Key words: active suspensions, optimal control, brakes, vehicle dynamics, angular dynamics, comfort.

Notations

M_s	rigid body mass of half-car,
$M_{nsv},\ M_{nsr}$	masses respectively of the front axle and the rear axle,
$l_v,\ l_r$	distances from center of gravity to vehicle front wheel, respectively, and to vehicle rear wheel,
I_p	vehicle pitch inertia about center of gravity,
θ	vehicle pitch angle about center of gravity,
h	height of center of gravity from the road,
$z_{sv},\ z_{sr}$	vertical displacements, respectively of the front and the rear of the rigid body,
$\dot{z}_{sv},\ \dot{z}_{sr}$	vertical velocities, respectively of the front and the rear of the rigid body,
$z_{rv},\ z_{rr}$	vertical displacements respectively of the front and rear axle,
$\dot{z}_{rv},\ \dot{z}_{rr}$	vertical velocities, respectively of the front and rear axle,
$z_{tv},\ z_{tr}$	road displacements, respectively on the front and rear wheel,
$k_{sv},\ k_{sr}$	spring constant of the secondary suspensions, respectively front and rear,

$b_{sv},\ b_{sr}$	damping coefficients of the secondary suspensions, respectively front and rear,
$k_{tv},\ k_{tr}$	spring constant of the primary suspensions, respectively front and rear,
$b_{tv},\ b_{tr}$	damping coefficients of the primary suspensions, respectively front and rear,
$f_{av},\ f_{ar}$	friction forces ,respectively of the front and rear wheels,
$f_{zv},\ f_{zr}$	normal forces, respectively of the front and rear wheels,
$u_v,\ u_r$	active control forces, respectively of the front and rear wheels,
$x, \dot{x},\ \ddot{x}$	position, velocity and acceleration of the vehicle,
$w_{av},\ w_{ar}$	angular velocity, respectively of the front and rear wheels,
$\dot{w}_{av},\ \dot{w}_{ar}$	angular acceleration, respectively of the front and rear wheels,
$T_{bv},\ T_{br}$	front and rear disc brake torque, respectively,
$J_v,\ J_r$	inertias, respectively of the front and rear wheels,
r	effective tyre radius,

1. Introduction

Many theoretical and experimental works propose applications of optimal control theories for the active control of mechanical systems and structures vibrations. Several works, such as those of Karnopp [1, 2, 3], in the field of vehicle suspensions have made it possible to show the performances obtained by active systems for vehicle comfort and stability improvements.

The interesting results obtained by this type of work on vehicle suspensions led us to raise the question of its possible application to other problems. This study proposes to extend its use to the improvement of road behaviour. During the braking phase for example, there are longitudinal and transverse load transfers, causing pressure loss on certain wheels. It is necessary to add a supplementary load on each unloaded wheel and discharge those which are overloaded. According to the Coulomb law ($T = \mu.N$), if one manages to increase the normal force (N), the force of friction (T) should also increase. That would contribute to adding loads to the discharged wheels and to obtain good deceleration of the vehicle.

For the same purpose, several mechanisms have already been installed on road vehicles. These mechanisms, such as ABS (Anti-lock Braking System) and ESP (Electronic Stability Program), have proved their effectiveness in improving the stopping distance and handling of vehicles. In the braking field, car manufacturers and the scientific community have optimized the parameters of vehicles to obtain effective braking and optimal reduction to the braking distance. Since people drive ever faster, it would be interesting to develop an innovative system adapted to this trend in driver behaviour. This paper offers then a new concept which is able to increase safety and to improve handling, and which could be added to the existing powerful systems (ABS, ESP...).

In this contribution, we propose a method which consists in increasing the friction force between the tire and the road while acting on the suspension.

For this purpose, we use a control law which will act on some of the vehicle degrees of freedom. This action represents the behaviour of an actuator which increases the normal force on the contact surface (between the tyre and the road), and which will affect the frictional forces. A study conducted in France by the car manufacturer Renault, on the circumstances of accidents, revealed that 36% of accidents take place in a straight line, 18% at roads intersections and 46% in curves. The greatest share of accidents occur in curves because of instabilities caused by the action of the driver, or by external actions. Among the instabilities caused by external actions, one can consider two cases. In the first case, the vehicle is in low adherence zone (in a discontinuous manner). A loss can then occur in the tracking forces on one or more tyres, generating instability. In the second case, the vehicle can also be subjected to aerodynamic disturbances, generating an additional yaw motion which could be a source of instability. Concerning instabilities caused by the driver, it corresponds mainly to the situation in which the driver imposes two or several successive changes of direction of the vehicle. This case could occur when trying to avoid an obstacle, a change of lane in an urgent situation or at an intersection in the presence of another vehicle. We will use the latter example in our simulations because the suspensions are strongly strained.

The work offered here uses optimal control features, takes into account the existing knowledge in terms of vehicle dynamics in order to put them in operational form and applicable to the design problem of vehicles. Models were developed to design the control device and to simulate the operation of the system in order to evaluate the law of control. Considering the optimal control principles, we proposed an active control law for various cases of constraints. This law is meant to significantly improve vehicle handling. Simulations were carried out in the braking phase because the vehicle's suspension is also strained when avoiding an obstacle. The paper is organized as follows: Sec. 2 gives basic equations describing the vehicle dynamics. It includes all relevant components description and details. Section 3 discusses deeply the cost functional representing the optimal vehicle in terms of braking capacities and performances. Section 4 offers some numerical simulations and includes main situations in an attempt to check the robustness of the proposed solution. Section 5 concludes the paper.

2. Vehicle Dynamics Model

2.1. Vehicle dynamics concept

To understand the concepts which will be referred to in this paper, we introduce here some elementary notions related to vehicle dynamics. Two reference frames are needed. The first reference frame is related to the road. The second

reference is fixed at the mass center G of the vehicle. We define the angle of rolling as being the rotation around the longitudinal axis (GX), the angle of pitch as being the rotation around the transverse axis (GY) and the angle of yaw, like that of rotation, around the vertical axis (GZ).

It is important to define the variables which will characterize the state of the vehicle. Among them are the parameters which will be useful for the study of contact between the wheel and the ground and those concerning to the tyres. The angle between the tyre and the vertical axis is the steering angle (α) and the angle between the velocity vector and the longitudinal axis is the drift angle (γ).

To simplify and reduce the calculations for asymmetrical braking, we study the dynamic behaviour of a vehicle whose trajectory is circular.

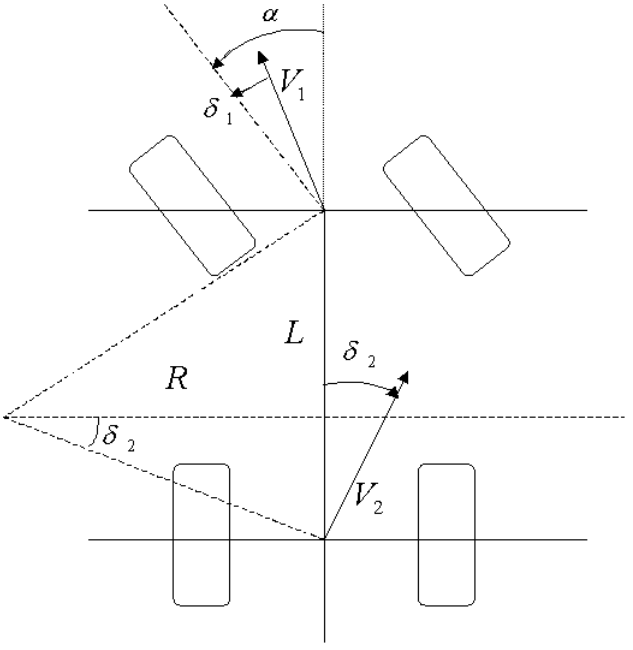

FIG. 1. Angular dynamics.

We assume in this model that the angles between the right wheel and the left wheel of the same axle are identical. δ_1 and δ_2 denote the drift angles of the right axle and the rear axle. δ is the drift angle at the mass center. If we impose a steering angle α, the vehicle runs in a circle whose radius is equal to $R = L/[\alpha - (\delta_2 - \delta_1)]$. If the drift angles of the right axle and the rear axle are known, the behaviour of the vehicle can be predicted. If $(\delta_2 - \delta_1) < 0$, the vehicle is oversteering or if $(\delta_2 - \delta_1) > 0$, the vehicle is understeering. And if $(\delta_2 - \delta_1) = 0$, the vehicle is on the trajectory.

If the vehicle is on a circular trajectory and we accelerate, if it is necessary to add steering to maintain the trajectory, the vehicle is understeering. On the other hand, if it is necessary to decrease steering, then the vehicle is oversteering. And there is a critical velocity beyond which the vehicle becomes unstable. It is necessary in this case to steer right in order to go left. This variation of angle, which characterizes the mode established in turns is called angular dynamics. Angular dynamics can be defined as being the partial derivative of the steering angle compared to transverse acceleration. Under these conditions, the vehicle remains on a circular trajectory of radius R at constant. The angular dynamics is expressed by:

$$da = \frac{d\alpha}{d\gamma_t}$$

where γ_t represents transverse acceleration. The sign of angular dynamics gives then the character of the vehicle. In order to simulate the behaviour of the tyres on a road, it is essential to know their characteristics. We introduce the concept of sliding. Sliding g represents a percentage. If the wheel is blocked and the vehicle is not stopped, then the sliding is equal to – 100%. But if the wheel slips and the vehicle is stopped, then the sliding is equal to 100%. For good adherence, Fig. 2 resulting from Pacejka's tyre model shows that friction force is maximum when sliding is around 10%.

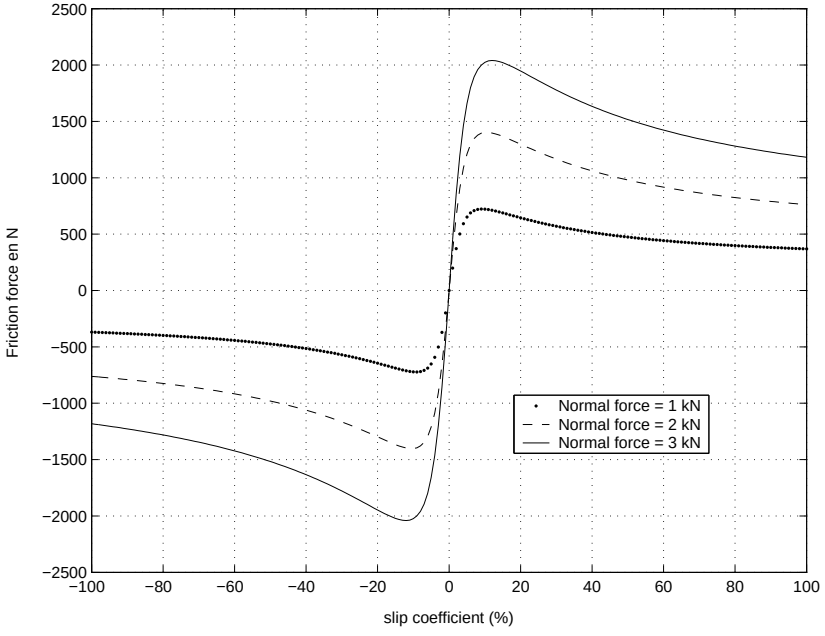

Fig. 2. Friction force according to the slip coefficient.

All the forces of the ground acting on the tyre can be divided into three principal components: F_x represents the trail of braking when the force is opposed to the wheel movement (during braking) or acceleration when it goes in the direction of the movement, F_y is the lateral force of guiding. It is related to the value of pneumatic drifts. F_z is the vertical load which acts on the tyre. It depends on the static weight of the vehicle but also on its dynamic state. It is greatly influenced by the transfers of load during acceleration, braking or curves.

2.2. Model and equations of the vehicle

This model [4, 5] includes the rigid mass of the vehicle's body and the four unsprung masses. It has 22 degrees of freedom, $(x_G,\ y_G,\ z_G,\ \theta,\ \varphi,\ \psi)$ for the vehicle's body, $(x_{ij},\ y_{ij},\ z_{ij})$ for each unsprung mass and (w_{ij}) for each wheel in rotation. We can simulate the dynamic behaviour of a vehicle in real time using this model. Thus, it facilitates experimentation on controlled frame systems using a control simulator, integrating the reactions of a real driver.

The index $i = 1$ is for the front wheel-axle unit, $i = 2$ is the rear wheel-axle unit. The index $j = 1$ is for the left-hand side, and $j = 2$ for the right-hand side.

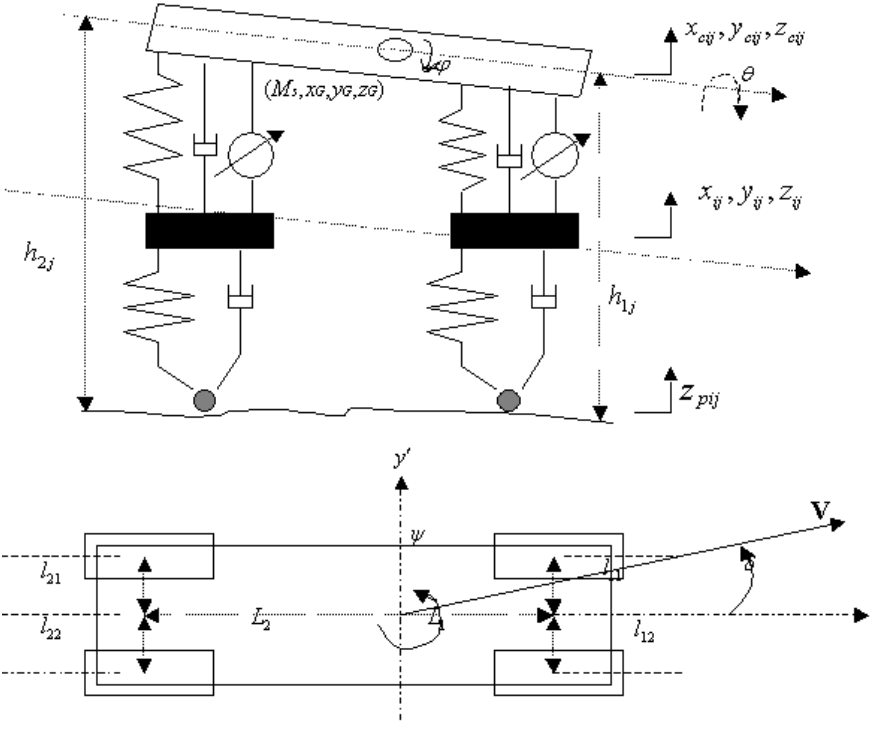

FIG. 3. Model of the complete vehicle.

2.2.1. Rigid mass of the vehicle. To determine the general equations of the model's movements in 3D, we used Lagrange equations [6]. Thus the equations of the vehicle's body are :

$$I_{x'x'}\frac{\partial^2\theta_G}{\partial t^2} = \sum_{i=1}^{2}(l_{i1}Fz_{i1} - l_{i2}Fz_{i2}) + \sum_{i,j=1}^{2} h_{ij}Fy_{ij} + M.g.h * \sin\theta, \tag{2.1}$$

$$I_{y'y'}\frac{\partial^2\varphi_G}{\partial t^2} = \sum_{j=1}^{2}(L_2Fz_{2j} - L_1Fz_{1j}) - \sum_{i,j=1}^{2} h_{ij}Fx_{ij}, \tag{2.2}$$

$$I_{z'z'}\frac{\partial^2\psi_G}{\partial t^2} = \sum_{i=1}^{2}(l_{i2}Fx_{i2} - l_{i1}Fx_{i1}) + \sum_{j=1}^{2}(L_1Fy_{1j} - L_2Fy_{2j}). \tag{2.3}$$

For the unsprung masses $(i, j = 1, 2)$, we can write:

$$M_{nsij}\ddot{z}_{ij} = -C_{sij}(\dot{z}_{ij} - \dot{z}_{cij}) - k_{sij}(z_{ij} - z_{cij}) - k_{pij}(z_{ij} - z_{pij}) - F_{aij}, \tag{2.4}$$

where F_{aij} represents the active force element to be controlled, F_{xij}, F_{yij} and F_{zij} represent the suspension forces under the wheels according to (Gx'),(Gy') and (Gz')axis of reference $R'(G, x', y', z')$ related to the vehicle mass center, C_{sij} represents the damping of the secondary suspensions, k_{si} and k_{pi} are respectively the stiffnesses of the secondary suspensions and the primary suspensions. $I_{x'x'}$, $I_{y'y'}$, $I_{z'z'}$ are respectively the inertias of the rigid body according to the axes of the $R'(G, x', y', z')$ reference related to the mass center of the vehicle. h_{1j} and h_{2j} are respectively the vertical distances from the ground to the axis of rolling at the front wheel-axle unit and the rear wheel-axle unit and h represents the vertical distance from the ground to the center of gravity of the unsprung mass. L_1 and L_2 are respectively the horizontal distances from the gravity center to the axis of rolling at the front wheel-axle unit and the rear wheel-axle unit and l_{ij} are the distances between the rolling axis and the vertical one which passes through the gravity center of each unsprung mass. M_s and M_{nsij} are respectively the masses of the rigid body and the unsprung masses ij. θ, φ and ψ are respectively the angle of roll, the angle of pitch and the angle of yaw of the rigid body. z_{pij} is the vertical road displacement and g is gravity.

The equations of the inertia center of the vehicle's movement which are obtained from the fundamental relation of dynamics are:

$$M.\ddot{x}_G - M.\dot{\psi}\dot{y}_G = \sum_{i,j=1}^{2} F_{xij}, \tag{2.5}$$

$$M.\ddot{y}_G + \dot{\psi}\dot{x}_G = \sum_{i,j=1}^{2} F_{yij}, \tag{2.6}$$

$$M.\ddot{z}_G = \sum_{i,j=1}^{2} F_{zij} - M * g, \tag{2.7}$$

with

$$M = M_s + \sum_{i,j=1}^{2} M_{nsij}.$$

The velocities of the gravity center in the reference R' are expressed by:

$$\begin{cases} \dot{x}_G = V.\cos\delta, \\ \dot{y}_G = V.\sin\delta, \end{cases}$$

and accelerations after linearization are:

$$\begin{cases} \ddot{x}_G = \dot{V}(1-\delta^2/2) - V\ \dot{\delta}\ \delta - \dot{\psi}\ V\delta, \\ \ddot{y}_G = \dot{V}\delta + V\ \dot{\delta} + \dot{\psi}\ V, \end{cases}$$

where δ represents the drift of the pneumatic and V represents the longitudinal velocity of the vehicle.

To study the vehicle's displacement in 3D, it is imperative to define a reference frame in which one will be able to consider the displacements in a straight line, but also the movements of yaw, pitch and roll. The selected references are: $R(\omega, x, y, z)$, the direct and fixed Galilean reference frame which is related to the ground reference frame. $R(G, x', y', z')$, the reference frame related to the mass center of the vehicle and obtained by rotation of angle ψ around the axis (G, z'). $R''(G, x'', y'', z'')$, the reference frame related to the mass center of the vehicle and obtained by rotation of angle φ around the axis (G, y''). And $R'''(G, x''', y''', z''')$, the reference frame related to the mass center of the vehicle and obtained by rotation of angle θ around the axis (G, x''').

The dynamic equations of the vehicle are established in the reference frame R'''. These equations are then expressed in the reference frame R, by using a matrix of passage P, linearized to the first order.

$$\mathbf{P} = \begin{pmatrix} 1 & -\psi & \varphi \\ \psi & 1 & -\theta \\ -\varphi & \theta & 1 \end{pmatrix}.$$

These equations are those of vehicle's body.

2.2.2. Wheels. The model of tyres used is a Pacejka model [7, 8], which allows the representation of tyre behaviour by taking account of the longitudinal/transverse coupling. The angles which we will refer to are those which are necessary for Pacejka's model and used for simulation. $(G,\ x_r,\ y_r,\ z_r)$ represents the reference frame of the wheel.

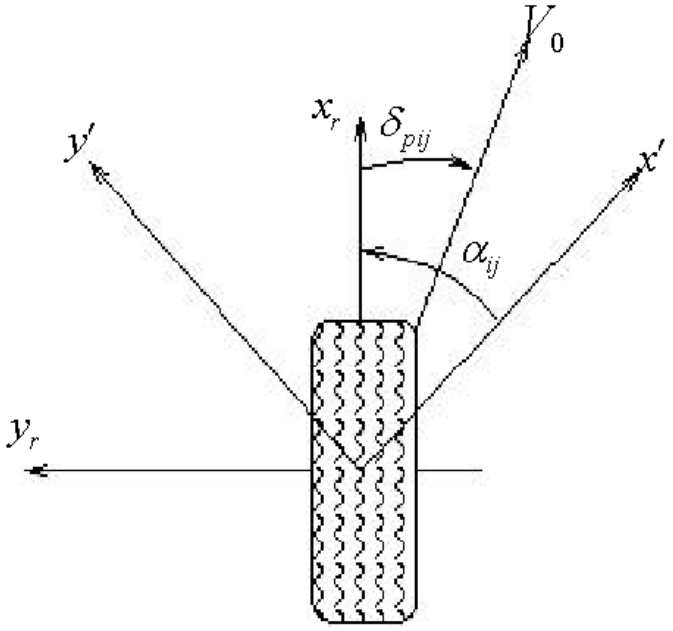

FIG. 4. Diagram of the tyre seen from above.

The pneumatic drifts (δ_{pij}) are expressed in the following way:

$$\delta_{pij} = \arctan\left(\frac{\vec{V}_0.\vec{y}_r}{\vec{V}_0.\vec{x}_r}\right) - \alpha_{ij} \tag{2.8}$$

where α_{ij} is the steering of the wheel's direction caused by the driver. The vertical efforts under each wheel are expressed in the following way

$$F_{zij} = -k_{pij}(z_{ij} - z_{pij}) - c_{pij}(\dot{z}_{ij} - \dot{z}_{pij}) + F_{zsij}, \tag{2.9}$$

where F_{zsij} is the static effort due to the load under each wheel. The forces given in the reference frame of each wheel are those of Pacejka's model. The passage of the efforts in the wheel reference frame to the frame R' is expressed as follows:

$$F_{xrij} = F_{xij}\cos\alpha_{ij} - F_{yij}\sin\alpha_{ij}, \tag{2.10}$$

$$F_{yrij} = F_{yij}\cos\alpha_{ij} + F_{xij}\sin\alpha_{ij}. \tag{2.11}$$

The pneumatic slip is defined by the following relation:

$$g = \begin{cases} \dfrac{(R.w - V) * 100}{V} & \text{if} \quad R.w < V, \\ \dfrac{(R.w - V) * 100}{R.w} & \text{if} \quad R.w > V. \end{cases} \tag{2.12}$$

All these equations enabled us to develop a software to simulate the road behaviour of a vehicle.

2.3. Description of the simulation software

The system is integrated in a simulation environment consisting of a complete model of the vehicle and is called VDS (Vehicle Dynamics Software). This model was developed by the structures and systems dynamics team of the Ecole Centrale de Lyon. This model enables simulation of the dynamic behaviour of a vehicle in real time, and thus allows experimentation on the frame using a control simulator, integrating the reactions of a real driver and the aerodynamics.

The model of tyre is also integrated in the tool for simulation and it takes account of the longitudinal/transverse coupling. The simulation tool was developed under MATLAB/Simulink.

3. Control laws developments

The objective of control is to find a suitable law to increase the normal force. We therefore minimize the vertical quadratic acceleration of the front and rear hubs and we limite the energy contribution necessary for control.

The parameters obtained for the front wheel on the 2D model is placed on the two front wheels of the 3D model. We proceed in the same way for the rear wheels. This is why the study of the control law was carried out on a 2D model.

The front and rear normal forces depend on movements in the vertical plane, which is the case of the displacements of the rigid body and the unsprung masses. We then separate the entry vector into two state vectors, one with the elements moving vertically and the other with the elements moving horizontally.

3.1. Model used

This model [9, 10, 11] of vehicle is composed of three rigid bodies. The suspended mass represents the rigid body and the two unsprung masses represent the front and rear axles. This model includes 9 (DOF) degrees of freedom: three degrees of freedom for the rigid body ($x,\ z,\ \theta$), two degrees of freedom for each unsprung mass ($x,\ z$), one degree of freedom for the rotation (w) of each wheel.

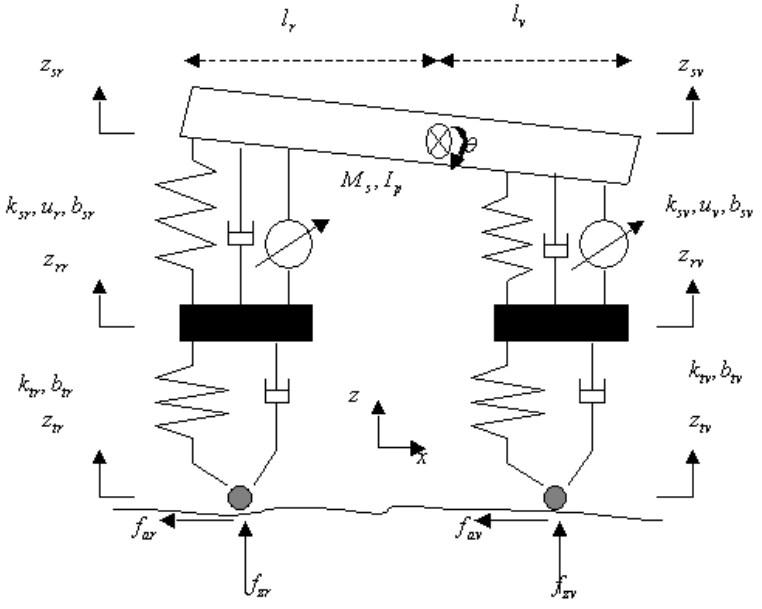

FIG. 5. Half car model.

The dynamic system can be expressed in the following form:

In the vertical plane,

$$\dot{Z} = A_1.Z + B_1.U + B_2(Z).F + B_3.W \tag{3.1}$$

with $A_1(8*8)$, $B_1(8*2)$, $B_2(8*2)$ as a function Z and $B_3(8*4)$.

In the horizontal plane,

$$\dot{X} = A_2.X + B_4.F + D.T \tag{3.2}$$

with $A_2(6*6)$,$B_4(6*2)$ and $D(6*2)$.

The vectors $\mathbf{X}$ and $\mathbf{Z}$ are:

$$\mathbf{X} = \begin{pmatrix} x \\ \dot{x} \\ w_{av} \\ \dot{w}_{av} \\ w_{ar} \\ \dot{w}_{ar} \end{pmatrix}, \qquad \mathbf{Z} = \begin{pmatrix} z_{sv} - z_{rv} \\ \dot{z}_{sv} \\ z_{rv} - z_{tv} \\ \dot{z}_{rv} \\ z_{sr} - z_{rr} \\ \dot{z}_{sr} \\ z_{rr} - z_{tr} \\ \dot{z}_{rr} \end{pmatrix}.$$

The choice of vectors was made for a suitable search for our control law, which constitutes an important stage of this study.

3.2. Expression of the criterion

The control law [12, 13] that we formulate is based on the minimization of a quadratic criterion for a linear dynamic system. This control provides the expression of the optimal forces according to the state variables of the system. Knowing the performance criterion and the equations of the system, we are able to identify the optimal forces to be applied for better road behaviour, regardless of the constraints related to the road state and the stochastic nature of the disturbances.

The variables to be minimized in our model are of two types: accelerations of the unsprung masses ($\ddot{z}_{rv}$ and $\ddot{z}_{rr}$), which would isolate the vehicle cockpit from irregularities in the road, thus making it possible to improve comfort of the passenger, and vertical displacements of the suspensions ($z_{sv} - z_{rv}$) and ($z_{sr} - z_{rr}$). To optimize the energy contribution necessary for the control forces, we have added the expressions J_5 and J_6 in the criterion of performance defined below. We define the criterion of performance as follows [14]:

J_1,J_2: being the quadratic evaluation of the front and rear accelerations respectively weighting the constants q_1 and q_2.

$$J_1 = \lim_{T\to\infty} \frac{1}{T}\, E \int_0^T q_1(\ddot{z}_{rv})^2 dt \tag{3.3}$$

$$J_2 = \lim_{T\to\infty} \frac{1}{T}\, E \int_0^T q_2(\ddot{z}_{rr})^2 dt \tag{3.4}$$

J_3,J_4: averages of squares of relative displacements between the rigid body and the axle, balanced respectively at the front and rear by the constants q_3 and q_4.

$$J_3 = \lim_{T\to\infty} \frac{1}{T}\, E \int_0^T q_3(z_{sv} - z_{rv})^2 dt \tag{3.5}$$

$$J_4 = \lim_{T\to\infty} \frac{1}{T}\, E \int_0^T q_4(z_{sr} - z_{rr})^2 dt \tag{3.6}$$

J_5,J_6: these terms are useful for limiting the control forces $u_v(t)$, $u_r(t)$ and thus controlling the strain energy of the suspension.

$$J_5 = \lim_{T\to\infty} \frac{1}{T}\, E \int_0^T \rho_v(u_v)^2 dt \tag{3.7}$$

$$J_6 = \lim_{T\to\infty} \frac{1}{T}\, E \int_0^T \rho_r(u_r)dt. \tag{3.8}$$

The coefficients ρ_v, ρ_r and q_i $(i = 1, ..., 4)$ are numerical constants whose values give predominance to one or the other of the performances to be achieved. The expression of the criterion will thus be

$$J = \sum_{i=1}^{6} J_i.$$

The square averages of these accelerations reveal a coupling and the index of performance can then be put in the form

$$J = \lim_{T\to\infty} \frac{1}{T}\, E \int_0^T (U^T.R.U + X^T.Q.X + 2.X^T.N.U)dt. \tag{3.9}$$

with

$$\mathbf{Q} = \begin{pmatrix} q_3 + q_1.a_1^2 & a_1.a_2.q_1 & a_1.a_3.q_1 & a_1.a_4.q_1 & 0 & 0 & 0 & 0 \\ a_1.a_2.q_1 & q_1.a_2^2 & a_2.a_3.q_1 & a_2.a_4.q_1 & 0 & 0 & 0 & 0 \\ a_1.a_3.q_1 & a_2.a_3.q_1 & q_1.a_3^2 & a_3.a_4.q_1 & 0 & 0 & 0 & 0 \\ a_1.a_4.q_1 & a_2.a_4.q_1 & a_3.a_4.q_1 & q_1.a_4^2 & 0 & 0 & 0 & 0 \\ 0 & 0 & 0 & 0 & q_4 + q_2.a_5^2 & a_5.a_6.q_2 & a_5.a_7.q_2 & a_5.a_8.q_2 \\ 0 & 0 & 0 & 0 & a_5.a_6.q_2 & q_2.a_6^2 & a_6.a_7.q_2 & a_6.a_8.q_2 \\ 0 & 0 & 0 & 0 & a_5.a_7.q_2 & a_6.a_7.q_2 & q_2.a_7^2 & a_7.a_8.q_2 \\ 0 & 0 & 0 & 0 & a_5.a_8.q_2 & a_6.a_8.q_2 & a_7.a_8.q_2 & q_2.a_8^2 \end{pmatrix},$$

$$\mathbf{R} = \begin{pmatrix} \rho_v + q_1.a_{10}^2 & 0 \\ 0 & \rho_r + q_2.a_9^2 \end{pmatrix}, \qquad \mathbf{N} = \begin{pmatrix} a_1.a_{10}.q_1 & 0 \\ a_1.a_{10}.q_1 & 0 \\ a_1.a_{10}.q_1 & 0 \\ a_1.a_{10}.q_1 & 0 \\ 0 & a_5.a_9.q_2 \\ 0 & a_5.a_9.q_2 \\ 0 & a_5.a_9.q_2 \\ 0 & a_5.a_9.q_2 \end{pmatrix},$$

$$a_1 = -ksv/M_{nsv}; \qquad a_6 = -bsr/M_{nsr};$$
$$a_2 = -bsv/M_{nsv}; \qquad a_7 = -ktr/M_{nsr};$$
$$a_3 = -ktv/M_{nsv}; \qquad a_8 = (bsr - btr)/M_{nsr};$$
$$a_4 = (bsv - btv)/M_{nsv}; \qquad a_9 = 1/M_{nsr};$$
$$a_5 = -ksr/M_{nsr}; \qquad a_{10} = 1/M_{nsv}.$$

The values used in the calculation of the criterion are given below [15]:

$$M_s = 730.0 \text{ kg}, \qquad I_p = 1230.0 \text{ kg.m}^2,$$
$$r = 0.3 \text{ m}, \qquad J_v = 1.4 \text{ kg.m}^2,$$
$$J_r = 1.0 \text{ kg.m}^2, \qquad k_{sv} = 19960.0 \text{ N/m},$$
$$k_{sr} = 17500.0 \text{ N/m}, \qquad b_{sv} = 1050.0 \text{ N.s/m},$$
$$b_{sr} = 900.0 \text{ N.s/m}, \qquad l_v = 1.011 \text{ m},$$
$$l_r = 1.803 \text{ m}, \qquad h = 0.508 \text{ m},$$
$$M_{nsv} = 40.0 \text{ kg}, \qquad M_{nsr} = 35.0 \text{ kg},$$
$$k_{tv} = 175500.0 \text{ N/m}, \qquad k_{tr} = 175500.0 \text{ N/m},$$
$$b_{tv} = 1500.0 \text{ N.s/m}, \qquad b_{tr} = 1500.0 \text{ N.s/m}.$$

The determination of the elements $u_v(t)$ and $u_r(t)$ and the law of control consists of finding the matrix which is the solution of the Riccati equation below:

$$P(t).A_1 + A_1^T.P(t) + Q - P(t).B_1.R^{-1}.B_1^T.P(t) = 0 \tag{3.10}$$

where P, Q and R are defined, symmetrical and positive matrices. The command which minimizes this criterion of performance is :

$$U(Z,t) = G(t).Z(t) \quad with \quad G(t) = -R^{-1}.B_1^T.P(t) \tag{3.11}$$

Elements $u_v(t)$ and $u_r(t)$ are written in the form:

$$\begin{pmatrix} u_v \\ u_r \end{pmatrix} = G.Z.$$

Generally, the development of a suspension is a compromise between the minimization of two variables (acceleration and vertical displacement), but the minimization of vertical displacement does not appear on the same level. So the choice of the ponderation coefficients, and thus of the optimal law, determines the control performance. As there is no suitable criterion for determining the

parameters, their adjustment is thus made in a dichotomic way. For the law of control, we choose the ponderation coefficients with the following values:

$$\rho_v = 1.75.10^{-9}, \quad \rho_r = 1.75.10^{-9},$$
$$q_1 = 10^{-8}, \quad q_2 = 10^{-8}, \quad q_3 = 0.9, \quad q_4 = 2.1,$$

We then examine the shape of the curves to decide on the effectiveness of the law of control.

4. Simulation

Active suspension control is intended to help the driver to deal with extreme driving situations generally leading to a loss of control of the vehicle, and thus an accident. Extreme situations targeted by a trajectory control system are for light vehicles, in the case of under and over-steering. The system equipped with an active suspension has to keep the vehicle on its trajectory, materialized by the steering wheel and guided by the driver. The command law synthesized in the previous paragraph was integrated on a vehicle. Among the emergency situations studied, we present the one which consists of avoiding an obstacle and then we will compare the behaviour of the active suspension-equipped vehicle with the behaviour of the one without such a system.

4.1. Skirting–cutting in

In the following, simulations correspond to the voluntary behaviour of the driver when an obstacle suddenly appears, as shown below (Fig. 6). The vehicle rolls at a speed of 130 km/h. On seeing the obstacle, the driver brakes one second later, steering the driving wheel to the left at a 60 degrees angle, then steers back to put the vehicle on its initial trajectory again.

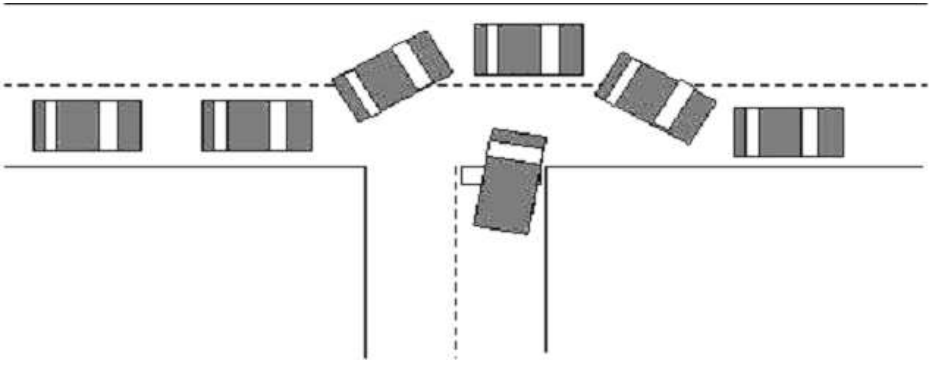

Fig. 6. The driver's maneuver.

During maneuvering the driver keeps his foot on the brake. This occurs with good grip corresponding to a dry road. The results obtained for vertical suspension control (as shown in Figures b) are compared with those without control (as shown in Figures a).

4.2. Results

Responding automatically to the driver's instruction, the vehicle is decelerated by pressing the brakes to around -9 m/s^2. This strong deceleration happens abruptly and leads to a loss of grip. The loss of grip decreases the braking. This leads to a loss of longitudinal deceleration (γ_x) after 3 seconds (Fig. 7a) in favour of acceleration (γ_y). While in Fig. 7b, the longitudinal deceleration (γ_x) of the controlled vehicle holds until the end of the maneuvering and the side acceleration is near zero after 3.5 seconds. Under these conditions, the vehicle equipped with active suspensions will follow the desired trajectory more easily and its wheels will transmit the lateral effort to the ground.

When the driver steers the wheel to the left, a lateral load transfer occurs which tends to unload the left-hand front and rear wheels in favour of the right-hand front and rear wheels. And braking generates a transfer of longitudinal load from the rear wheels to the front ones. The left rear wheel, unloaded from a large share of its load, is then on the verge of losing contact with the road. This wheel cannot therefore transmit any effort to the ground and for severe decelerations (> -8 m/s^2), it quickly locks (Fig. 8a).

The right-hand rear wheel, partly unloaded from its load by the longitudinal transfer, also locks equally during the braking phase. The wheel cannot compensate the transversal effort lost at the level of the left rear wheel.

With the deceleration imposed by the driver of the non-controlled vehicle, the longitudinal transfer generates an additional overload on the right front wheel which saturates completely. Longitudinal friction forces are thus stronger (Fig. 11a). The left front wheel unloaded during the turn receives the same braking order as the right front wheel. Under these conditions, the left front wheel blocks itself quite quickly ($slipping = -100\%$) and thus cannot transmit any lateral effort. The right front wheel, saturated and greatly longitudinally stressed, cannot provide enough lateral effort to compensate the blocking of the left front wheel. All four wheels are then blocked (Fig. 8a).

The active force synthesized by the control law and drawn in Fig. 8c, instantly balances the load of the suspended mass by adding an additional load when a wheel becomes unloaded, and by releasing the wheel when it is saturated.

Through its action, the active force allows the left front and rear wheels to return to a slip value (-10%) easing the driver's maneuvering.

a)

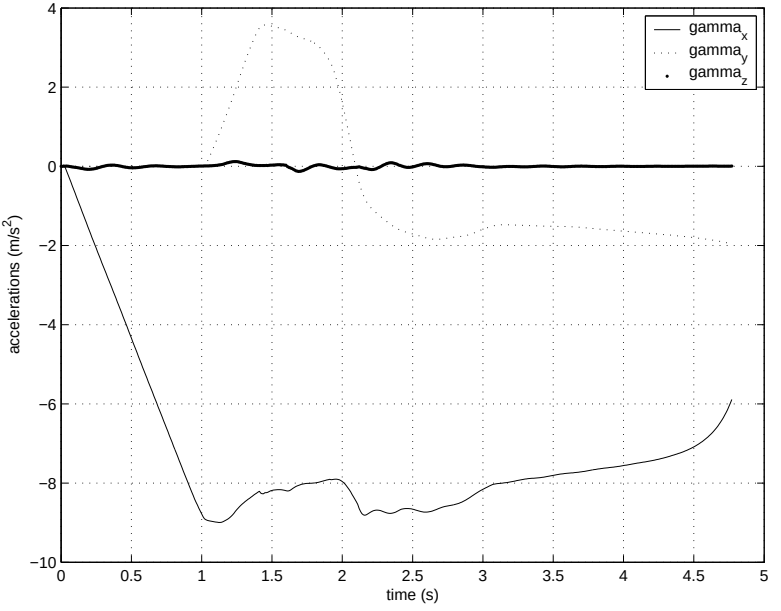

b)

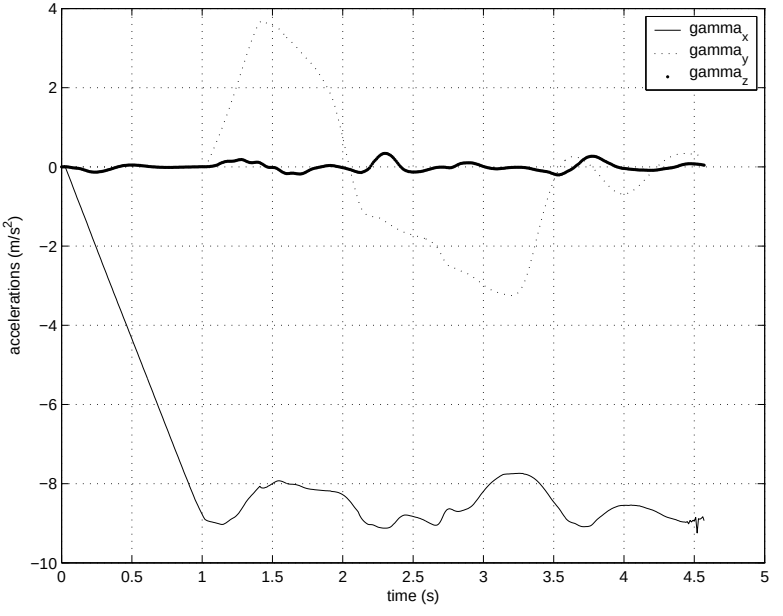

FIG. 7. a) Accelerations of non-controlled vehicle; b) Accelerations of controlled vehicle.

a)

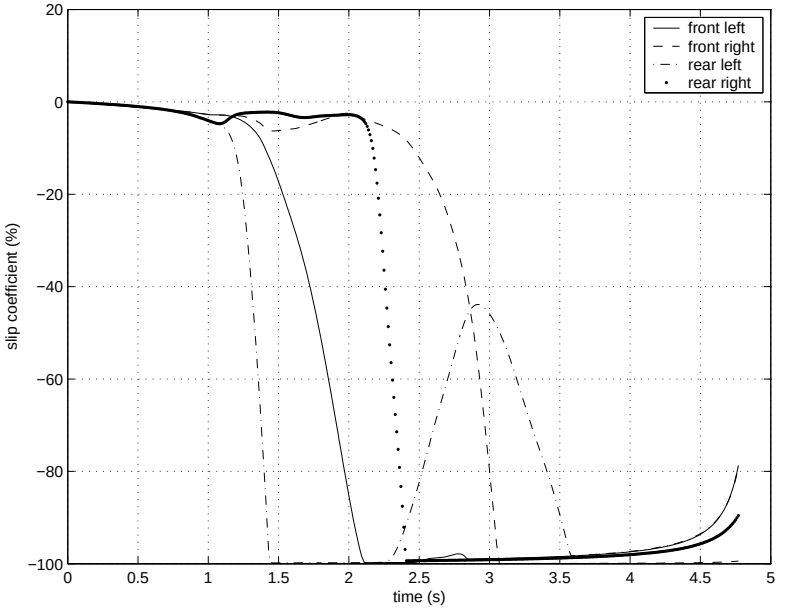
front left
front right
rear left
rear right
slip coefficient (%)
time (s)
20
0
−20
−40
−60
−80
−100
0
0.5
1
1.5
2
2.5
3
3.5
4
4.5
5

b)

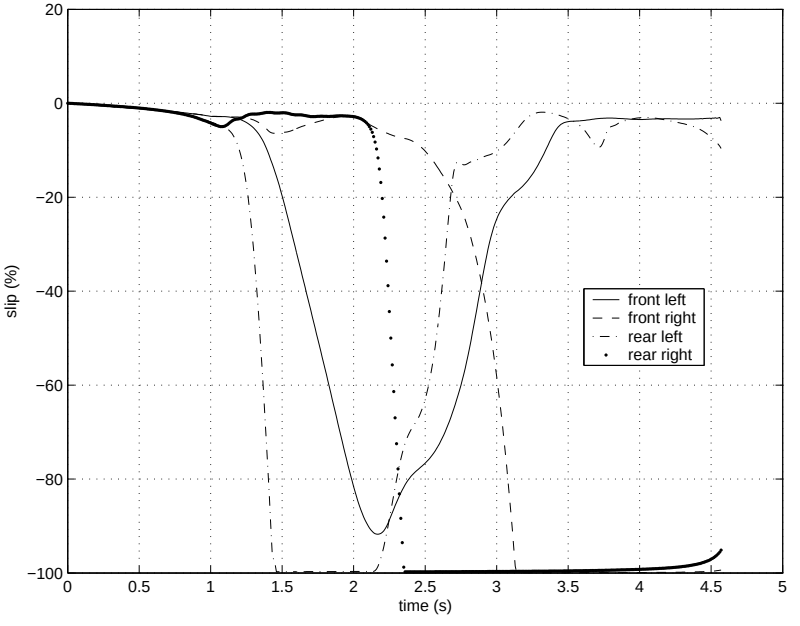
front left
front right
rear left
rear right
slip (%)
time (s)
20
0
−20
−40
−60
−80
−100
0
0.5
1
1.5
2
2.5
3
3.5
4
4.5
5

[Fig. 8a,b].

c)

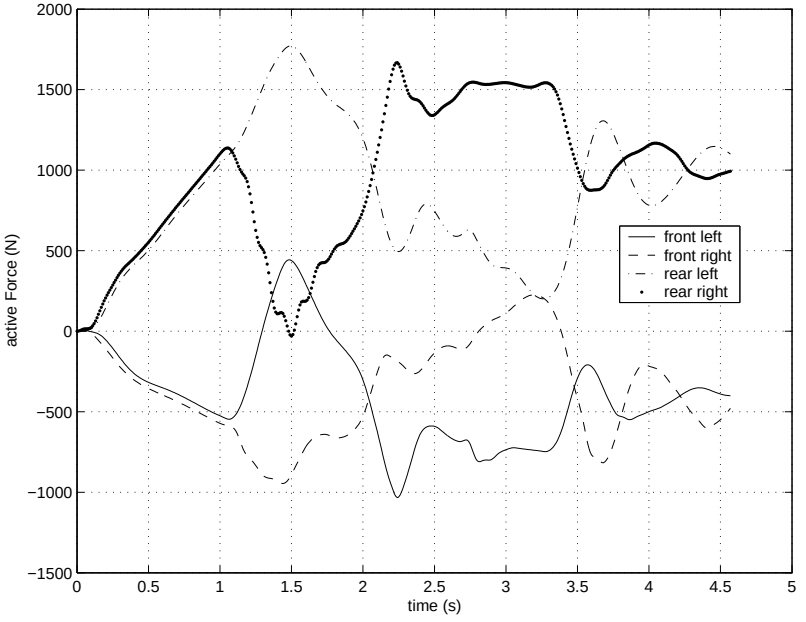

FIG. 8. a) Slip coefficient of non-controlled vehicle; b) Slip coefficient of controlled vehicle; c) Active force

Figure 9a shows the roll, pitch and yaw angles of the uncontrolled vehicle and Fig. 9b displays the same angles for the controlled vehicle. The roll on the controlled vehicle is lower than on the non-controlled one. This result means that the lateral load transfer is lower on our controlled vehicle. It is also the case for pitch which is lower on the controlled vehicle. This decreases the longitudinal load transfer. The front wheels will thus be less loaded and the rear ones less unloaded. The reduction of roll and pitch increases the vehicle stability, makes it more confortable and enables better braking thanks to better distribution of the load on the wheels.

When we analyze the rotation around axis (Gz) during the maneuver, the controlled vehicle has less yaw at the end of the maneuver, than the vehicle without control. This means that the non-controlled vehicle is far from the initial direction of its movement. The driver will have more difficulty putting his vehicle back to its initial direction. This generates a large lateral drift of the vehicle's center of gravity (Fig. 10a). Whereas the controlled vehicle has a lower drift angle at the center of gravity (Fig. 10b). It will be easier for the driver in this case to return to the initial direction of his movement.

a)

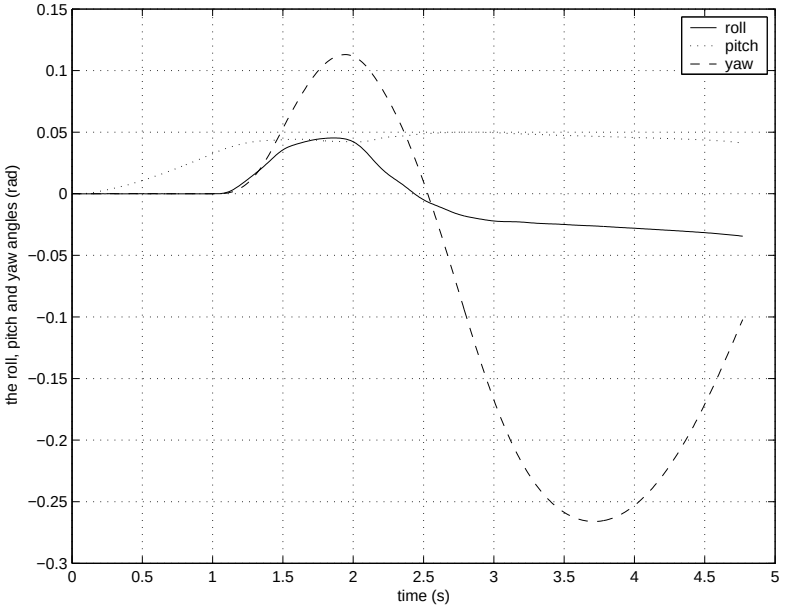

b)

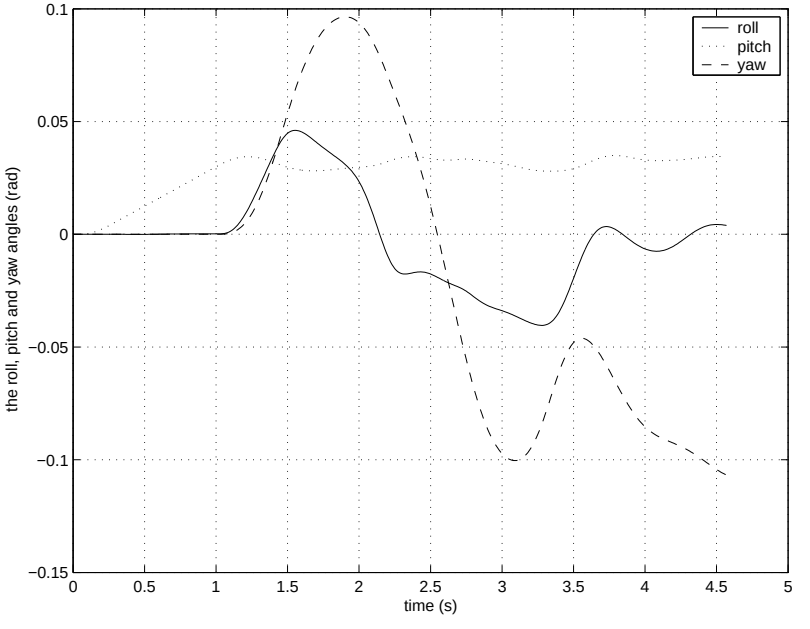

FIG. 9. a) Angles of non-controlled vehicle; b) Angles of controlled vehicle.

a)

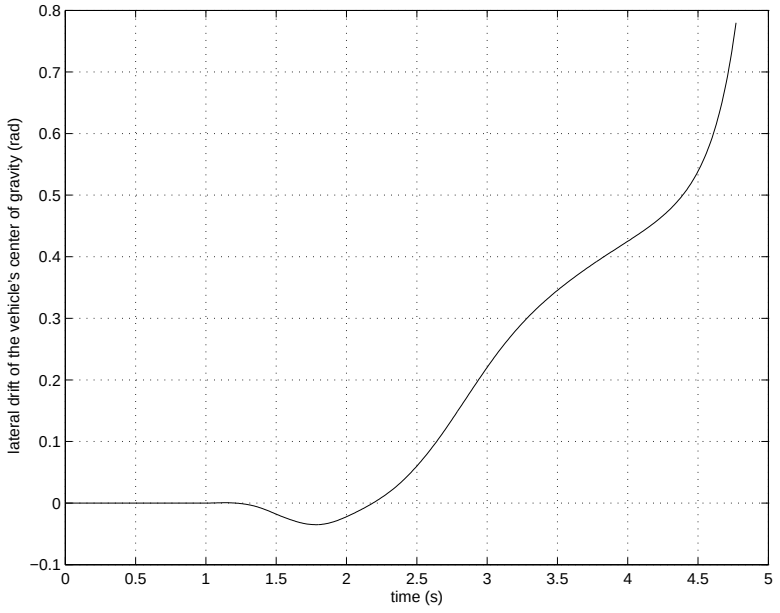

b)

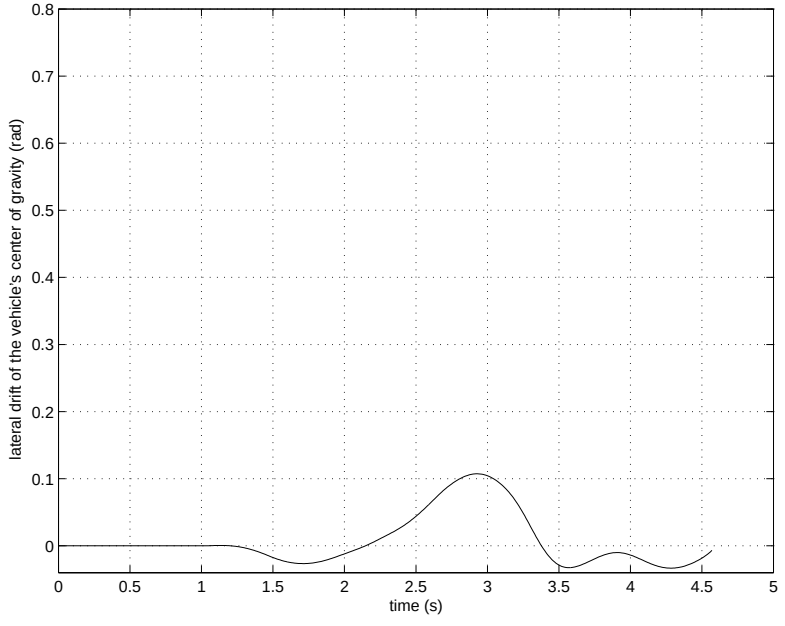

FIG. 10. a) Non-controlled vehicle: lateral drift of vehicle's center of gravity; b) Controlled vehicle: lateral drift of vehicle's center of gravity.

Longitudinal transfer during braking saturates the front wheels and unloads the rear ones. Furthermore, light vehicle manufacturers tend to load the front more than the rear. The friction of the front wheels becomes greater than that of the rear wheels (Fig. 11a and Fig. 11b).The exponential increase of drift at the center of gravity and the locking of the wheels of the non-controlled vehicle lead to an important loss of friction forces of the front wheels (Fig. 11a).

In Fig. 11b it can be seen that the longitudinal braking of the controlled vehicle is not decreased. This is caused by a decrease of the slip of the left front wheel and also to a hold of the transverse acceleration at around 0 $\mathrm{m/s^2}$.

For the vehicle without control, all wheels are locked, the center of gravity drift is high and the longitudinal deceleration is impaired. Under these conditions, the vehicle will have great difficulty responding to the driver's orders. The controlled vehicle holds its longitudinal deceleration until the end of the maneuver. Moreover, the drift at the center of gravity is lower than in the case of the non-controlled vehicle. The left front and rear wheels do not lock and so they compensate the locking of the two other wheels to ensure the trajectory desired by the driver.

In Fig. 12, the trajectories seen in the two previous cases are superposed.

The non-controlled vehicle cannot respond to the driver's orders. It moves 4 m sideways, which can cause it to leave the road. Whereas the controlled vehicle perfectly follows the desired trajectory.

a)

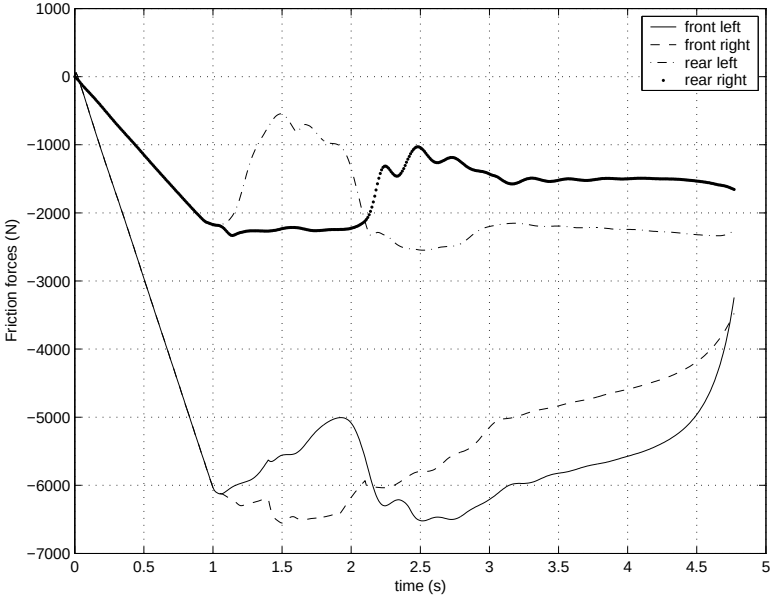

[Fig. 11a].

b)

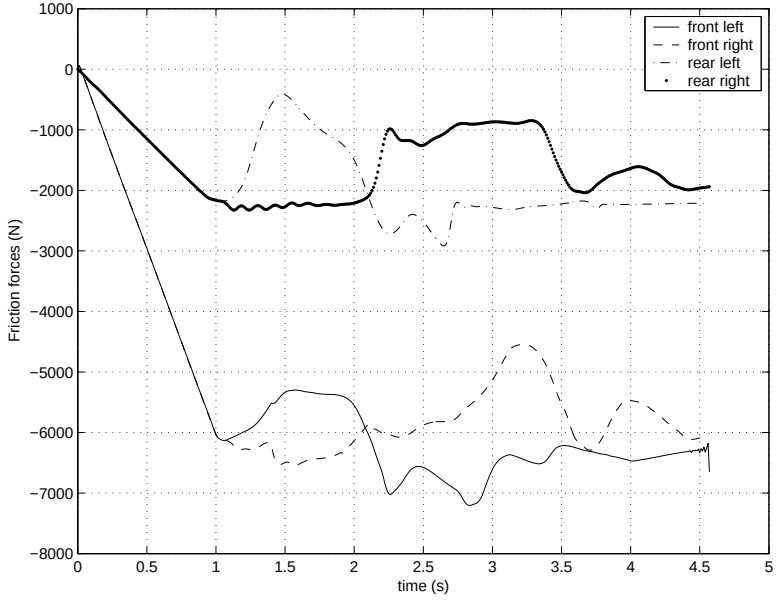

FIG. 11. a) Friction forces of non-controlled vehicle; b) Friction forces of controlled vehicle.

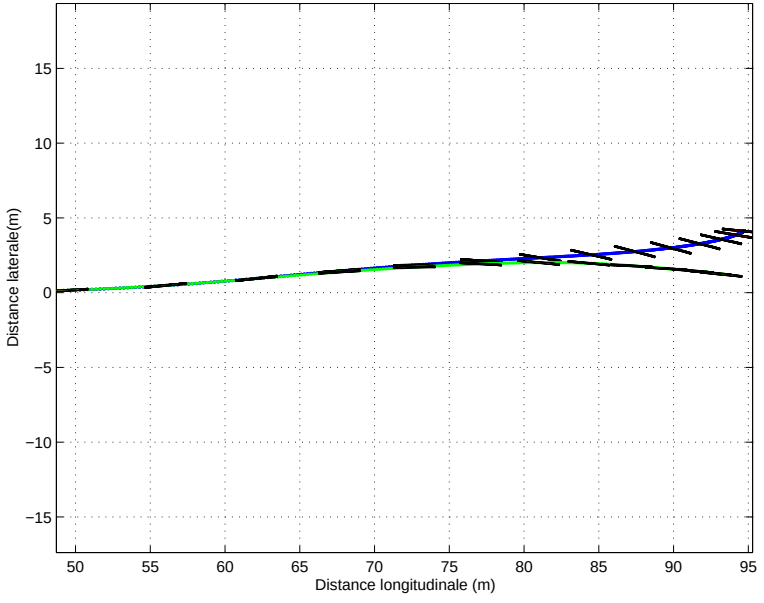

FIG. 12. Vehicle's trajectories.

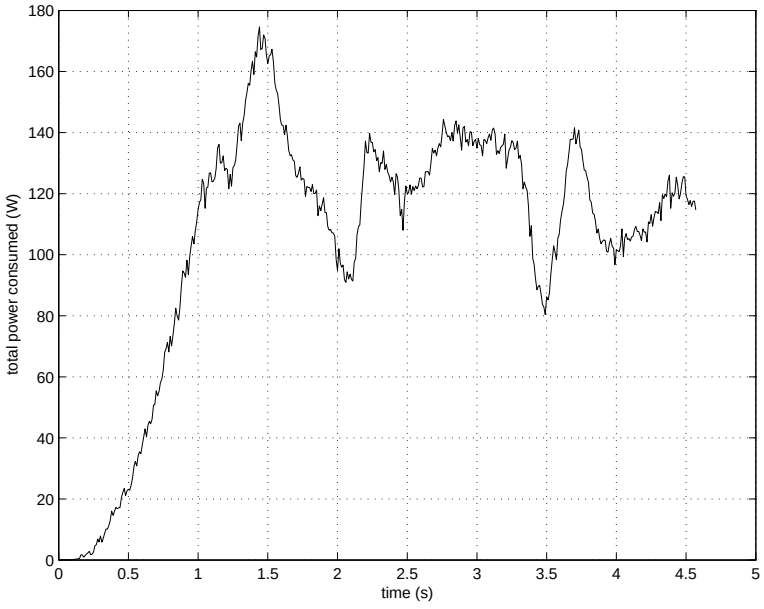

Fig. 13. Total power consumed.

Figure 13 shows the total instant power consumed by the four wheels during the maneuver.

It never exceeds 200 W, what is very reasonable. Energy consumption is a primary factor if the system is to be put in use because current vehicles occasionally have high consumption levels. A system adding greatly to energy consumption has little chance of acceptance.

Many maneuver simulations have been conducted, notably while turning or driving in a straight line. The results of all these trials show that the controlled suspension system gives a better trajectory hold and better respect of the angle order of the steering wheel, with low friction, which is a clear ad-vantage.

5. Conclusion and perspectives

In this study we have analyzed, modelled and simulated an active suspension to improve the traction of a car during the braking phase.

Our margin for obtaining satisfying results was limited. Indeed today's tyres are employed at around 95% of their maximum efficiency. As tyres are designed to endure up to 110% of their capability, we can add a reasonable supplementary load.

From the general results of the optimization, an active command law on a nonlinear system was synthesized. As these theoretical laws are only rarely applied to real systems, we had to devise the control strategies integrating the technological constraints linked to the structure control. For example, taking into account the energy failure for the control of some structures, considering the measurability of states or ascertaining the stability and observability of the systems to be controlled. A control law was validated on the numerical model of real structures in the field of automotive suspensions.

For a good description of a vehicle on the verge of slip, it appears necessary to use a non-linear tyre model and a description of the vehicle taking into account at least the longitudinal and lateral speeds, the yaw, pitch accelerations, the rotations of the four wheels and the maximum side slip of the tyres.

In this study, we have obtained an improvement of traction thanks to piloted suspensions. This was done without any loss of comfort. A numerical study consisting of associating these piloted suspensions with existing active safety systems (ABS, ESP, ...) may be undertaken for application in the future vehicles.

References

1. D. Karnopp, M.J. Crosby, R.A. Harwood, *Vibration control using semi-active force generators*, ASME, Journal of Engineering for Industry Transport, 2–8, 1974.
2. D. Karnopp, S.G. So, *Energy flow in active attitude control suspensions: a bond graph analysis*, Vehicle System Dynamics, **29**, 69–81, 1998.
3. H.E. Tseng, J.K. Hedrick, *Semi-active control laws – optimal and sub-optimal*, Vehicle System Dynamics, **23**, 1994.
4. O. Yaniv, *Robustness to speed of 4WS vehicles for yaw and lateral dynamics*, Vehicle System Dynamics, **27**, 221–234, 1997.
5. D.E. Williamsand W.M. Haddad, *Active suspension to improve vehicle ride and handling*, Vehicle System Dynamics, **28**, 1–24, 1997.
6. A. Gentile, A. Messina, A. Trentadue, *Dynamic behaviour of a mobile robot vehicle with a two caster and two driving wheel configuration*, Vehicle System Dynamics, **25**, 89–112, 1996.
7. E. Bakker, H.B. Pacejka, L. Lidner, *A new tire model with and application in vehicle dynamics studies*, SAE paper No 890087, 1989.
8. E.J.H de Vries, H.B. Pacejka, *Motorcycle tyre measurements and models*, Vehicle System Dynamics, **28**, 1998.
9. R.G. Langlois, R.J. Anderson, *Preview control algorithms for the active suspension of an off-road vehicle*, Vehicle System Dynamics, **24**, 65–97, 1995.
10. E. Esmailzadeh, F. Fahimi, *Optimal adaptative active suspensions for a full car model*, Vehicle System Dynamics, **27**, 89–107, 1997.

11. D.C. Rutledge, M. Hubbard D. Hrovat, *A two DOF model for jerk optimal vehicle suspensions*, Vehicle System Dynamics, **25**, 113–136, 1996.

12. P. de Larminat, *Automatique - commande des systems linéaires*, Hermes.

13. A.G. Thompson P.M. Chaplin, *Force control in electrohydraulic active suspensions*, Vehicle System Dynamics, **22**, 1993.

14. T.R. Ori, *Suspensions actives et comportement dynamique des véhicules lors du freinage*, PHD Thesis n°2001-23, Ecole Centrale Lyon, 2001.

15. A. Alleyne, *Improved Vehicle performance using combined suspension and braking forces*, Vehicle System Dynamics, **27**, 235–265, 1997.

Received March 20, 2006.

ENGINEERING TRANSACTIONS • *Engng. Trans.* • **55**, 2, 181–192, 2007
Polish Academy of Sciences • Institute of Fundamental Technological Research

A COMPARATIVE ANALYSIS OF THEORETICAL MODELS OF GRAVITY MOVEMENTS OF COHESIONLESS GRANULAR MEDIA

W. S z c z e p i ń s k i

Institute of Fundamental Technological Research
Polish Academy of Sciences
Świętokrzyska 21, 00-049 Warsaw, Poland

Three different theoretical models for the analysis of movements of granular media caused by the gravity forces only are critically discused. In each of them the motion is treated as a purely kinematical problem. It has been shown that in application to varoius practical problems, they lead to different displacements patterns (e.g. funnel or mass flow, formation of shear bands or a flow without such bands). Examples of applicaion illustrate the discussion.

1. INTRODUCTION

In numerous important practical problems, the movement of granular media is caused by gravity forces only. The movements in bins and hoppers, sand avalanches, subsidence of terrain caused by underground exploitation are the typical examples. It seems to be reasonable to treat such motions as purely kinematic processes. It is interesting to note that recently in physics, the movement of grains in sand piles is used as an illustration of the so-called "self-organized process" – see e.g. [1, 2]. In these papers the analysis was limited to the movements of grains in a pile of sand. More applications of engineering significance have been discussed in [3], among them an analysis of movement of granular materials in hoppers.

The method used in the mentioned papers is based on the "discrete cellular automata" concept, which is much simpler than continuous differential equations, as stated in [1]. To illustrate the idea of "self-organized criticality", the authors of [1] considered a "pile of sand" built by randomly adding a grain at a time. When the slope of the pile reaches a critical value called the "angle of repose", the added sand will slide down.

A theoretical model based on this concept will be used in the following Sec. 2 for the analysis of movements of loosely packed granular material in a hopper and for similar problems.

An analogous model for densely packed granular media will be discussed in Sec. 3. Section 4 is devoted to the discussion of a probabilistic treatment of the problem.

2. A model for loosely packed granular media

The theoretical model (cellular automaton) mentioned above is shown in Fig. 1. It is composed of a number of identical cicrular (spherical) "grains" forming a regular, loosely packed array. The movements of grain in the model are governed by two simple rules:

1. If an empty space is located under that occupied by a grain, the grain moves downwards filling the empty place – cf. Fig. 1b
2. The difference of the heights of two neighbouring columns of grains cannot be larger than the diameter of a single grain. When it is larger, the upper grain falls down to the lower position in the next column – cf. Fig. 1c.

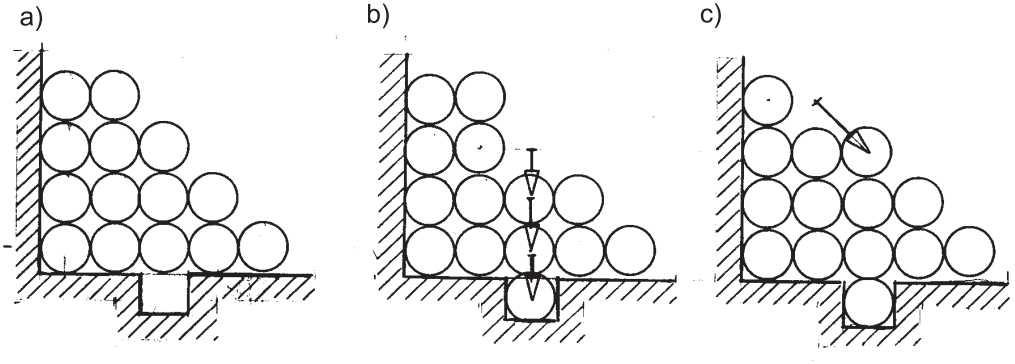

Fig. 1.

Using the two rules one can solve numerous problems of practical significance. As an example let us analyse displacements of grains in a bin. The initial stage of motion is shown in Fig. 2a when four grains have left the outlet. In Fig. 2b is presented a more advanced stage of the movement. The medium flows through a vertical funnel, while the rest of the bulk remains motionless. Thus the model predicts the well-known phenomen of the often observed so-called funnel flow in hoppers – see e.g. [4–7].

Let us note that this simple model does not predict the existence of any horizontal interaction (pressure) between the granular medium and the container's wall. The stress state in the medium reduces everywhere to uniaxial compression increasing towards the bottom. This unrealistic result is caused by the specific arrangement of grains in the model.

As a next example, let us consider the problem of terrain subsidence caused by partial tectonic translation of bedrock uder the sand-like layer resting on it – Fig. 3. The empty space formed by this translation must be filled by granular medium of the upper layer.

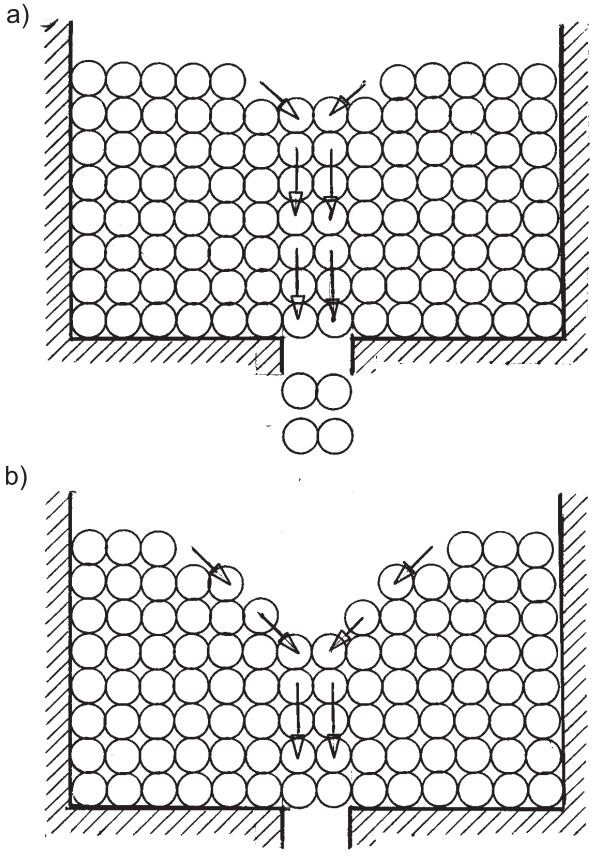

Fig. 2.

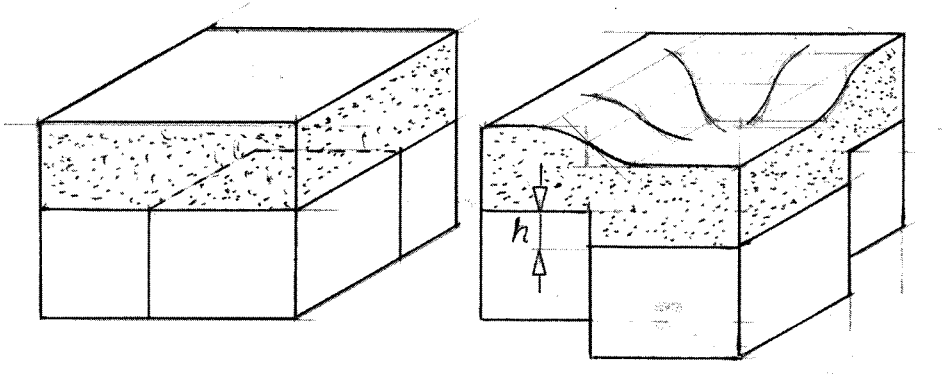

Fig. 3.

The solution is shown in Fig. 4. Elememts of granular medium have been presented in a cuboidal form. Such a presentation assures better visualization of the shape of deformed upper surface of the medium.

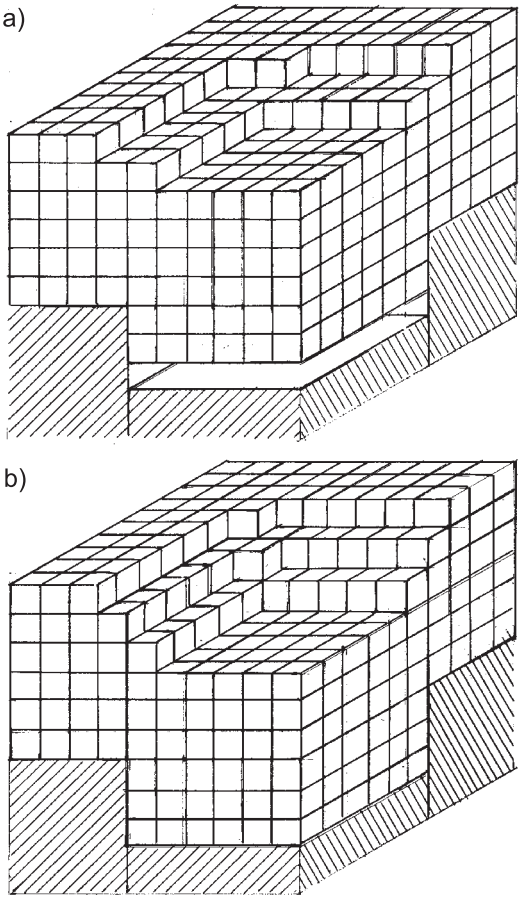

Fig. 4.

3. A model for densely packed granular material

A regular dense packing of elements of a granular medium is shown in Fig. 5a. As an illustrating example let us assume that at the bottom, the container is equipped with a feeder moving downwards. When the bottom of the feeder moves, the grains of the medium above it also move until each of them reaches the position assuring the smallest possible potential energy (the lowest possible position). Using this simple rule we can find the momentary translation vectors

for all particles. They are shown in Fig. 5b and c for two subsequent positions of the bottom of the feeder. Comparing these patterns of translations with those shown previously in Fig. 2, one can see that the present model leads to a solution with the "mass flow" instead of the funnel motion predicted by the previous model.

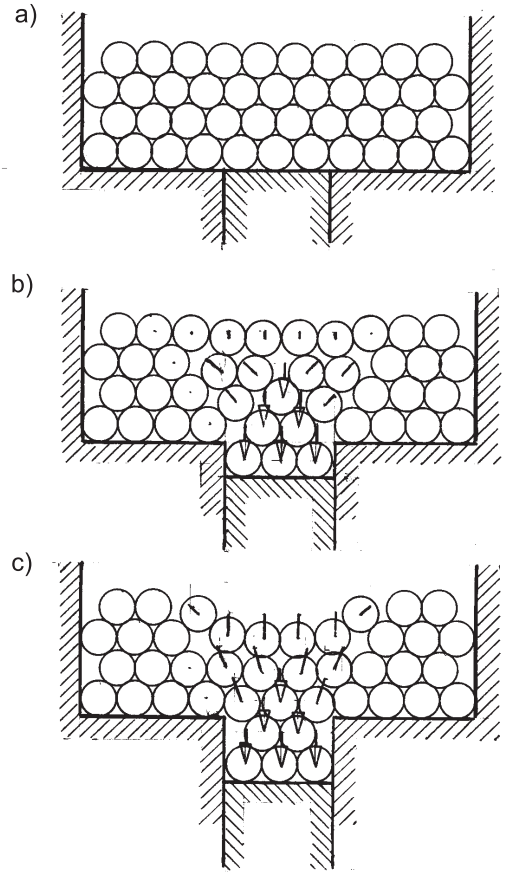

FIG. 5.

A more advanced example of momentary movement in a hopper is shown in Fig. 6. When calculating the momentary translation vectors of particular elements in an assembly of grains, we must often arbitrarily decide which of the adjacent grains moves towards the empty place below. Thus the procedure of determining the translation vectors is influenced by certain random factors. Slightly different translation patterns may result from the calculation procedure. In Fig. 6 is presented one of the possible solutions. It corresponds to the stage when fourteen elements have left the outlet of the bin.

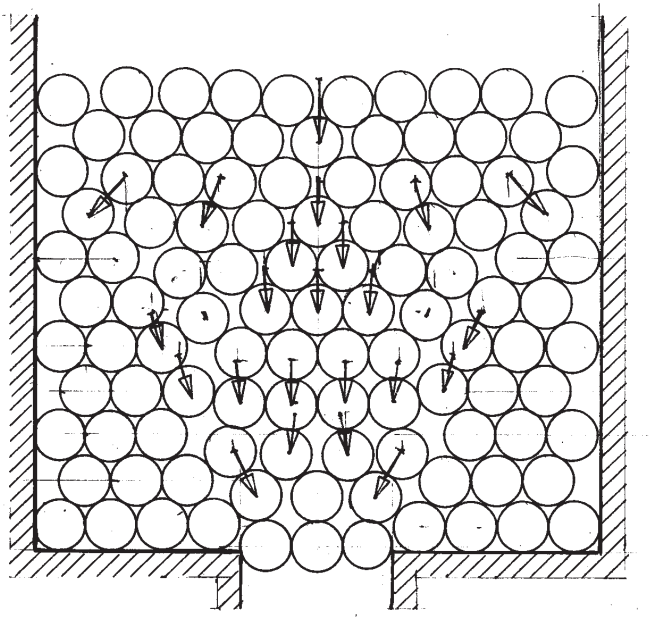

Fig. 6.

Let us note that during the flow of grains the packing of them becomes less dense. Such a loosening of the packing has been observed in deformed granular materials in experiments performed with the use of X-ray method – see e.g. [8–11].

The pattern of particle translation and loosening of the packing was also experimentally investigated in [12]. In a simulation test an assembly of coins has been used. The coins were located on a glass plate in the initially horizontal position. Then the plate was inclined with respect to the horizontal plane. The coins slid downwards due to gravity forces. The obtained translation pattern of coins was similar to that shown in Fig. 6.

Using this model we can calculate the forces of interaction between the medium and a retaining wall. This can be done when the friction between the grains and the surface of the wall is neglected. In Fig. 7 are presented the calculated interaction forces. It was assumed that the weight G of a single grain is equal to unity ($G = 1$). To the right of the row $A - B$ of grains, the system of interaction forces reduces to the uniaxial compression in vertical direction. Within the triangle $A - B - C$ this system is disturbed by contact of grains with the wall. It is seen that the influence of the contact is strongly localized.

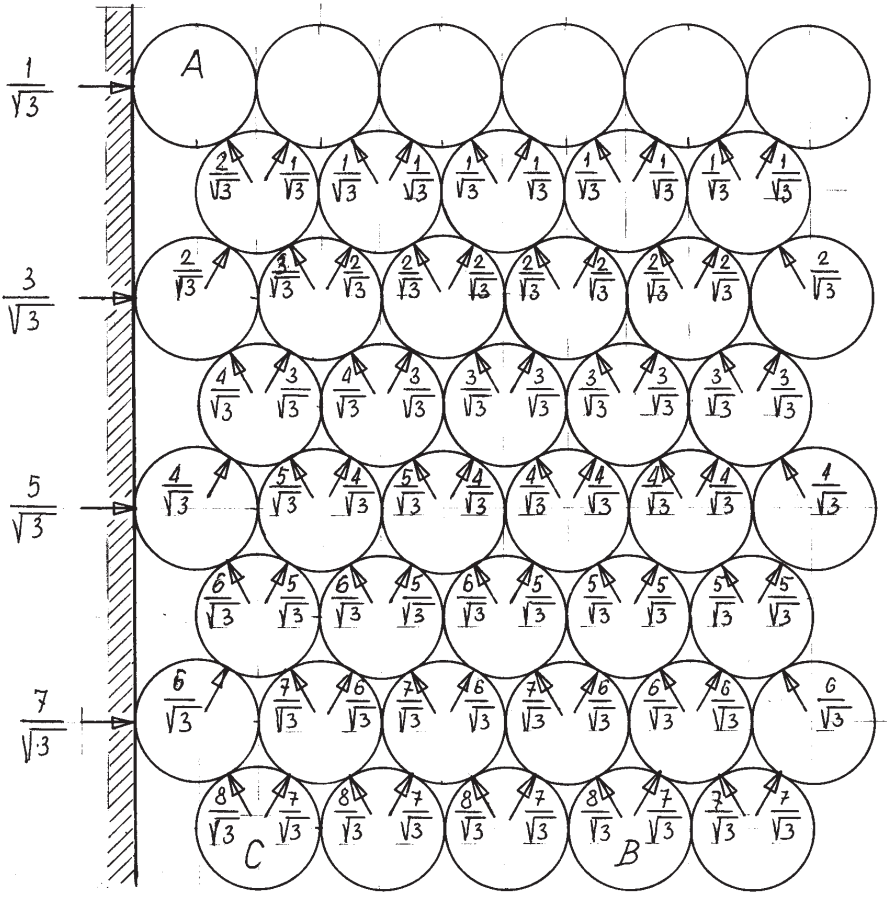

FIG. 7.

Using the model discussed in this section we can solve numerous two-dimensional problems. However, application of the model to the analysis of three-dimensional problems may prove to be difficult.

The model allows us to determine a general layout of the system of slip-lines (displacements discontinuity). Two simple examples are presented in Fig. 8. They concern the movements of elements of the model caused by displacement of the retaining wall. In Fig. 8a the wall slightly rotates about the point at the bottom. In the triangle ABC there appear several slip-lines. Such an effect has been confirmed in numerous experiments – cf.e.g. [9–10]. In the case shown in Fig. 8b, when the wall has been slightly shifted horizontally, the movement of the medium reduces to a displacement of the triangle ABC as a rigid body along the single slip-line $B - C$.

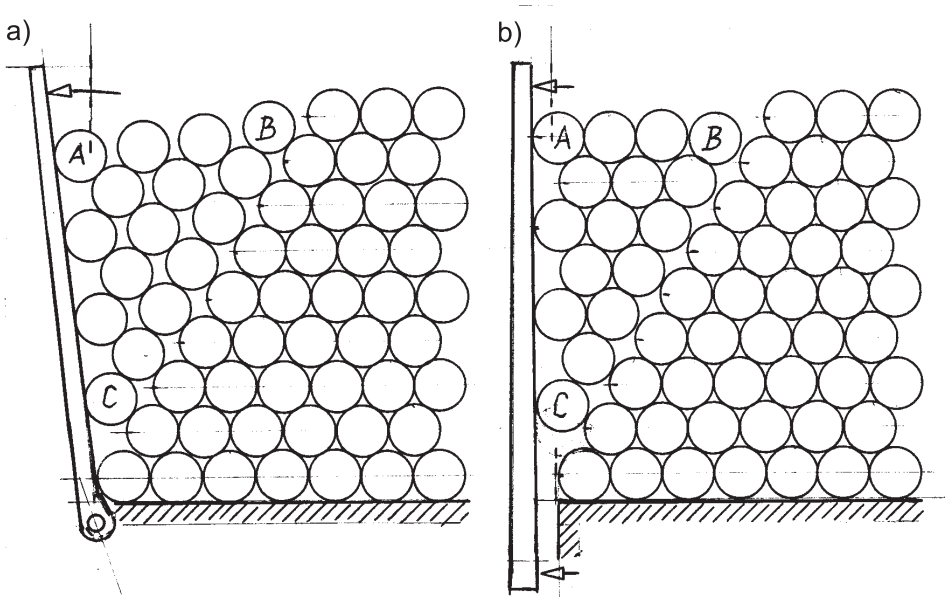

Fig. 8.

4. Stochastic finite cells model for granular media

The stochastic model is based on the concept of J. Litwiniszyn [13–15]. According to this concept displacements in a granular medium caused by gravity forces are of the mass character of random changes of mutual contacts between the particles. Consequently, the displacements of particles are random.

As the starting point let us imagine a device composed of a number of plates (layers) resting one on the other. Each plate is formed by a regular array of cuboidal cells with square holes (Fig. 9). The cells in subsequent plates are arranged with respect to each other in such a manner that central axes of the holes in a plate coincide with the common line of four corners of cells in the plate located just below or above.

Let us assume, similarly as in the so-called Galton's board (cf.e.g. [16]) for two-dimensional cases, that small balls falling down from a particular cell in a plate and striking the common vertical edges of four cells in the plate below are randomly directed into one of these cells with the probability equal to 1/4. The random path of consecutively falling balls is repeated for each plate below. Finally the balls fall at random into one of the separate containers at the bottom. The distribution of the number of balls in these containers shown at the bottom of Fig. 9 approaches the circular normal distribution.

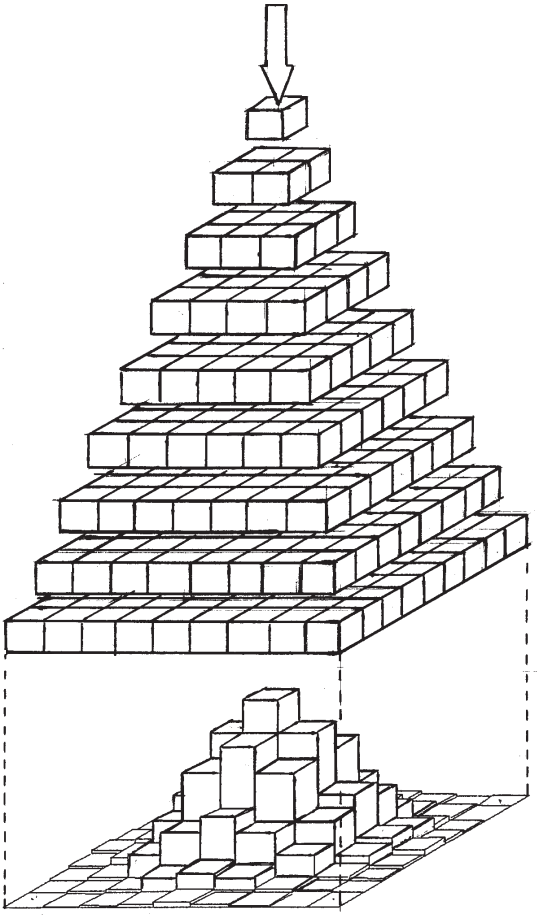

FIG. 9.

Litwiniszyn analysed an inverse two-dimensional problem, in which cavities existing in the bulk of a loose medium migrated randomly upwards to the upper surface of the bulk. This idea has been generalized for three-dimensional cases. In this generalized procedure, systems of finite cells were used to calculate the formation of local depressions in the upper surfaces of granular media, in which there exist systems of cavities [17, 18].

As an example of application of the finite cells procedure, in Fig. 10 is shown a step-wise approximation of the deformed upper surface of the layer of a granular medium, resting on the bedrock with the initial narrow cuboidal cavity. The cavity has been divided into eighteen units. In the calculating procedure, these unit cavities are assumed to migrate randomly upwards through an assumed system of plates with cells such a those shown in Fig. 9.

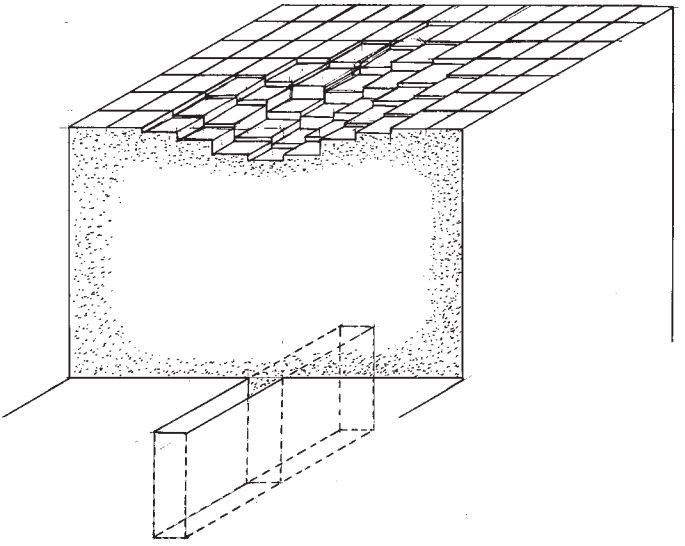

Fig. 10.

Using the stochastic finite cells procedure it is possible to calculate the displacement vectors of the particles of the medium – cf. [18]. The calculated vectors in the longer symmetry plane are shown in Fig. 11.

Let us notice that the finite cells model leads to realistic solutions even if the initial cavity is located very deeply. In such cases the model discussed in Sec. 2 gives unrealistic results concerning the funnel flow of the medium.

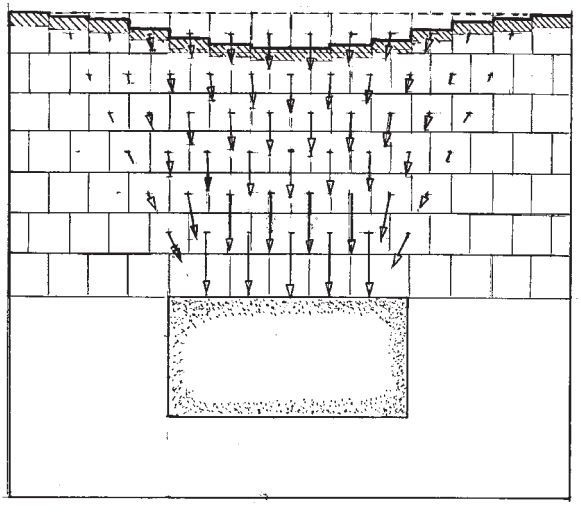

Fig. 11.

5. Concluding remarks

In all three theoretical models of granular media, their movements caused by gravity fores without any external action are treated as a purely kinematical problem. Application of each of these models is limited to a certain class of problems.

The model discussed in Sec. 2 predicts the so-called funnel flow observed sometimes in bins and hoppers. However, it cannot be used in the cases when the so-called mass flow is expected. As an example let us mention the motion in a bulk of granular medium leading to filling a deeply located empty space.

The model of a densely packed granular medium (Sec. 3) predicts mass flow of the medium. It gives good results when it is used for the analysis of two-dimensional problems. Its application to three-dimensional cases is difficult. However, using it in two-dimensional problems we can rationally analyses the pressure exerted by the medium on the retaining walls. Note that the previous model (Sec. 2) does not predict any pressure between the medium and the wall. Moreover, the model predicts formation of shear bands in the medium often observed in experimental tests.

The stochastic finite cells model (Sec. 4) predicts the mass flow of the medium and may be used for the analysis of any three-dimensional problem. However, it does not predict formation of shear bands in the granular medium.

References

1. P. Bak, C. Tang, K. Wiesenfeld *Self-organized criticality*, Phys. Review A., **38**, 1, 364–374, 1988.
2. C.P. Prado, Z. Olami, *Interia and break of self-organized criticality in sandpile cellular-automata models*, Phys. Review A., **45**, 2, 665–669, 1992.
3. D.Müller, *Techniques informatiques pour la simulation de mileux granulaires par la méthode d' élements distincs*, Thése No. 1545, Ecole Polytechnique Fédérale de Lausanne, 1996.
4. A. Jenike, *Better design for bulk handling*, Chemical Engineering, 1954.
5. J. Johanson, *The use of corrective inserts in bins*, Journal of Engineering for Industry, 224–230, 1966.
6. J. Nachimowicz, J. Piwnik, S. Poskrobko, *Dead zones in the gravity flow in bins* (in Polish), Trans. of the Białystok Technical Univeristy, Ser. Mechanics **10**, 45–62, 1993.
7. I. Sielamowicz, *Experimental analysis of granular material flows using the technique of digital particle image velocimetry*, Engng. Trans., **53**, 197–229, 2005.
8. J.R.F. Artur, *Strains and lateral forces in sand*, PhD Thesis, University of Cambridge, 1962.

9. G.W.E. Milligan, *The bahaviour of rigid and flexible retaining walls in sand*, PhD Thesis, University of Cambridge, 1974.

10. D. Leśniewska, *Analysis of shear band pattern formation in soil*, Institute of Hydroengineering of the Polish Academy of Sciences, Gdańsk 2000.

11. A. Drescher, T.W. Consens, P.L. Bransby, *Kinematics of mass flow of granular material through a plane hopper*, Geotechnique, **28**, 27–43, 1978.

12. Z. Kotulski, W. Szczepiński, *On a model for prediction of the movements of a crowd in narrow exits*, Engng. Trans., **53**, 347–361, 2005.

13. J. Litwiszyn, *Application of the equation of stochastic processes to mechanics of loose bodies*, Arch. Mech. Stos., **8**, 393–411, 1956.

14. J. Litwiszyn, *On application of the random walk argument to the mechanics of granular media*, Proc. of the IUTAM Symp. on Rheology and Soil Mechanics, Springer Verlag 1966.

15. J. Litwiszyn, *Stochastic methods in mechanics of granular bodies*, CISM Courses and Lectures, **93**, Udine, Springer Verlag 1974.

16. Z. Kotulski, W. Szczepiński, *Error analysis for engineers* [in Polish], WNT, 2004.

17. W. Szczepiński, *On the stochastic approach to the three-dimensional problems of strata mechanics*, Bull. of Polish Academy of Sciences, Technical Sciences, **51**, 335–345, 2003.

18. W. Szczepiński, *On the movement of granular materials in bins, Part II – Three-dimensional problems*, Engng. Trans., **51**, 433–444, 2003.

Received May 11, 2006; revised version October 3, 2006.